Chapter 1

Introduction

1.1 Introduction

Gaseous discharge and gas discharge plasma have been explored and studied since the early of 17^{th} century. The history began with the observation of glowing light in a partially evacuated glass tube when charged by static electricity. Since then, the investigations on the phenomenon of electric arc were carried out to understand the phenomenon as it has been found that the light produced was more intense compared to an incandescent light bulb. The term "gas discharge" refers to the electrical breakdown of gas due to an applied electric field, typically in the order of several hundred volts.

The term of "plasma" was introduced by Irving Langmuir in the 1920's to describe the partially ionized gas produced in a discharge tube of uniform electric field. The number of ions and electrons within the discharge tube were almost equal that resulting a very small space charge. Today plasma is studied in the laboratory either to enhance the understanding of plasma phenomenon or to utilize its high temperature high density characteristics for practical application like production of light source and fusion energy.

There are several methods of plasma generation in the laboratory for research or application, pulsed discharge is one of them. In fact, the oldest method used in order to generate high temperature Dense Magnetized Plasma (DMP) was based on high voltage

pulsed discharge between metal electrodes. The simplest configuration was a set of two conical, hemispherical or plane electrodes placed at a chosen distance inside a vacuum chamber filled with selected working gas or gas mixture. The discharge was then initiated by a high voltage pulse discharged across the two electrodes.

Plasma produced by a pulsed discharge in the Plasma Focus (PF) device demonstrated in 1965 has shown to produce neutrons in the magnitude of 10^8 per pulse. Research based on the plasma focus soon became a hot topic. The plasma focus device is a simple coaxial accelerator that produces short-lived pinched plasma by electromagnetic acceleration and compression. The dense transient plasma formed at the end of coaxial plasma accelerator was reported to has a plasma densities $n > 10^{19}$ particles/cm^3 and a temperature of few kilo electron volts $T_e \sim$ 1-3 keV. The lifetime of the plasma was measured to be about hundreds of nano seconds (Mather, 1965). Confinement of the plasma to a longer duration was soon found to be hindered by the onset of hydromagnetic instability (Mather & Bottoms, 1968).

Nevertheless, early research was concentrated on improving the performance of the plasma focus device as a nuclear fusion facility. Works have been conducted to understand the instabilities and aimed to prolong the lifetime of the hot and dense plasma for thermonuclear fusion. Various experimental evidence and theoretical treatment of the marco- and micro-instabilities in the plasmas were reported (Lehnert, 1967) , (Comisar, 1969), (Lu, 1996), (Kies, et al., 1998),(Haruki, et al., 2006).

The conceptive design of the plasma focus device for fusion research was first investigated independently by Filippov (Filippov, Filippova, & Vinogradov, 1962) at the Kurchatov Institute in Moscow (U. S. S. R.) and Mather (Mather, 1964) at Los Alamos (U. S. A.) in the early sixties. Therefore, the two independently developed

plasma focus devices, which were of different configurations were named after their founders, the Filippov type (Filippov, et al., 1962) and Mather type (Mather, 1964).

The Filippov type plasma focus was originated from the modification of the *Z*-pinch configuration whereas Mather type plasma focus was evolved from the electromagnetic shock tube. The electrode geometries of Filippov type and Mather type plasma focus are similar with the major difference lie in the aspect ratio of the electrodes diameter, d and their length, l as shown in (Figure 1). The Filippov type plasma focus usually has a large aspect ratio with $d/l > 1$ that the electrodes are of short length and the inner electrode is relatively large in diameter. The Mather type has small aspect ratio $d/l < 1$ with long electrode length and small diameter inner electrode. The electrodes are usually made of copper or stainless steel.

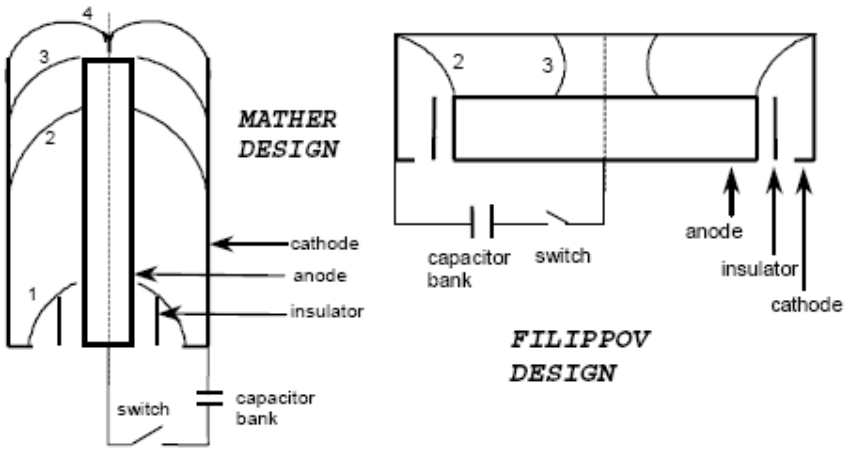

Figure 1: Schematic drawings of Filippov design and Mather design Dense Plasma Focus devices.

The plasma focus can operate with the capacitor bank energies ranging from 1 *kJ* to 1 *MJ*. The device can be classified into three categories based on the input energy; the small plasma focus of 1 – 15 *kJ*, the medium plasma focus 15 – 50 *kJ* and large plasma focus of 150 *kJ* – 1 *MJ*. Sub *kJ* plasma focus was also investigated since 1978 (Shyam & Srinivasan, 1978) with the input energy as small as 0.1 *J* (Soto, et al., 2009). It has also been shown the evidence of the plasma pinching in a nano Joule plasma focus. The pinched plasma has been recorded by image techniques made by a single-frame image converter camera with 4 *ns* exposure time.

The phenomenon of plasma pinching and various other plasma parameters are about the same in the wide range of input energy. A 3 *kJ* Mather type plasma focus system is used in the current project, with maximum current of about 180 kA, and plasma life time of about 100 *ns*.

1.2 Literature Review of The Plasma Focus Discharge

Since the development of plasma focus device, considerable interest was directed to plasma fusion technology and plasma applications. Many works have been carried out by the researchers in order to study and understand the mechanism of the dense transient plasma discharge. Some theoretical works have been done to relate the plasma focus dynamics with the experimental observation. However, there is still a big challenge for plasma physicists to fully understand the mechanism of plasma focus phenomena.

In his first report on the plasma focus, Mather reported two modes of operation by using deuterium as the working gas (Mather, 1964). The mode 1 operation worked like a coaxial plasma gun, where fast deuteron ions with energy many times the applied charging voltage were produced. On the other hand, in mode 2 operation, a high density focused plasma was formed at the end of the electrodes and neutrons were registered. Further work on his mode 2 operations yielded an intense neutron pulse of more than 10^{10}. Image of the focused plasma was obtained through the soft X-ray pinhole imaging technique. The recorded images showed that plasma column was situated at a distance of about 1.5 *cm* away from the center electrode.

He then investigated the evolution of the plasma from the breakdown to the formation of pinched plasma (Mather & Williams, 1966). The pinch effect formed a plasma column at the open end of the center electrode was due to the rapid conversion of the stored magnetic energy in the focus tube and the external circuit to the plasma energy (Mather, 1971). The pinching effect of the current sheath in a coaxial plasma gun has also been observed in Japan in 1966 (Nakano, Hirano, & Mitadera, 1966).

Formation of the high density plasma column at the end of the coaxial accelerators was believed to depend on the dynamics of the collapsing current sheath. In 1972, Jalufka observed the collapse of the current sheaths in a 25 *kJ* plasma focus with the employment of two image-converter cameras operated in the streak mode (Jalufka & Lee, 1972). One of the cameras viewed the region above the end of the center electrode and the other viewed the region at the area above the center electrode. The recorded streak photographs were summarized and he concluded that the neutrons and the hard x-ray emission were originated from the plasma column.

A study (Oppenlander, Pross, Decker, & Trunk, 1977) showed that only a fraction of the discharged current flowed in the current sheath and formed the plasma column. The author measured the pinch current of the plasma column by placing a magnetic probe close to the final pinch region. Pinch current measured was in the order of 80 % of the total discharged current. The scaling law to relate the correlation between neutron yield and pinch current is described as $Y \sim I^{4.1}$. The author also found that formation of spokes during the breakdown phase results in very small neutron emission as the effect of low pinch current. Thus, he believes that higher average pinch current correlated to higher neutron yield.

Lee developed the Radiative Dense Plasma Focus Computation Package (S. Lee) to simulate and compare with the experimental data of various plasma focus devices. The plasma enthalpy in the stationary pinch column was attributed to the work done by the current sheath driven by the magnetic piston (S. Lee, 1983). The pinch ratio of the plasma column can be computed and is dependent only on the specific heat ratio, γ, of the pinched plasma. A pinch ratio of 0.14 for the deuterium plasma column was computed for γ = 5/3 and is very close to the measured value of 0.13 from streak photograph.

The dynamic behavior of the collapsing current sheath in focus region was observed by Yamamoto using interferometry method in streak mode and framing mode together with neutron measurement (Yamamoto, Shimoda, Kobayashi, & Hirano, 1984). The images captured by Mach-Zehnder interferometric system showed that the plasma column formed at the end of center electrode has a diameter of about 0.8 *mm*. Due to the growing of m = 0 instability, the plasma column started to expand and finally disrupted into plasma cloud. The presence of m = 0 instability was seen to have no effect on the

production of neutrons. Thus, the author suggested that the acceleration of ion beam caused neutron emission was due to the abrupt rise of the plasma resistivity rather than the rapid change in the plasma inductance.

Another researcher, Moreno obtained the images of plasma dynamics in a small plasma focus device of bank energy 50 *J* with a single frame ICCD camera couple with micro-channel plate operated at 5 *ns* exposure time (Moreno, Silva, & Soto, 2003). An evidence of the plasma pinching during the maximum compression was observed in the plasma images. The plasma column was observed to be stable momentary for about 50 *ns* with its radius measured to be about 0.7 *mm*. The velocity of the radial collapse was determined to be in the order of 10^5 ms^{-1}. However, the dip in current derivative signal was not observed, which indicated the change of plasma impedance was not significant in comparison with the external circuit impedance.

Koshelev and co-workers reported an observation of the micropinch formation in a plasma column with the presence of heavy gas impurities (Koshelev, et al., 1988). Number of micropinches or so called "hot-points" of up to 10 or more were observed along the plasma column axis by the pinhole imaging technique. Such phenomenon was also observed in the megajoule plasma focus (Scholz, et al., 2004). The number of mircopinches were found dependent on the quantities of the heavy gas doping. Micropinches were found when the concentration of xenon gas doping was more than 0.5% and became the brightest and smallest at xenon concentration of 1-2 %.

In 1992, current efficiency in the pinching was investigated (Tou, Chin, & Chen, 1992) based on the measured voltage and current signals. The run down velocity of the current sheath in a plasma focus was simulated by using a modified snowplow model.

The results were computed for deuterium and argon discharge and the rundown velocity obtained are 9.2 $cm/\mu s$ and 7.5 $cm/\mu s$, respectively. The results obtained showed that there was leakage current, which stayed behind near the insulator. About 27 % and 33 % of the total discharge current in deuterium and argon, respectively contributed to the leakage current. The magnetic energy was thus lower due to the current leakage and it was believed to be an important factor that could influence the neutrons' output. The importance of magnetic energy for the performance of plasma focus device also has been reported by Zhang (Zhang, Rawat, et al., 2006).

Polarity of the plasma focus electrode was investigated again in 1998, after Mather concluded that the plasma focus should have a positive polarity in the inner electrode in 1965 (Mather, 1965). Generally, plasma focus is operated with inner electrode of positive polarity. Mathuthu (Mathuthu, Zengeni, & Gholap, 1998) compared the results of a 2.3 *kJ* plasma focus with inner electrode of negative polarity and positive polarity. The length of the electrodes was also varied. The results obtained showed shorter inner electrode length (40 *mm*) was better with negative polarity while in positive polarity, longer electrode (150 *mm*) has to be used. In negative polarity operation, it was found that shorter electrodes helped to reduce the contamination due to ablated inner electrode material and also improved the focus action at higher filling pressure where the focus action occurs at the peak discharge current.

At the same year, Serban studied the performance of a plasma focus device with the enhanced axial sheath velocities (Serban & Lee, 1998). He modified the geometry of the anode to a double-stage-stepped anode configuration. The region of the speed-enhanced section was tested to be long enough for speed enhancement but short enough to avoid the separation between the shock front and the magnetic piston. Peak axial

speeds of 15 $cm/\mu s$ were achieved and the thermonuclear neutron emission is found to be correlated with the peak axial speed. Neutrons and X-rays production were found to be increased as the current sheath velocities increases. A scaling law for the neutron yield from the thermonuclear origin is proposed as $Y_{th} \propto (I_p V_{axial})^4$.

In recent years, works has also been devoted to the enhancement and application of the plasma focus for neutrons and ion beams production [(Pouzo & Milanese, 2003), (Yasin, Ali, Solaija, Younis, & Zakaullah, 2004), (Soto, 2005), (Verma, et al., 2009), (El-Aragi, 2010)]. It can be made a unique high intensity neutron source as well as high energy ion beam source for the generation of directional neutrons via beam-target mechanism.

A report in 2010 by Roshan (Roshan, et al., 2010) found that there is two pressure regimes for the plasma focus to be operated either as neutron source or ion beam source. He correlated the deuteron beam energy and neutron yield with the time-integrated images of focused plasma. At low pressure, very high deuteron beam energy (about 500 *keV*) was produced and found to be correlated with the bright area on the anode surface of the pinch images. The bright area was the effect of high energy electron beam bombardment of the anode surface. While the high pressure range, was optimum for neutron production, but the deuteron beam energy registered was in the range of 40-50 *keV*.

Correlation of the plasma focus radial compression phase with the neutron emission from the Tens-of-Joules small plasma focus has been recently reported by Saldivia (Tarifeño-Saldivia, Pavez, Moreno, & Soto, 2011). The dynamic of the plasma focus is observed by interferometric measurements and the radial phase is measured to

last for about 50 *ns* with peak radial sheath velocity of 10 *cm*/μs. The plasma column of pinch densities 1.6 x 10^{25} m^{-3} is confined to about 6-10 *ns* before disrupted and produces 1.6 x 10^{4} neutrons per shot. The ratio of the ionized particles to the neutral gas was estimated to be 25 % in their earlier report (Soto, Pavez, Tarifeño, Moreno, & Veloso, 2010), which was of the same order of magnitude as in plasma focus device of sub-kilojoule to megajoule stored energy. Thus, fruitful results with plasma focus application as pulsed neutron source or ion beam source can be expected.

1.3 Ion Beam Acceleration/Production Mechanism

The mechanisms responsible for the appealing neutron yield in the early research were thought of due to thermonuclear fusion. However, abundant of results have proof otherwise (Bernstein & Hai, 1970), (J. H. Lee, Shomo, Williams, & Hermansdorfer, 1971), (Hübner, Bruhns, & Steinmetz, 1978). The mechanisms of neutron productions need to be understood before we could efficiently enhance the neutron output. Measurement of the prime product, the energetic ions was the key diagnostics that could give us useful information. Several important models have been proposed to explain the ion acceleration mechanism, include the induced electric field model (Bernstein, 1970), (Peter Gary & Hohl, 1973), (Imshennik, Osovets, & Otroschenko, 1973), (Kondoh & Hirano, 1978), (Zambreanu & Doloc, 1992), anomalous resistive electric field model (Peter Gary, 1974), gyro-reflection-acceleration (Deutsch & Kies, 1988), resistive ion acceleration model (Tanimoto & Koyama, 1982) etc.

In 1970, Bernstein's model (Bernstein, 1970) computed the trajectories of ions under crossed electric and magnetic fields, which vary only as a function of the radial coordinate. These fields were assumed to be generated by the rapid transition of current distribution in the plasma column. Deuteron ion measured were accelerated by the induced electric field of magnitude 200 *kV*/*cm* and above up to energy of 600 *keV*. He also observed experimentally the presence of non-thermonuclear origin for the neutron production (Bernstein & Hai, 1970).

Later, Gary (Peter Gary & Hohl, 1973) extend the model developed by Bernstein (Bernstein, 1970) by add in axial electric field in the centre axis of plasma column, which was assumed to be zero in Bernstein model. The ion trajectories subjected to electric and magnetic field in the plasma column were calculated from numerical integrations of three-dimensional equations of motion. This assumption is shown to be more effective in terms of energy transfer, where the ions can be accelerated to very high energy instead of moderate heating due to cyclotron acceleration in the case of Bernstein model. An experiment to correlate the rapid current drop and ion runaway has yielded good evidence for the validity of the model (Peter Gary & Hohl, 1973). This model also implied that ions are accelerated by strong electric field during the focus phase.

About the same year, Imshennik (Imshennik, et al., 1973) attempted to explain the acceleration of the ions with the magnetohydrodynamic (MHD) theory. He postulated that strong local electric filed was induced by the development of m = 0 instabilities that was responsible of accelerating the ions to the measured energy. The potential differences of the electric field calculated agree quite well with the measured energy of the accelerated ions observed in experiments assuming their ions were emitted

from the boundary of the plasma column. The potential difference was the highest at the boundary.

In 1978, Kondoh (Kondoh & Hirano, 1978) investigated the motion of ions in a Z - pinch type plasma focus from the theoretical approach with the assumption of uniform current density in the plasma. The equation of motion of ions is solved numerically with the presence of electromagnetic field induced in the pinch phase from fluid and circuit equations. It is shown in the collapse phase, a betatron-like acceleration process with negligible drift velocity appears to be the most efficient process of transferring energy to the ions. Whilst in the expansion phase, a strong free-streaming acceleration process evolved to be the most efficient process for acceleration of ions due to a decreasing current density.

Zambreanu (Zambreanu & Doloc, 1992) proposed a model to compute the ion trajectories under the assumption of a uniform current density in the plasma and approximation of infinite plasma column length. The motion of ions was computed to have axial component and radial component. Uniform accelerated dynamics and non-uniform accelerated dynamics for the column stage were considered in this model. In the uniform case, results obtained showed that ions have only very small energy in the range 10 – 20 *keV* while gyrate with small drift along the z-axis (end on). In the later, high energy ions were produced owing to more efficient acceleration process during the expansion phase and m = 0 instability. The results also suggested that expansion of the plasma column play an important role for the acceleration mechanism.

In 1974, Gary (Peter Gary, 1974) suggested an anomalous resistive electric field model, which is an extension to his previous theoretical model (Peter Gary & Hohl,

1973). He calculated the electric and magnetic field based on a simple plasma model. He assumed that there is an enhancement of anomalous resistivity during the collapsing of the current sheath, which leads to the diffusion of electric and magnetic field into the plasma and hence accelerates the ions. Deuteron ions with large axial speed and random perpendicular (radial drift) velocities were computed from the model. However, this model is far from satisfactory to explain presence of the strong induced electric in producing high energy ions.

In the resistive ion acceleration model (Tanimoto & Koyama, 1982), Tamimoto discussed the acceleration of ions by the enhanced resistivity due to the insulation of current by a self-induced magnetic field for the non-relativistic case. A strong resistive electric field was believed to be dominant than inductive electric field in the plasma column, which accelerated ions to several *MeV*. A scaling law was obtained for the maximum ion energy based on the model. A relation was also obtained where the ion acceleration by resistive electric field is 16 times more dominant than the inductive one. In this model, the energy of the accelerated ions was only limited by the duration of axial electric field to the transit time of ions over the length of plasma column.

Deutsch (Deutsch & Kies, 1988) suggested gyro-reflection acceleration model for large and high performance plasma focus device to account for the evidence of neutron emission even though no m = 0 instability was detected. The model was extended from the induced electric field model by add in supplementary field due to current sheath acceleration. In this model, ions are assumed to be accelerated by a magnetic piston effect of the current sheath.

1.4 Pulsed Plasma Radiation Source

Plasma Focus has been studied intensively by many researchers because of its special characteristic as high energetic ion beam source, of characteristic energy ranged from tens of kiloelectronvolts to megaelectronvolts (Gerdin, Stygar, & Venneri, 1981), (Sadowski, Zebrowski, Rydygier, & Kucinski, 1988), (Zakaullah, Ahmad, et al., 1998), (Bostick, Kilic, Nardi, & Powell, 1993). Nevertheless, plasma focus is also well known as a rich plasma source of producing multi-radiation such as X-ray, electron beam and neutrons if deuterium or deuterium and tritium are used as the working gas.

Numerous studies of ion beam emission has been carried out from experimental and theoretical approach in order to discover the information about the ion source, ion acceleration mechanism and also its application in the various emerging technological fields. However, there are some difficulties in the measurement of ion beam emission due to its transient phenomena. High temporal resolution diagnostic tool is required to resolve the information from the ion beams emitted. Several diagnostic techniques commonly used for the determination of ion beam energy spectrum include time-of-flight (TOF) technique (Bostick, et al., 1993), (Bhuyan, Chuaqui, Favre, Mitchell, & Wyndham, 2005), (Yap, 2006), Thomson parabola spectrometer (Sadowski, et al., 1997), (Skladnik-Sadowska, Baranowski, & Sadowski, 2001), (Malinowski, Skladnik-Sadowska, & Sadowski, 2005), nuclear activation technique (Gullickson & Sahlin, 1978), Faraday cups (Gerdin, et al., 1981), solid state nuclear track detectors (Szydlowski, et al., 2004), (Castillo, et al., 2007), thin silicon detectors (Musseau, et al., 1998), ion pinhole camera (Skladnik-Sadowska, Baranowski, Milanese, et al., 2001) and etc.

In 1980, Gerdin (Gerdin, et al., 1981) studied the ion beam emission from Faraday cup analysis using time-of-flight technique. He successfully designed and operated the faraday cup as secondary electron emitter (SEE mode) and as an ion collector (MIC mode). The results obtained in these two modes shown to be consistent and deuteron energies down to ~ 25 *keV* were able to resolve with biasing voltage of - 400 Volts.

Another research group (Nardi, et al., 1988) reported the results on the stimulated acceleration and confinement of the deuterons by employing a suitable field distortion element in the inter-electrode gap. The research group successfully extends the ion confinement time in the pinch region, which in turns enhanced the average neutron yield by a factor of 3 and more. The energy spectrum of the deuteron beam obtained cover the range of 70 *keV* – 8 *MeV* as determined from Thomson Spectrometer, Magnetic analyzers and Faraday cups.

Moo (Moo, Chakrabarty, & Lee, 1991) investigated the ion beam emission from the observation of neutron yield using a copper obstacle and deuterated target. The neutron yield is investigated as a function of target/obstacle distance from anode tip. The obtained results showed that neutron yield is dependent on target distance and more than 85 % of the neutron yield resulted from the deuteron beam - deuterium gas interaction in the region 20 - 60 *mm* from the anode end. The results suggested beam-target mechanism for the neutron production.

This group later resolved the neutron emissions due to non-thermonuclear and thermonuclear reaction with time of flight method (Yap, Wong, Choi, Dumitrescu, & Moo, 2005). The non-thermonuclear neutron was believed due to energetic deuteron

beam and attempt was made to enhance its yield by changing the system inductance with electrode of different length (Wong & Yap, 2005). Three different electrodes length at 16 *cm*, 22 *cm* and 27 *cm* were investigated and optimum pressures for each were determined. Average deuteron beam with energy of 50 to 200 *keV* was consistently produced with the highest energy observed at 27 *cm* electrode.

A time-of-flight method was suggested by Bostik (Bostick, et al., 1993) to study the energy spectrum of the ion beam in a 5.4 *kJ* plasma focus device. Ion beam was detected with faraday cup housed in a differentially pumped drift tube separated from plasma chamber. Deuterons energy in the range of 0.3 – 9 *MeV* were obtained by time of flight method and the result is consistent with the measurement of a differential filter method. He correlated the ion beam intensity with operating pressure, neutron yield and hard X-ray. Maximum ion beam intensity at corresponding neutron yield is increases with the increase of hard X-ray amplitude.

Measurement of deuterons and nitrogen ions from the registration of ion tracks on solid state nuclear track detectors was reported by Sadowski (Sadowski, et al., 1997). The primary objective of the author was to calibrate the characteristic of CN-type films and CR-39 solid state nuclear track detectors. Deuteron and nitrogen ions were separated and registered as parabola track on the detectors with the use of Thomson parabola spectrometer. These detectors are shown to be applicable for the measurement of deuteron ions within the energy range from 100 to 500 *keV* as well as nitrogen ion of characteristic energy from 0.2 to 3 *MeV*.

The technique making use of track detectors was further enhanced by coupling them with aluminium foil filters (Skladnik-Sadowska, Baranowski, Milanese, et al.,

2001). The angular distribution and energy spectrum of deuteron ions in a 1.9 *kJ* plasma focus was investigated using ion pinhole camera equipped with aluminium foils of different thickness interposed between ion beam and LR 115. Ion energy range from 80 *keV* to 2 *MeV* was obtained. Average ion flux density of 3.3 x 10^9 ions/cm^2 was determined from the deuteron tracks registered on the LR 115 film and high energy ion beams were found to be well collimated.

Similar technique applied in a larger plasma focus device of 44 *kJ* (Skladnik-Sadowska, Czaus, Malinowski, & Sadowski, 2005) found protons and deuterons with energy ranged from 30 *keV* to 400 *keV*. Local minimum in the ion angular distribution obtained is similar with the previous observation. The authors interpreted this phenomenon due to the lack of deuterons within a tunnel of an ion Larmour diameter. On the other hand, in order to resolve low energy ion beam, they employed an additional acceleration system together with a Thomson parabola spectrometer (Skladnik-Sadowska, Baranowski, & Sadowski, 2001). The accelerating system can further increase the energy of ions up to 20 *keV* without disturb the shape of the energy distribution. This method made possible the registration of low energy ions on the solid state nuclear track detectors, whenever the ions energy is lower than the registration threshold of the detector.

Ion beam emissions in methane plasma was reported (Bhuyan, et al., 2005) on a 1.8 *kJ* plasma focus device. The maximum ion energy for H^+, C^{+4}, and C^{+5} were in the range of 200 - 400 *keV*, 400 - 600 *keV* and 900 - 1100 *keV*, respectively. He correlated the ion beam signal with the emission of soft X-ray pulses. The results supported the idea of ion acceleration mechanism by anomalous resistivity electric field model. The model was also consistent with the results, where the dominant charge states of carbon

ions presented are C^{+4} and C^{+5}. The anisotropy of ion emission was reported later (Bhuyan, Favre, Valderrama, Chuaqui, & Wyndham, 2006). The author explained that the ion emission at five different angular directions to the center axis of anode (0^0, 10^0, 15^0, 20^0 and 90^0) was due to the effect of ion Larmor radius. The maximum ion emission was observed to be confined within a solid angle of 15^0. The results also showed that ion emission strongly dependent on operating pressure with the maximum ion emission when focus formation occurs at peak current.

Much efforts and endevour has been done in the past in order to optimize the neutron production of plasma focus. Nisar et al. (Nisar, Khattak, Murtaza, Zakaullah, & Rashid, 1993) used a special designed cascading plasma focus device in producing sequential burst of neutrons. The neutron output was measured at different distances from the cascading anode. He placed a copper disc target in front of the anode tip to study the neutron yield as a function of target distance from the anode tip. The average neutron yield was found to be independent of target distance beyond 5 *cm* from the anode tip. He observed that the average neutron yield has increased significant when a same target having 2 *mm* hole in the center is used. This result suggested that the neutron production is due to beam target mechanism. He also successfully cascaded the focusing action by reducing the gap between the target and anode tip to ~ 1 – 1.2 *cm*. The voltage signal shows a second weaker focus spike after 1 μs interval from the first focus spike, which is also coincide with the neutron signal.

Anisotropic neutron emission was reported by Castillo (Castillo Mej á, Milanese, Moroso, & Pouzo, 1997). Evidence of high angular anisotropy neutron flux at the axial direction was confirmed by the measurement of ion beams with faraday cup. Ion beam energy spectra of 0.7 – 5 *MeV* was obtained from the analysis of ion tracks. Imaging of

the evolution of plasma dynamics obtained with Cordin model 511 image converter camera (ICC) at 5 *ns* exposure time can explain the possible mechanism for the generation of ion beams with energies up to 5 *MeV*. Plasma jet and ion beams were obtained, which was also observed by Lim (Lim, Ngoi, Yap, Wong, & Saadah, 2009).

Some measurement on temporal and spatial evolution of neutron emission (Yap, 1998), (Yap, et al., 2005) revealed two different kinds of neutron production mechanisms. They investigated the profile of neutron emission under pure deuterium and deuterium-argon admixtures filling. The existence of two phases of neutron emission was observed for the first time in a small energy plasma focus device. In deuterium doped argon discharge, about 65 % of total neutron yield attributed to beam target mechanism whereas in pure deuterium discharge, contribution to total neutron yield by beam target mechanism is less than 35 %. Observation of two or three neutron pulses of about 2 μs apart was also recorded in large focus device of 1 *MJ* stored energy (Szydlowski, et al., 2004).

In 1997, Mohanty (Mohanty, Srivastava, & Rawat, 1997) reported for the first time quantitative measurement of X-ray emission in the presence of external magnetic field and compared with that of no external magnetic field. X-ray energy as well as electron temperature was observed to be lower with the application of external axial magnetic field. Reduction about 40% of X-ray energy was obtained. Electron temperature determined at the presence as well as absence of magnetic field is 1.8 ± 0.3 *keV* and 2.4 ± 0.6 *keV*, respectively. Electron temperature is found to be less deviated from its mean value with the application of external magnetic field, which was inferred by the author due to formation of more stable pinched plasma column. Measurement of the electron temperature of a magnetically compressed plasma also has

been reported in many literature (Mather, 1965), (Jahoda, Little, Quinn, Sawyer, & Stratton, 1960) , (Zakaullah, et al., 2001), (Asif & Ikram, 2004).

Another works (Van Paassen, Vandre, & White, 1970) on X-ray emission in a paraboloidal type plasma focus device investigated that X-ray energy as high as 350 *keV* can be produced. X-ray emission was investigated at two plasma focus devices with different capacitor bank energy, one with 13.6 *kJ* and another is 54 *kJ*. The obtained results suggested high energy X-ray spectra (350 *keV*) are not dependent on capacitor bank energy, filling gas, or anode composition. On the other hand, total intensity of X-rays in the lower energy range (5.46 *keV*) is found to be dependent on capacitor bank energy, anode material and geometry.

Application of the plasma focus as a hard X-ray source for ultrafast imaging (Raspa, et al., 2004) and flash radiography (Raspa, Moreno, Sigaut, & Clausse, 2008) has been investigated recently. X-ray energy in the range of 40 - 150 *keV* was obtained with maximum intensity around 60 -80 *keV*. X-ray emission was observed to be enhanced with small doping of argon to deuterium gas. Radiation output of 50 *ns* resolution allowed good contrast and rapidly rotating object to be recorded, which open the possibility of its application in defect testing of materials.

Despite ion beam, X-rays and neutrons, electron emission was found strongly correlated with the operating pressure (1.5 – 5.5 *mbar*) and the X-ray emission (Patran, et al., 2005). Magnetic electron energy analyzer and Rogowski coil were used as diagnostic tools to monitor the electron beam emission. The electron energy spectra are in good agreement with the measured photon energy of hard X-ray. Most of the measured electron energies lies below 200 *keV* and electron current up to 10 *kA* have

been obtained in this device. Maximum electron emission was obtained at 4 *mbar* with the features of tunable electron beam source as a function of pressure.

Neog (Neog & Mohanty, 2007) also obtained electron beam with characteristic energy in the range of 10 *keV* to more than 200 *keV* in a low energy plasma focus device (2.2 *kJ*). The most probable electron energy distribution is found to be confined within 80 to 110 *keV*. At optimum operating condition, where the maximum compression occurs at the peak of discharge current, maximum average electron beam current of 13.5 kA was obtained. The author also correlated the electron beam current signal with the corresponding current derivative signal and found that the multi spike in the electron beam signal has a strong correlation with different pinch stage, which is classified here as pre-pinch, at pinch and post-pinch phase. The first spike is thought to be the breakaway electrons from the collapsing current sheath due to positive anode voltage before the maximum compression. The second spike occurs at the time of maximum compression where the FWHM is comparable to pinch lifetime. Hence, the electron beam is believed to be emitted from pinch column. The authors explained that the last spike may be resulted from turbulent plasma after the breakup of plasma column, which is referred as post-pinch phase.

Kelly (Kelly & Márquez, 1996) took into account the elastic and inelastic interaction of the low energy ions with the background gas and found that the density of low energy ion is very high and plays an important role in the neutron production. The results also suggested a beam target mechanism for the neutron production in, which low energy ions in the range of 20 to 60 *keV* play an important role for the total neutron yield. These results were supported by the report of Springham (Springham, Lee, & Rafique, 2000) from the analysis of deuteron energy spectra with an automated track

measurement system. The author concluded that low energy deuterons (predominatly 30 - 60 *keV*) are the major contributors to the neutron production.

Simultaneous measurements of ion beam, electron beam, X-ray were investigated by Zakaullah (Zakaullah, Ahmad, et al., 1998). They used argon as the filling gas and recorded the X-ray pinhole image at different operating pressures. Ion beam, electron beam and X-ray emission were found to be dependent upon operating pressures and argon energy in few tens of *MeV* was obtained. X-ray emission was observed to be delayed at longer time as the operating pressure is increases, which is in contrast to ion beam emission, where larger delay time is observed at lower pressure. X-ray pinhole imaging revealed that wider emitting zone at lower pressure while the pinch filament squeezes with increase in pressure.

The angular distribution of ion emission with the employment of CR-39 nuclear track detectors is carried out and correlates with the neutron and X-ray emission (Zakaullah, Akhtar, et al., 1998). Neutron yield was observed to be the highest (~2 x 10^8) with low fluence anisotropy (~1.5) at pressure 2.5 – 3 *mbar*. Whilst at lower pressure (1 – 2 *mbar*), low neutron yield (~7 x 10^7) with high anisotropy (~3.5) was obtained. The authors believed this may be due to the trapped energetic deuteron within the plasma column to undergo D-D fusion reactions and is also in accordance with the result of high anisotropy (~6) deuteron flux obtained at pressure 2.5 – 3 *mbar*.

In 2002, Heo (Heo & Park, 2002) investigated the characteristic of argon ion beams and correlated with X-ray emission as an alternative route to study the mechanism of charge particle acceleration in a plasma focus. Maximum energy of argon ions over 1 *MeV* and the most probable energy of about 200 *keV* were obtained as

determined from time-of-flight method. Ion beam emission was observed started before the X-ray emission. The result also shown that ion beam energy increases when there is X-ray emission. The author suggested this phenomenon can be explained by the induced electric field model in conjunction with anomalous resistivity and Hall Effect.

Correlation between pinch dynamics, neutron and X-ray emission from PF-1000 facility was reported by Scholz etc (Scholz, et al., 2004) in order to study the possible mechanism of neutron emission. The pinch dynamic was observed by three-frame optical camera with an exposure time of 1 *ns*. Micropinch in the plasma column was observed and neutron emission of 10^{10} -10^{11} neutrons per burst was measured. Two neutron pulses were observed in most of the discharge. The author was able to identify the thermal and non-thermal mechanism of neutron production from the correlation of neutron and X-ray emission.

Other work on the time integrated measurement of angular distributions of fusion products (protons and neutrons) and X-rays emission was performed by Castillo (Castillo, et al., 2007). CR-39 plastic track detector was used as the film for the registration of fusion products and X-rays were detected by means of thermolumuniscent TLD-200 dosimeters. Smaller size tracks attributed to protons were observed on the film compared to neutron. Both fusion products were observed to be confined within angle of $\pm 40^0$ and strongly peaked on the axis. However, the angular measurement of X-rays with energy above 15 *keV* shown two maxima peaked at $\pm 20^0$.

Soft X-rays with total duration up to 300 *ns* were observed to be emitted corresponding to different pinch stages, which was analogous with the electron beam emission (Neog, Mohanty, & Borthakur, 2008). Estimated effective hard X-ray photon

energy (~110 *keV*) was obtained to be consistent with electron beam distribution. Coincidence of ion beam and electron beam signal indicates both phenomena are related to each other and are accelerated by the same local accelerating field. Higher intensity of soft X-rays at subsequent focus action was also observed compared to previous one. The author believed this manner is due to more turbulent formed plasma column corresponding to subsequent focus than the earlier plasma column.

The features of plasma focus device producing energetic ion beams within wide energy range and high flux density are particularly an appealing outstanding research subject. These studies provide extremely important information not only for academic studies but can also serve as foundation for future applications in diversified emerging technological fields either in scientific or industrial sectors. Some potential applications in material science have been explored, such as surface properties modification (Agarwala, Annapoorni, Srivastava, Rawat, & Chauhan, 1997), (Sadiq, Shafiq, Waheed, Ahmad, & Zakaullah, 2006), (Ngoi, et al., 2011), ion implantation (Gribkov, et al., 2003), (Feugeas, Llonch, De Gonzâlez, & Galambos, 1988), (Sánchez & Feugeas, 1997), thin film deposition (Gupta, Srivastava, Balakrishnan, Kodama, & Peterson, 2004), (Rawat, Chew, Lee, White, & Lee, 2003), semiconductor doping (Nayak, Acharya, Mohanty, Borthakur, & Bhuyan, 2001), ion assisted coating (Kelly, Lepone, Márquez, Lamas, & Oviedo, 1996) and synthesis of nano particles (Zhang, Thomas Gan, Lee, Ramanujan, & Rawat, 2006) are reported elsewhere.

In spite of many efforts and works, both theoretical and experimental studies have been investigated since the past and much are devoted to understand the ion production and acceleration mechanism, the physical mechanism involved in their generation are still not clear and remains as an interesting topic of research. In this

regard, it is necessary to further investigate and provide more comprehensive information for the exact correlations of the ion beam emission mechanism with other plasma focus phenomena. In the previous works, it has been reported that the ion acceleration process may be explained by a hybrid model, which involved two or more ion acceleration mechanism. Consequently, a more comprehensive study has to be carried out to compromise with existing theoretical model in order to explain the ion beam emission.

1.5 Objective/Motivation of the Research Project

The self attraction of the plasma focus device as pulsed ion beam source has been the subject of continuing interest for over five decades. Study of ion beam has been given much attention for its possible correlation with fusion reactions where application of the ion beam has been proposed as the source for neutron production mechanism by beam-target reaction. In addition, to the recent years, research has been expanded to explore its potential application as distinct neutron source or ion beam source as well as in material sciences and various emerging technological fields. This motivated us to extend our study of the 3.3 *kJ* plasma focus to characterize the ion beam emission at its optimum condition.

The main objective of current project is to characterize the plasma focus discharge operated with deuterium gas at a low operating pressure. It has been observed that the ion beam produced at low pressure is much more significant that at normal pressure of several *mbar*. We also aim to improve the current understanding of the mechanism involved in the ion beam emission. It has been reported that a good focusing

action can be obtained when the peak axial current sheath velocities lies within the range of 6-10 *cm/μs* and drive parameter of about 89 *kA/cm* (S. Lee & Serban, 1996).

This has instigated us to employ a matching electrode length and enable the low operating pressure of less than 1 *mbar* where the peak axial current sheath velocity should achieve up to 10 *cm*/μs. The low-pressure regime for enhanced ion beam production will be investigated.

1.6 Dissertation Layout

A brief introduction and history about the gas discharge and plasma focus device is given in chapter 1. In this chapter also, literature reviews on the plasma focus research with special attention paid to the ion beam emission is described. A brief review about the previous works on the pulsed radiation emission from the plasma focus and some proposed ion beam acceleration mechanisms is given as well. The motivation of the research project is explained. In chapter 2, the dynamics of the plasma focus discharge is outlined. A brief description at each phase of plasma focus evolution is discussed.

The experimental setup and diagnostic technique used in this project is presented in chapter 3. Discussion and analysis of the experimental results is presented in chapter 4. This chapter is divided into three main sections. The first part describes the basic electrical measurement from the plasma focus device such as discharge voltage and current signal. Second part discusses in details the ion beam emission from the plasma

focus while third part describes briefly the X-rays emission and some correlation between ion beam and X-rays emission.

Finally, the discussion and conclusion of the experimental results are summarized in chapter 5.

Chapter 2

Plasma Focus Discharge

2.1 Introduction

Advanced in pulsed power has allowed generation of pulsed discharge plasma in an efficient way. Plasma Focus is one of the machines that produce short lived plasma using the principle of pulsed discharge. For instance the current project uses a single capacitor of 30 μF discharged onto the load, which gives total store energy of 3 *kJ*. If the energy is efficiently couple to the plasma, it can produce a pulsed current with peak value of about 180 *kA*. In more extreme case, a several *MJ* system can be made with parallel capacitors of 1332 μF and charged to 40 *kV*, like the PF 1000 in ICDMP in Warsaw. In this way, plasma of temperature up to few *keV* and discharge current in the range of *kA* to *MA* can be achieved.

In all the range of plasma focus discharge, the principle of producing the pinched plasma is similar. The capacitor stored energy is discharged in a short pulse to the electrodes. An insulator between the electrodes limits the path for the voltage breakdown and lead to the formation of a uniform current sheath. The current sheath focus at the end of the electrodes produces very high temperature plasma column through magnetic compression and/or joule heating mechanism. The heating mechanism for magnetic compression is inductive in nature while it is resistive for joule heating.

Generally, plasma can be considered as equivalent electrical components in a discharge circuit, represented by a combination of a time varying resistor and a time varying inductor. An equivalent circuit of the plasma focus discharge is schematically shown in Figure 2.1.

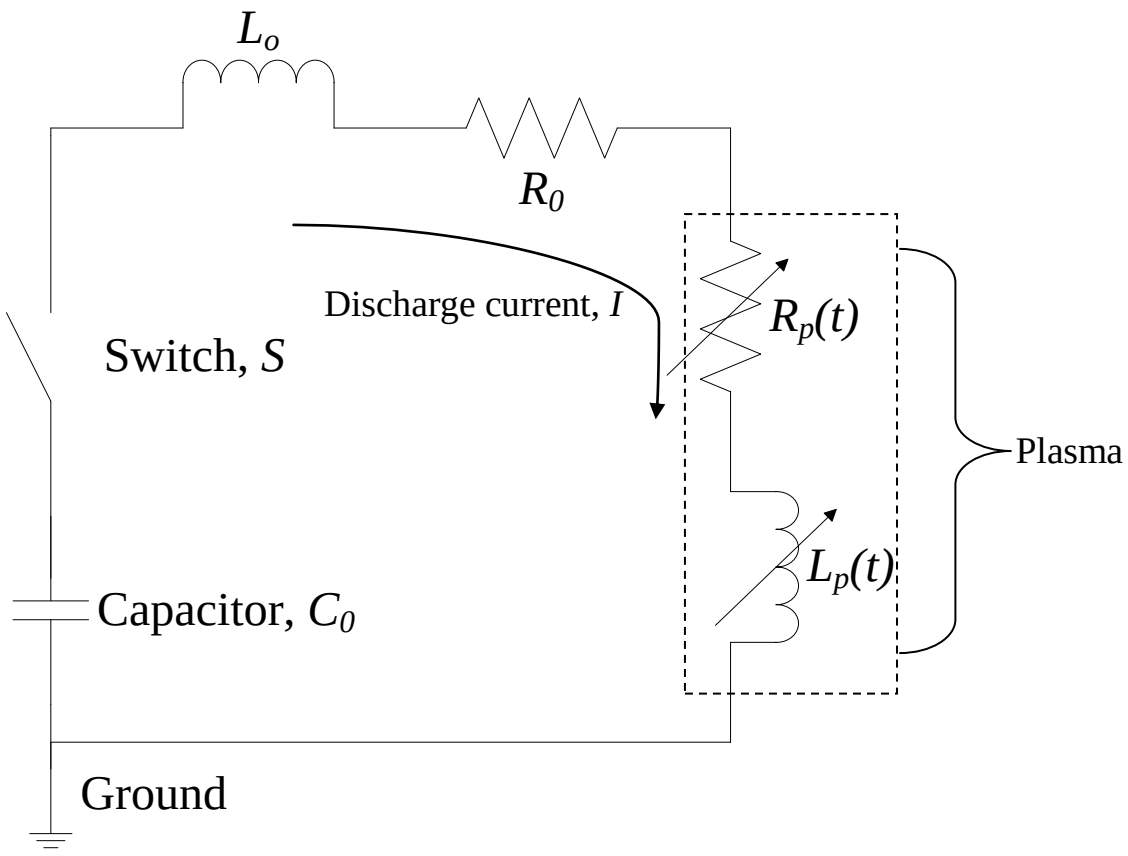

Figure 2.1: Concept of plasma in the equivalent circuit of the plasma focus tube.

In the circuit, symbols C_0, R_0, and L_0 represent the circuit capacitance, resistance and inductance, which depend on the specified setup. $R_p(t)$ and $L_p(t)$ are the plasma resistance and inductance, respectively where their value changes during the discharge. When the capacitor C_0 is charged up to a voltage V_0, upon closing of the switch S the capacitor is then discharged through the circuit where the voltage will be distributed to

all the circuit components including the plasma. By applying Kirchhoff's second law, the circuit equation can be expressed as

$$V_o = \frac{1}{Co}\int_0^t Idt + \frac{d}{dt}[(L_o + L_p)I] + I(R_0 + R_p)$$

The voltage across the plasma, V_p which is marked in the box can be written as

$$V_p = \frac{d}{dt}L_p I + IR_p = V_o - \frac{1}{Co}\int_0^t Idt - \frac{d}{dt}L_o I - IR_0$$

From the equation, it can be seen that the measurement of discharge current I and the voltage across the discharge tube V_p reveals important information of the dynamic and conditions of the plasma. The time varying values of V_p and I can be corresponded to the various phases of the plasma focus discharge.

In plasma focus discharge, the first step is to obtain electrical breakdown in the working gas that forms a uniform current sheath. In correct operating condition, the current sheath successful formed in the breakdown phase will be accelerated by the Lorentz force parallel to the electrode axis. Further from the axial acceleration phase, the current sheath will finally proceed to focusing phase or radial compression phase upon reaching the end of the electrode.

2.2 The Breakdown Phase

The breakdown phase also known as inverse pinch phase is the first important process that occurs in the plasma focus discharge. The breakdown or current filaments may glide vertically across the backwall of the focus tube or along the surface of a cylindrical insulator, placed between the inner and outer electrode. The breakdown initialization may occur in two different modes depend on the presence or absence of the insulator sleeve, as shown in Figure 2.2. In our Mather type plasma focus device, a 26 *mm* long insulator sleeve is used, thus the breakdown is first formed along the surface of the insulator. In this mode of breakdown, a longer breakdown path is introduced by the presence of the insulator sleeve.

Upon formation of the current sheath, it will be lifted off from the insulator surface, as depicted in Figure 2.3. The initial current sheath near the insulator surface is thick and it propels radially outwards in an inverse pinch manner by the $(J \times B)_r$ force until it reaches the outer electrode. When a uniform current sheath in cylindrical shape is formed, this marks the end of the breakdown phase.

The breakdown and formation of current sheath also depends on the operating pressure. The operating pressure regime can be divided, empirically into three regimes (Bruzzone & Vieytes, 1993). At low pressure regime, which is 0.1 *mbar* to 1 *mbar*, a volumetric discharge is formed in between the electrode space. At middle pressure (1 *mbar* to 5 *mbar*), a single and uniform current sheath is formed on the surface of the insulator. At higher pressure (5 *mbar* to 20 *mbar*), multi layers of current sheath with filamentary structure may be formed across the electrodes at the end of the insulator.

A uniform or symmetry current sheath is desired for good performance of plasma focus discharge (Amrollahi, Habibi, & Shahshenas, 2009).

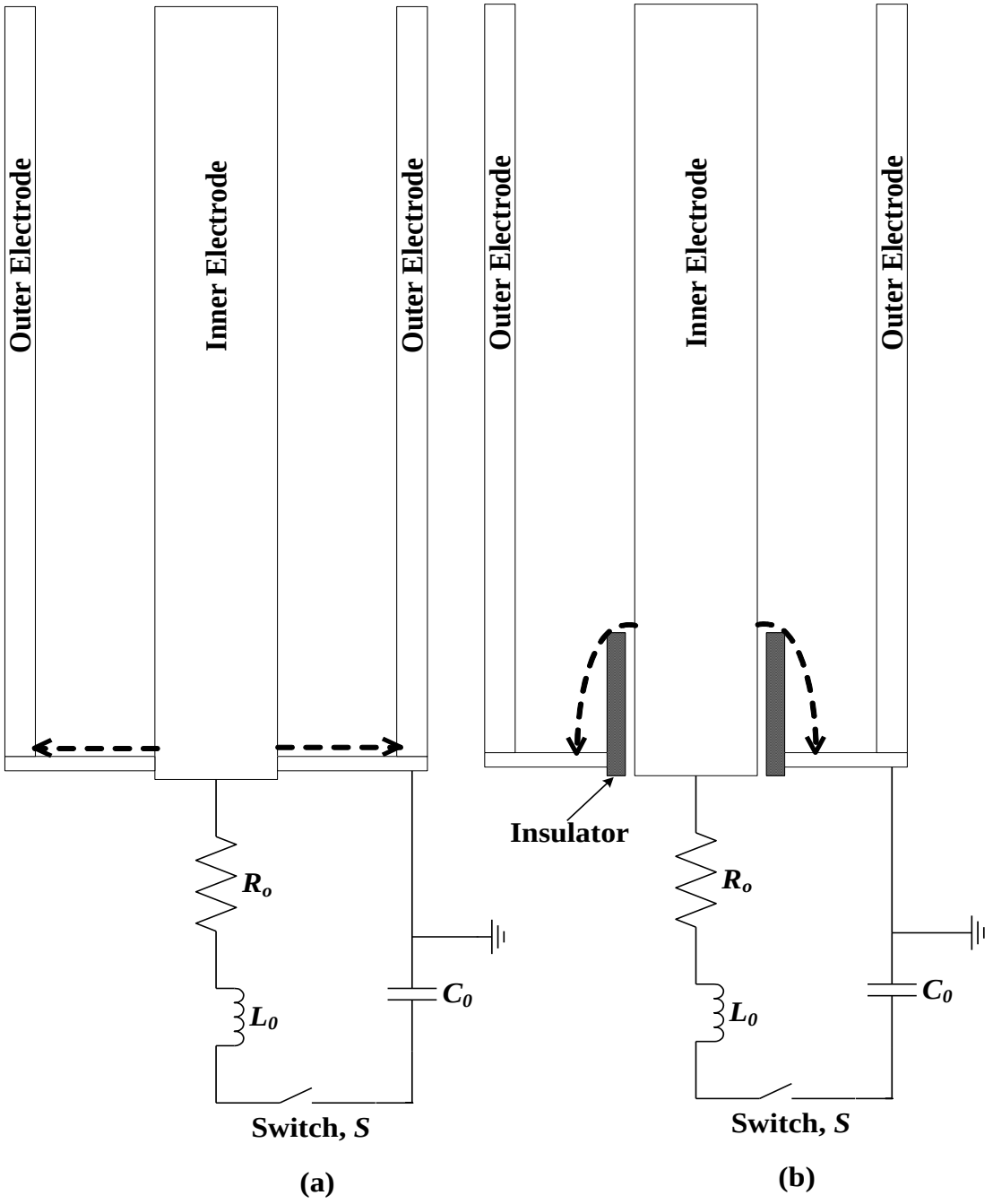

Figure 2.2: a) Mode 1 operation of initial breakdown.
b) Mode 2 operation of initial breakdown.

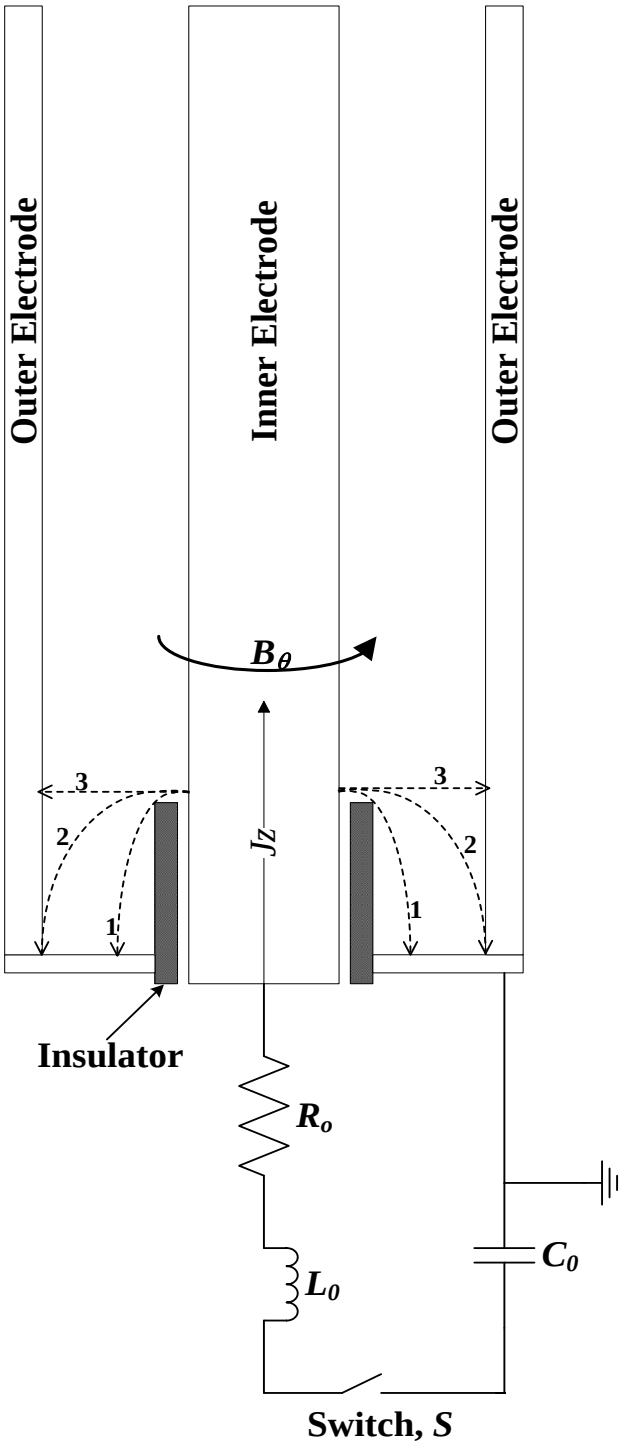

Figure 2.3: Schematic presentation of breakdown phase in plasma focus development.

2.3 The Axial Acceleration Phase

In the second phase, also known as axial rundown or axial acceleration phase, the current sheath starts to propagate along the electrodes with the $(J\ X\ B)_z$ Lorentz force (Figure 2.4).

Along the axial propagation, the current sheath driven by a magnetic piston collects all the gas particles it encounters. This process resembles the snowplow effect in an electromagnetic shock tube. The rundown of the current sheath that is driven by the Lorentz force depends also on the magnetic field, which varies with $1/r^2$. As the results, the current sheath near the surface of the inner electrode is accelerated more. Thus, the current sheath is usually slightly canted in the forward (z) direction at the inner electrode. Practically not all the discharge current will flow through the current sheath. Computation based on experimental results shown that at least 20 % to 30 % of the total discharge currents is left behind and could be treated as leakage current. When the current sheath reaches the end of the anode, the next phase, which is radial compression phase, takes place.

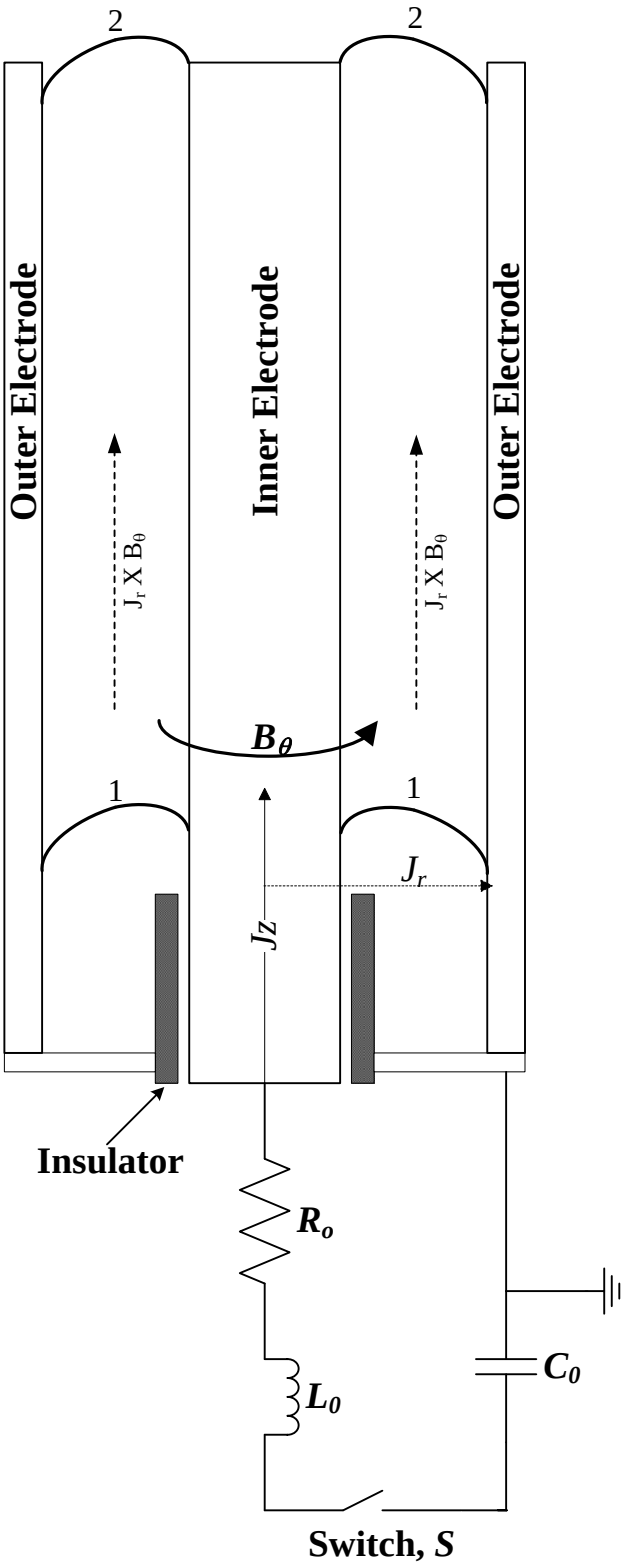

Figure 2.4: Schematic presentation of axial acceleration phase in plasma focus development.

2.4 The Radial Compression Phase

The most important phenomena in focusing discharge are the radial compression phase where the plasma will eventually be compressed into a very high temperature and high density plasma column. As the plasma focuses to form a pinch, the device was named as plasma focus. Generally, at the end of axial phase when the current sheath has been accelerated to the open end of the electrodes, one end of the current sheath that attached to the inner electrode will be driven by the $J_z B_\theta$ force and slide across the face of the inner electrode in the radial inward direction. The other end of the current sheath that attached to the outer electrode will continue its motion in axial direction. This is illustrated in Figure 2.5. In this way, the current sheath that implodes radially inwards will have the shape of fountain-like, hollow cylindrical shape. This electromagnetic compression of plasma is called as "pinch". Following the radial compression phase, multi bursts of pulsed plasma radiation are produced.

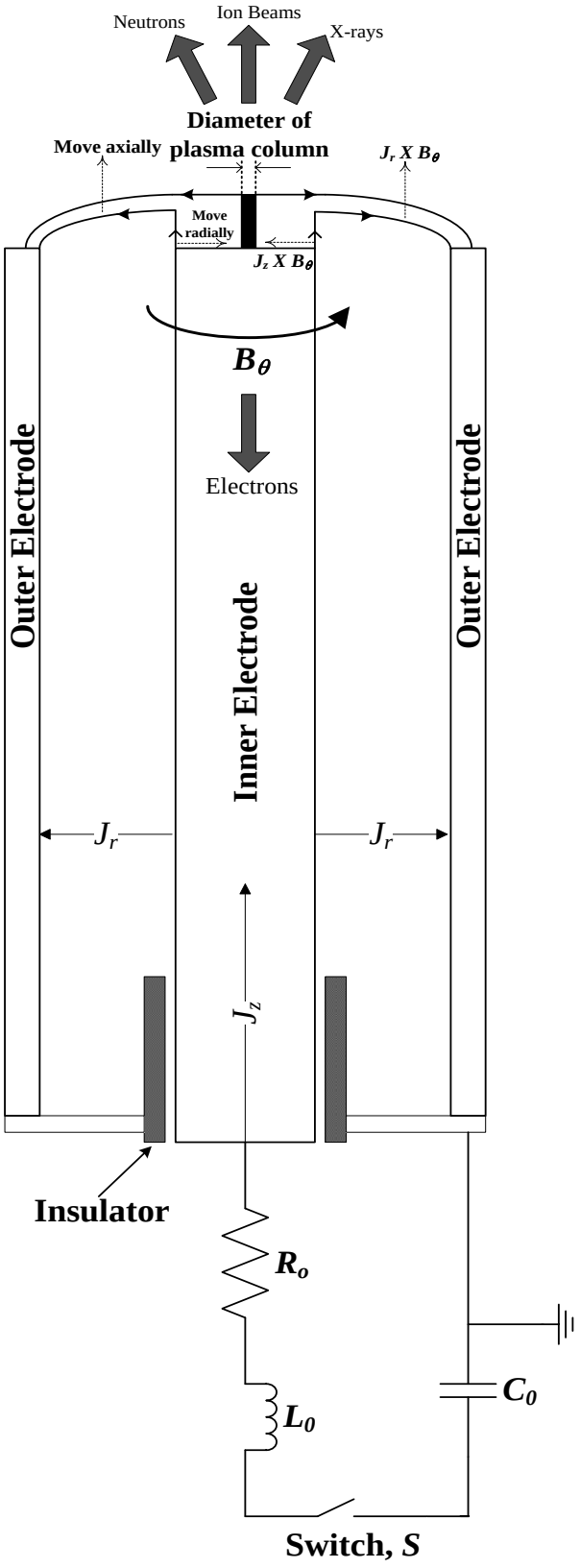

Figure 2.5: Radial compression phase during plasma focus development.

The dynamics of the radial compression phase is rather complicated, it can be sub-divided, empirically into five sub phases: (i) Compression Phase (ii) Very Dense Phase (iii) Quiescent Phase (iv) Unstable Phase and (v) Decay Phase.

(i) Compression Phase

This is the first stage of the plasma implosion, which begins as the current sheath starts to sweep around the end of the inner electrode radially and axially. At the beginning of this phase, the length of the plasma column is considered zero while its radius is considered same as the anode radius. As it pinches inwards, the length of the plasma column elongates while the radius becomes smaller. In this phase, the plasma is compressed adiabatically thus forming a very high temperature and high density plasma column. The plasma column is elongated with its dimension depending on the electrode geometry, typically of 1-15 *mm* in diameter and 10-70 *mm* in length.

Heating and compression of plasma can be achieved due to the pinch effect. However, this will lead to rapid growth of hydromagnetic instabilities. The Rayleigh – Taylor instabilities usually observed to set in 30 *ns* before the end of this phase (Peacock, Hobby, & Morgan, 1971). However, this type of instabilities are damped out when the radial velocity diminishes (Jeffrey & Taniuti, 1966).

(ii) Very Dense Phase

During the pinching, the leading shock front will be reflected and propagates outward. When this reflected shock meet the radially inward motion of the current sheath, it stops the current sheath and thus plasma column reaches its minimum radius. The plasma column remain in the minimum radius with the highest particle density for a short duration for about 10 *ns* (Decker, et al., 1976). The minimum radius of the

electromagnetically pinched plasma column is gas dependent and is found to achieve at smaller size for heavier gas (S. Lee, 1983).

During this phase, magnetic field diffuses into the plasma column (Decker, Kies, & Pross, 1983) and leads to increasing plasma resistance and inductance (Chen & Lee, 1973). The increase in resistivity might be due to reduction of electron mobility in the plasma column (Decker, et al., 1983). The electron temperature of the plasma also increased (Decker, et al., 1976).The sudden increase of plasma impedance results in the observed sharp rise of voltage and dip in the current signals. Discharge current and voltage signals measured with distinct current dip and voltage spike, respectively are used to mark this characteristic features of focusing discharge.

(iii) Quiescent Phase

In this phase, an energy exchange occurs between ions and electrons owing to the temperature difference among them where electrons were colder than the ions. Due to this collisions process in the plasma column, the dimension of plasma column starts to expand rapidly. Because the total number of ions and electrons remained constant in this phase, the particle density drops as the plasma expands. The phase usually last for about 30 *ns*.

The sudden change of inductance induces a high electric field that will accelerate the ions and electrons. Thus, electrons and ions are emitted in opposite direction. The induced electric fields are to maintain the current flow in the plasma column. Towards the end of this phase, m = 0 instabilities start to grow. The growth of m = 0 instabilities will in turn disrupt the plasma column.

(iv) Unstable phase

This phase marks the onset of instabilities. The m = 0 instabilities enhances the induced electric field and part of the plasma is compressed again, causing it "necked" off locally (Bhuyan, Mohanty, Neog, Bujarbarua, & Rout, 2004). Consequently, ions and electrons are accelerated to higher energy. The duration of this phase lasts for about 20 *ns*. The pinch lifetime (t_{pf}) is defined as the duration of the existence of the plasma from the very dense phase to the unstable phase. The disruption causes the plasma density drops, and the whole plasma column expand and breaks up to form a hot and thin plasma cloud.

(v) Decay Phase

This phase commences when the plasma column has been broken up completely to form a large diameter, hot and thin plasma cloud. Multi-radiations are produced while the plasma is cooling down. This also indicates the end of the radial compression phase. The whole process usually lasts tens of nanoseconds for a small focus (several *kJ*) to a fraction of microsecond for a large focus device (Mega Joule). The correlation between the discharge voltage signal and dynamics for the radial compression phase can be demonstrated as in Figure 2.6.

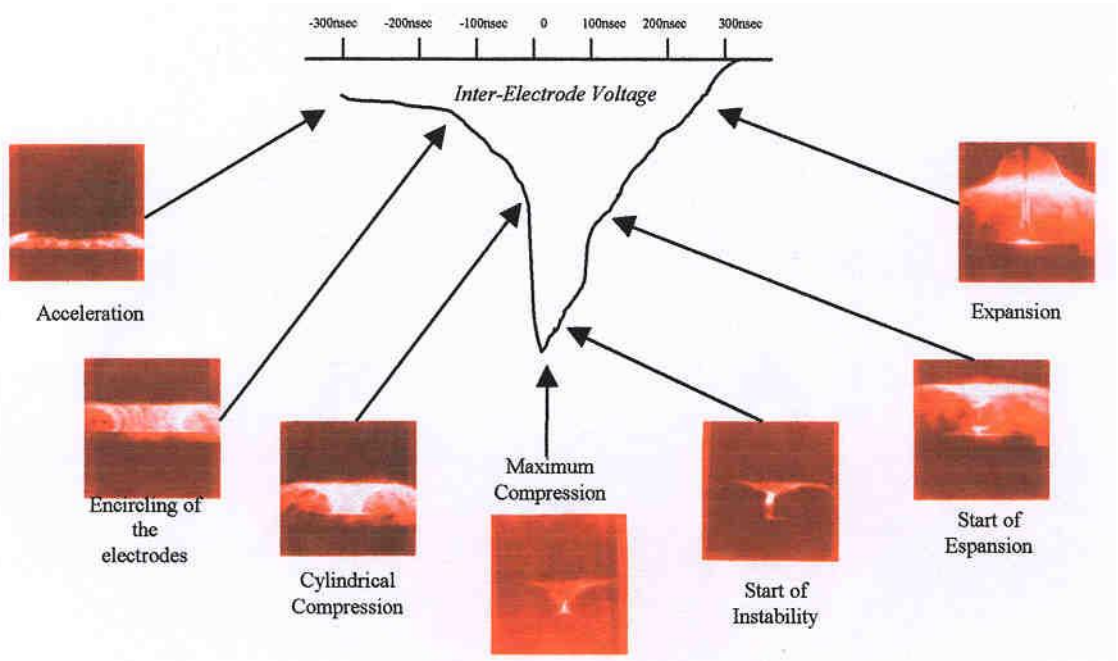

Figure 2.6: Dynamics of plasma focus discharge in radial compression phase.

Chapter 3

Experimental Setup and Diagnostic Techniques

3.1 Introduction

In this project, Mather type plasma focus device filled with deuterium as a gas medium has been used for the entire experiments. The plasma focus device is driven by a low inductance 30 μF Maxwell capacitor, charged to a voltage of 15 *kV*, which gives the maximum energy of 3.3 *kJ*. The capacitor is capable of delivering a peak current up to 180 *kA* at 15 *kV*.

The focus tube consists of a set of coaxial electrodes immersed in a cylindrical chromed mild steel vacuum chamber of diameter 15 *cm* and height of 30 *cm*. The plasma focus chamber is evacuated to a pressure below 10^{-2} *mbar* by means of Edwards high vacuum rotary vane pumps of model E2M5 before filling with fresh deuterium gas. The pressure inside the chamber is monitored by Pirani gauge and Capsule-type dial gauge. Figure 3.1 shows the schematic diagram of the plasma focus device.

a) Side View 1

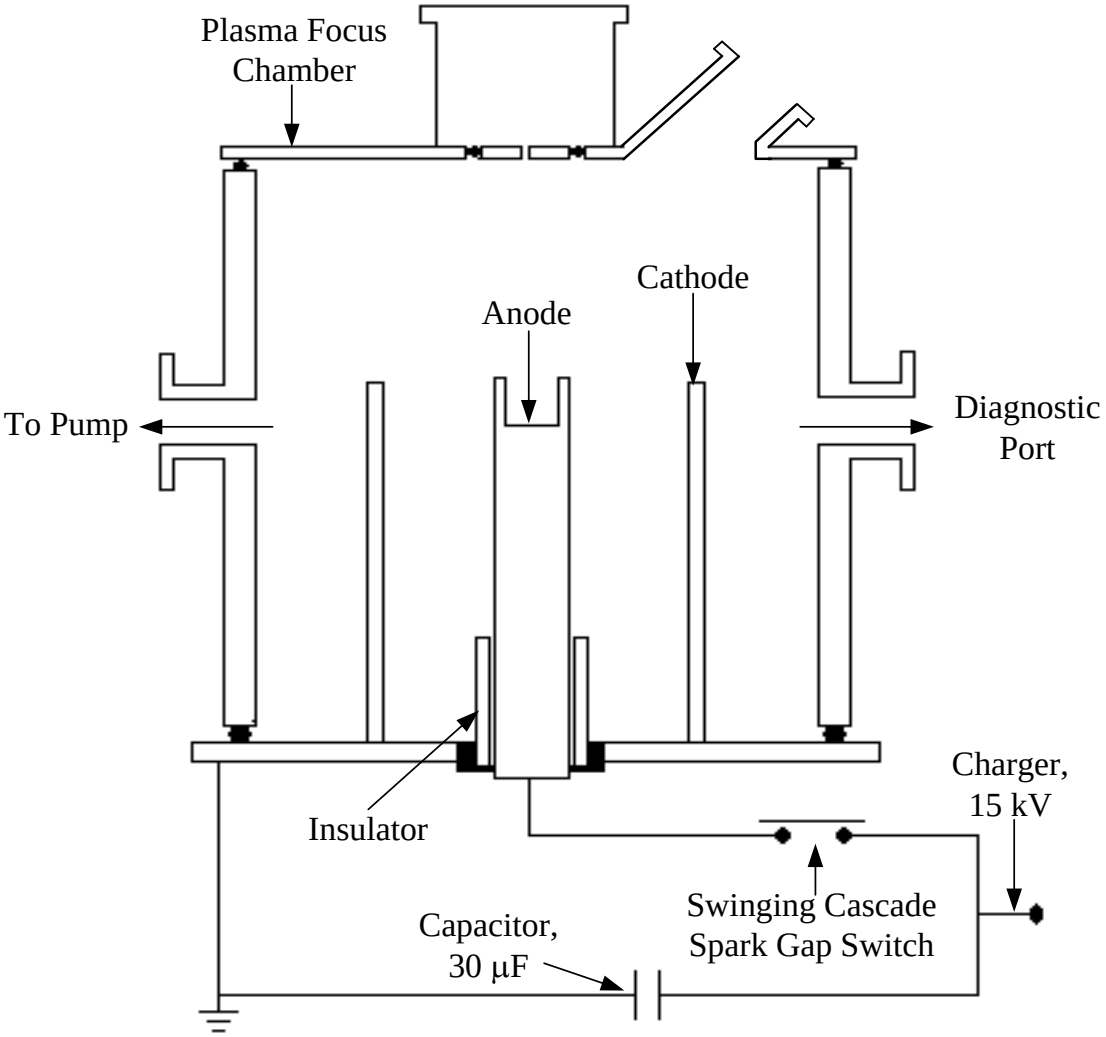
Plasma Focus
Chamber
Cathode
Anode
To Pump
Diagnostic
Port
Charger,
15 kV
Insulator
Swinging Cascade
Spark Gap Switch
Capacitor,
30 μF

b) Side View 2

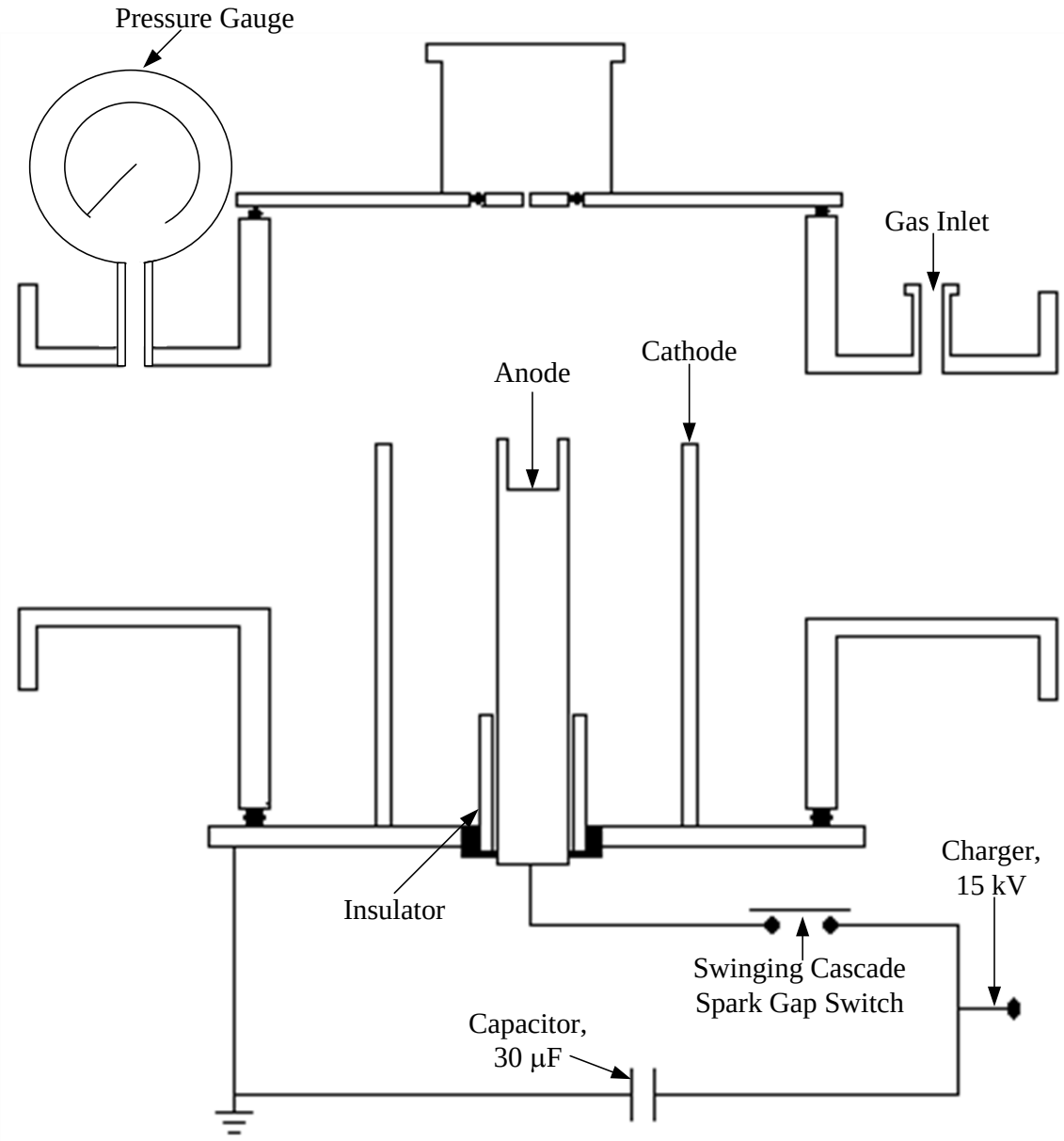
Pressure Gauge
Gas Inlet
Anode
Cathode
Insulator
Charger,
15 kV
Swinging Cascade
Spark Gap Switch
Capacitor,
30 μF

c) Top View

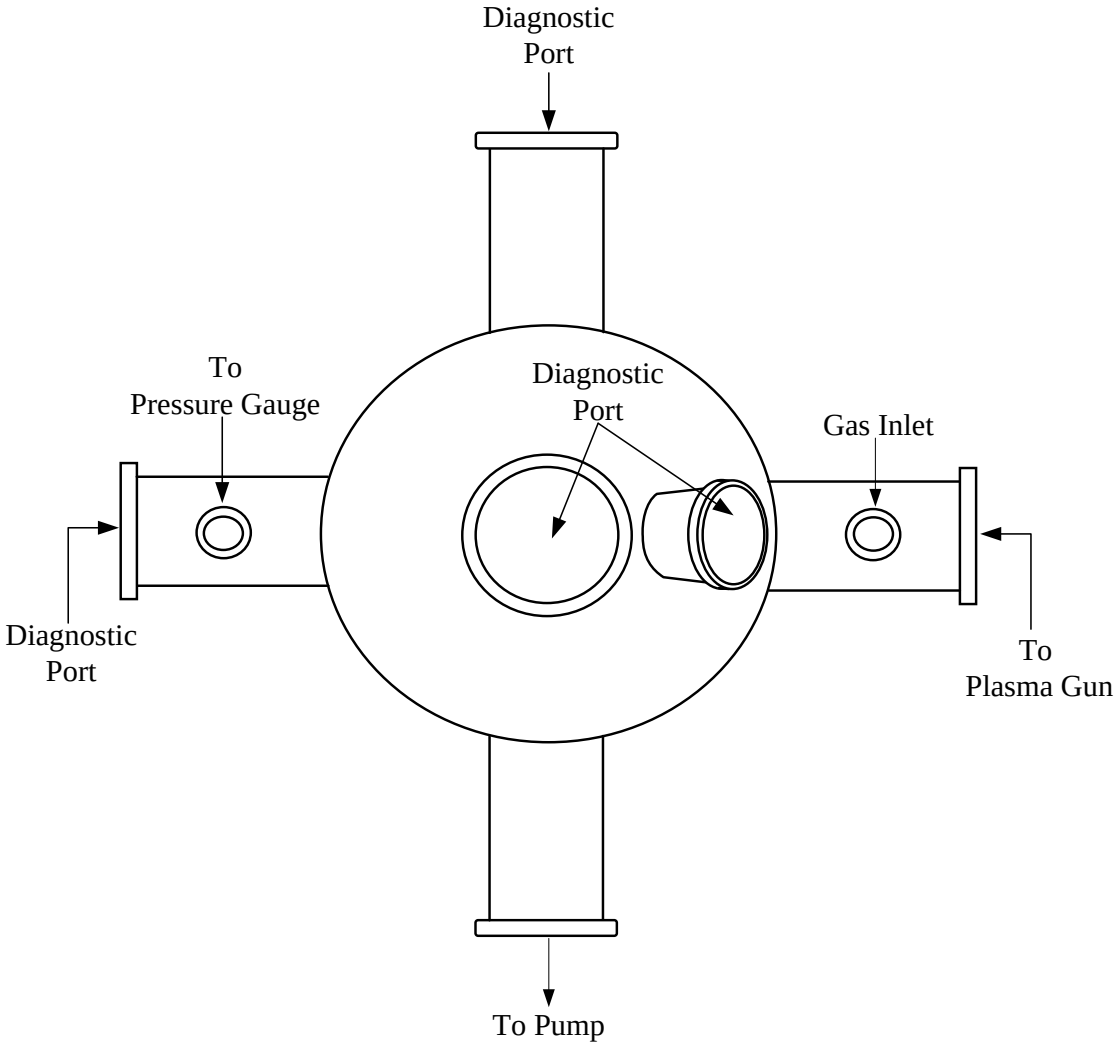

Figure 3.1: Schematic diagram of the Plasma Focus System.

a) Side view 1 b) Side view 2 c) Top view

Other subsystems include the capacitor, high voltage charger, high voltage cable, spark gap switch, triggering electronics, and turbo molecular pump. In the plasma focus tube, the electrode system consist of six outer electrodes (cathode) arranged concentrically around an inner electrode (anode) Figure 3.2.

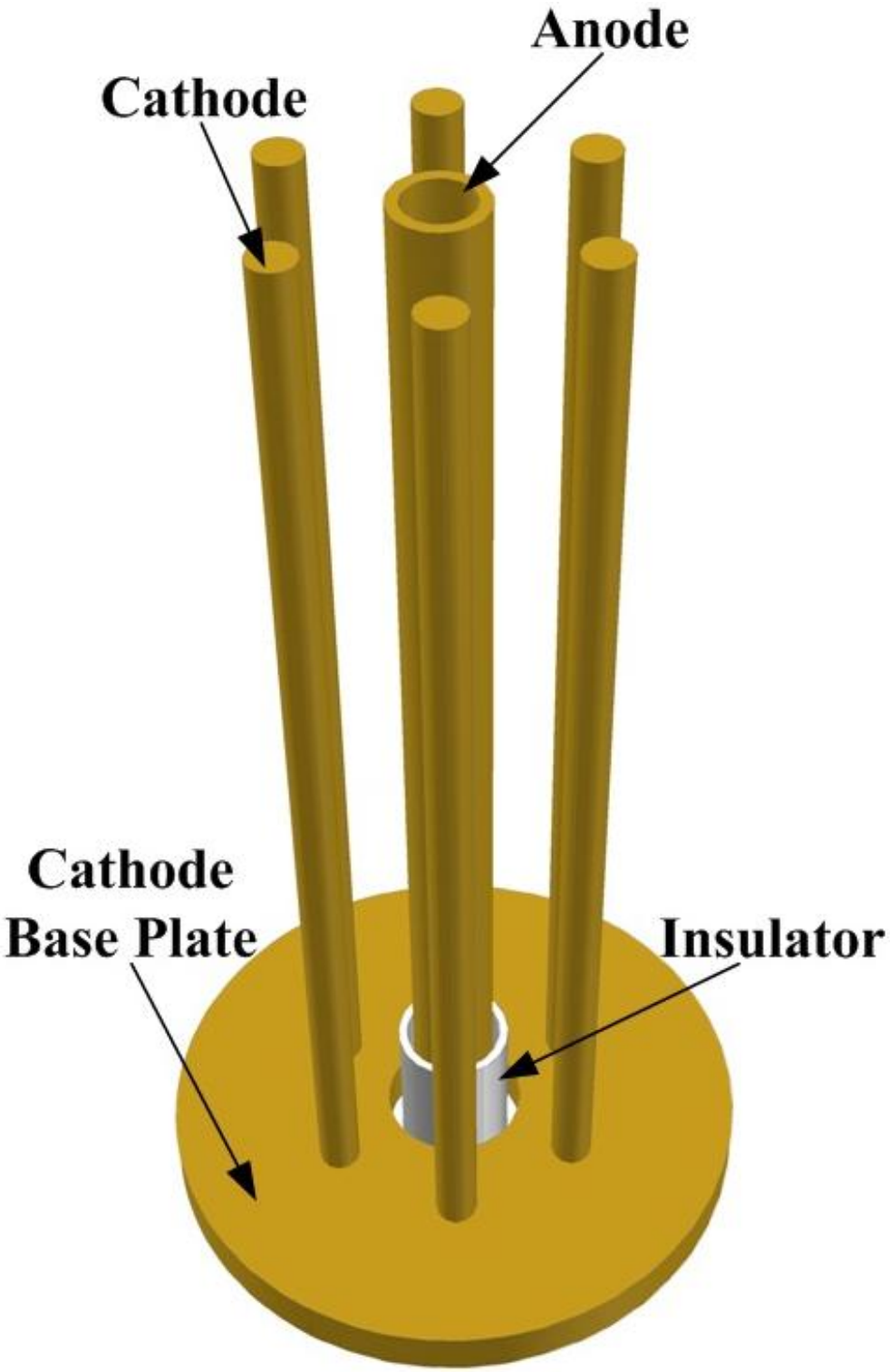

Figure 3.2: The Plasma Focus Tube.

The electrodes are made of copper rods and they are 27 *cm* in length with inner electrode of 19 *mm* in diameter and outer electrode rods of 9.5 *mm* in diameter. The open end of inner electrode is engraved to 4 *cm* deep. The inner electrode is electrically separated from outer electrode behind the back wall with the use of Mylar and Perspex sheets together with a silicon rubber gasket.

The glass insulator is made of cylindrical Pyrex glass of 26 *mm* long and 2 *mm* thickness. The Pyrex glass insulator provides the path for the initial breakdown between the electrodes. At the long electrodes configuration, the system is required to operate at low pressure in order to match the electrical characteristic time and dynamic time. For this purpose, a set of delayed triggered plasma gun is in-cooperated in the system to enhance the breakdown of the current sheath at the surface of backwall insulator.

A block diagram of the plasma focus device including the sub systems is schematically shown in Figure 3.3.

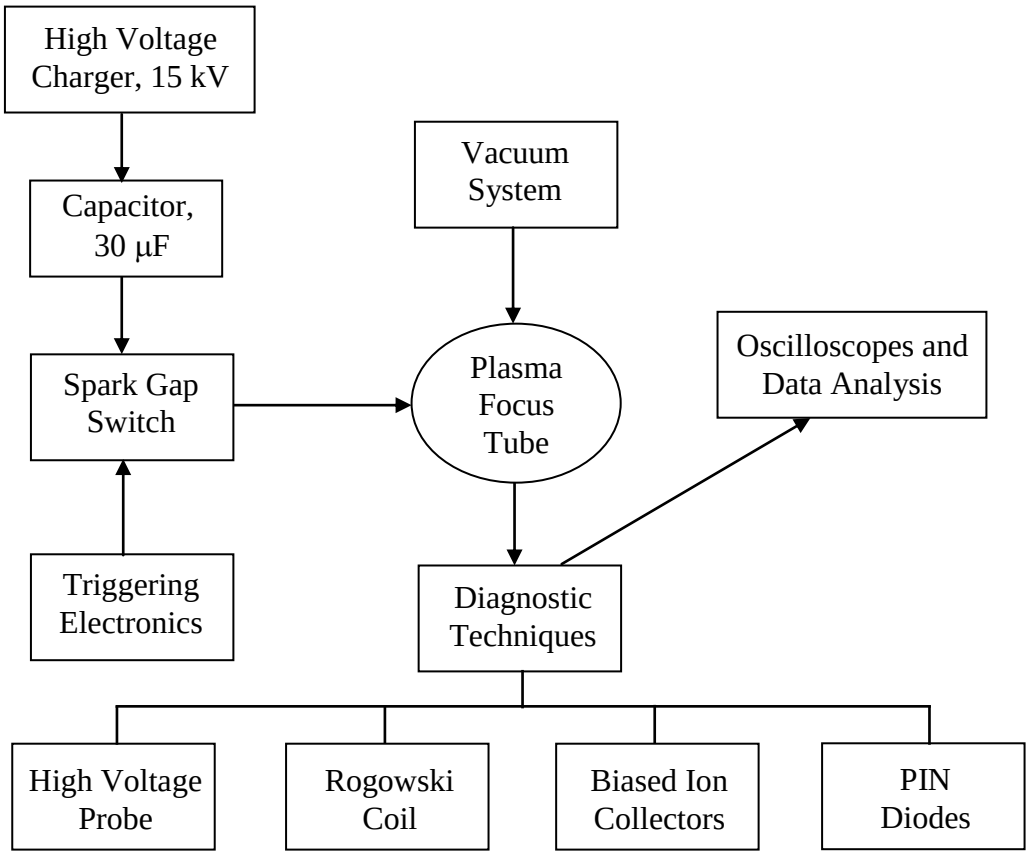

Figure 3.3: Block diagram of the experimental arrangement.

For the data acquisition, the most commonly used plasma diagnostics for the measurement of discharge current and transient voltage across the focus tube is the Rogowski coil and high voltage probe, respectively. Both measurements give the most basic and quick information about the plasma focus discharge. Other diagnostic techniques employed to govern the by-product such as ion beam and X-ray emission of the plasma focus discharge are biased ion collectors and filtered BPX 65 PIN diodes. All the signals are recorded by digital oscilloscope and data analysis is done in a computer.

Due to high electromagnetic noise that is generated by the transient phenomena during the focusing discharge, all the diagnostic tools and measuring instruments are shielded in a screened room. All the electrical signals are transmitted to the screen room via coaxial cables that have been insulated from electromagnetic noise with copper piping.

In addition to ion beam measurement, an additional diagnostic port or so called drift tube is attached to the top plate of the focus tube for the recording of time resolved ion beam signals. All the electrical signals from the high voltage probe, Rogowski coil, ion beam and X-rays are recorded on four channels digitizing oscilloscopes of 1 *GHz* sampling rate with an effective bandwidth of 500 *MHz*.

In order to correlate the electrical signals with ion beam or X-rays signals, the measurement are carried out simultaneously. This is necessary because there is variation of the plasma focus dynamics from shot to shot even though general same features can be observed at the same condition and geometry. All the oscilloscope signals are properly synchronized for time correlation purpose. However, due to limited channels of the digital oscilloscope some of the signals may have to be sacrificed. The details of the subsystem of plasma focus device and diagnostic technique are discussed in the following sections.

3.2 Subsystem of the Plasma Focus Device

A single low inductance Maxwell capacitor is used as the energy storage for the plasma focus device. It is rated at capacitance of 30 μF and breakdown voltage of 15 kV with equivalent series inductance of about 27 nH. In each of the discharge, the capacitor is charged via a high voltage capacitor charger, which gives a maximum energy of 3.3 kJ at 15 kV.

A swinging cascade spark gap switch capable of switching 280 kA with jitter within 50 ns has been used as a switch to transmit high current pulse from the capacitor. The ratio of the gap is set at 3:2 (4.5 mm : 3 mm) which is suitable for the operating voltage (13 - 15 kV) in the plasma focus device.

Another important part of the experimental setup is the triggering system. It is required to generate a pulse with very sharp rise and fall times in order to trigger the spark gap switch for best switching performance. The triggering system mainly comprises of an isolating capacitor, two SCR triggering units and a TV flyback transformer. There are low voltage SCR units, which upon trigger can produce 22.5 V output pulse. This pulse is then transmitted to trigger the high voltage SCR unit. The 800 V negative pulse generated by the high voltage SCR unit is stepped up by a TV transformer up to 17 times. Eventually, the stepped up pulse signal is sent from a 100 pF isolating capacitor to trigger the spark gap switch.

3.3 Plasma Diagnostic Techniques

3.3.1 Measurement of Discharge Current

In plasma focus discharge, pulsed discharge current is measured by Rogowski coil. A Rogowski coil, named after Walter Rogowski, is an electrical device for measuring alternating current (*AC*) or transient current pulses. It is essentially a multi-turn solenoid, which is bent into the shape of a torus. The reason for choosing Rogowski coil for current measurement over other types of current transformer is that it can be made open-ended and flexible.

Moreover, the sensitivity of Rogowski coil is independent of its position as long as it is topologically equivalent to a torus enclosed around a live conductor (Leonard, 1965). The coil is wound over polythene tubing, insulated in a plastic piping hose and placed at the backwall of the plasma focus device surrounding the inner electrode. The design of the Rogowski coil is shown in Figure 3.4.

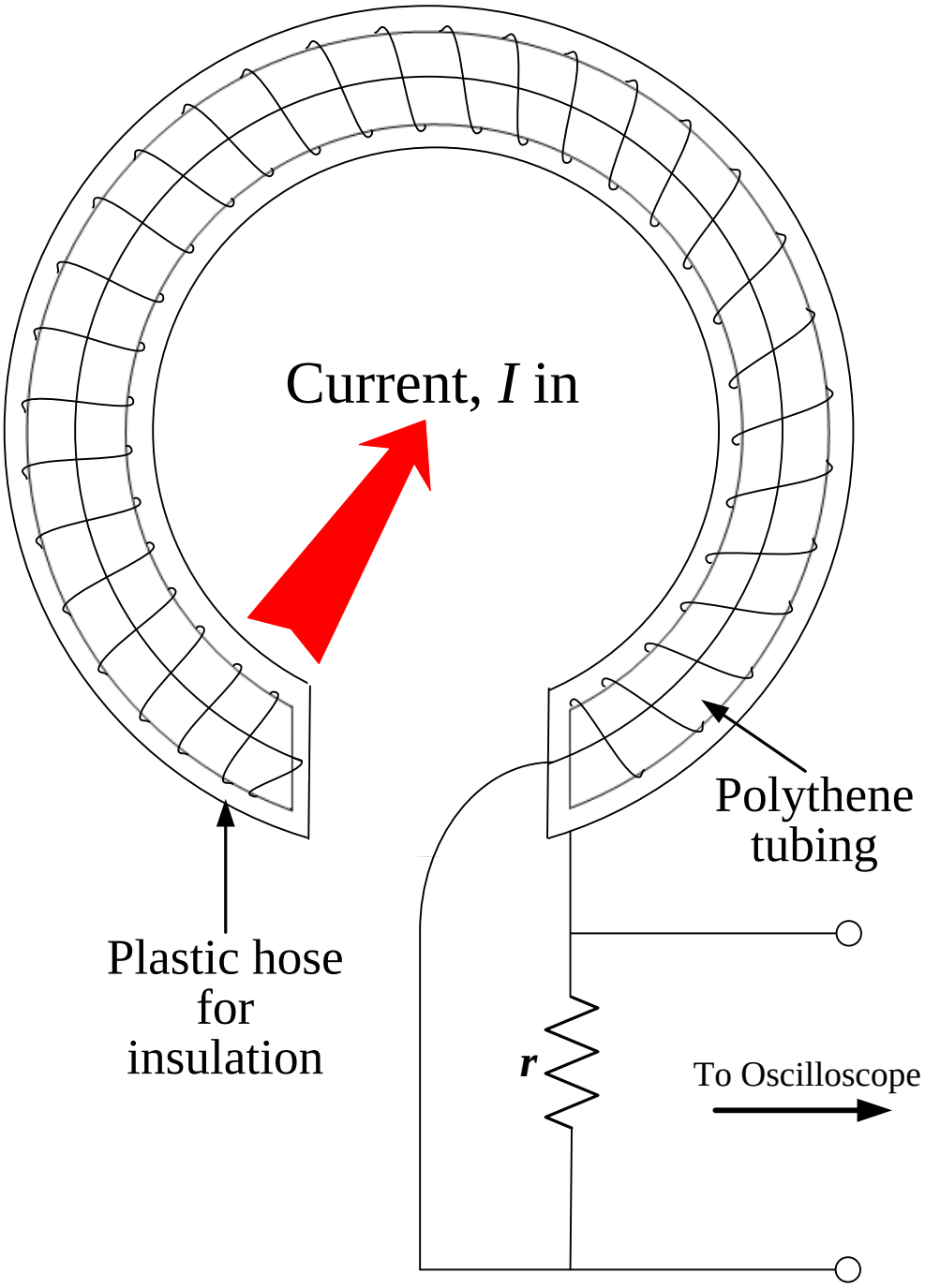

Figure 3.4: Schematic design of Rogowski coil.

3.3.1.1 The Rogowski Coil as a Current Transformer

When the discharge current *I(t)* passes through the centre of the coil as shown in Figure 3.4, magnetic field is induced by the current and the voltage induced across the terminal of the coil is the rate of change of the discharge current *dI/dt*.

However, the coil can be operated as a current transformer by terminating it with a low inductance resistor, with r ~ 0.1 *ohm*. This also allowed it to fulfill the condition of $\omega L_c << r_c$, where ω represent the frequency of the varying discharge current, L_c is the inductance of the coil and r_c is the resistance of the coil. Such criterion is needed to ensure that the diagnostic tool is at sufficient high resolution to measure a rapidly changing current. The equivalent circuit of the Rogowski coil is illustrated in the Figure 3.5.

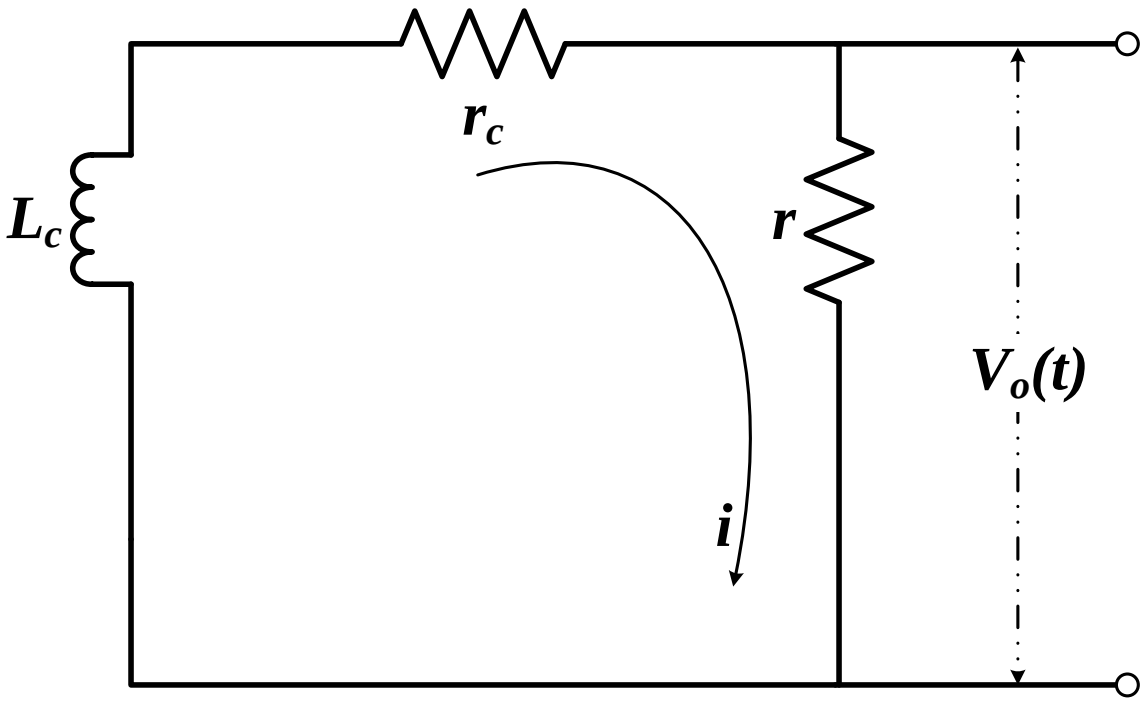

Figure 3.5: Equivalent circuit of Rogowski coil as current transformer.

From the equivalent circuit, the circuit equation can be written as:

$\frac{d\phi}{dt} = L_c \frac{di}{dt} + i(r_c+r) = k\frac{dI}{dt}$, i is the induced current in the coil and I is the discharge current.

When $L_c \frac{di}{dt} >> i(r_c+r)$,

$$L_c \frac{di}{dt} = k\frac{dI}{dt}$$

$$i = k\frac{I}{L_c}$$

Thus, the output voltage across the terminal can be expressed as:

$$Vo(t) = ir = (k\frac{I}{L_c})r$$

$$= \frac{krI}{L_c}$$

$$= KI \propto I(t)$$

It is shown that the potential difference across the small resistor r is proportional to discharge current going through the coil. The factor K will be determined by calibrating the Rogowski coil.

3.3.1.2 Calibration of the Rogowski Coil

The Rogowski coil has been calibrated by using an in-situ method. For the calibration purpose, plasma focus was operated at high pressure at about 10 *mbar* of deuterium. The measured current waveform produced resembled the under damped *LCR* discharge waveform.

The peak current I_0 of an *LCR* discharge, by considering conservation of charges flowing in and out from capacitor can be calculated from the expression below (S. Lee, 1969):

$$I_0 = \frac{\pi C_0 V_o (1+f)}{T},$$

where C_0 = capacitance of capacitor

V_0 = charging voltage

f = reversal ratio of the current trace

T = Time of one cycle current discharge

The value of f and T can be obtained from short circuit signal of the current waveform. Practically, it is advised to take the average of several consecutive peak values to get a more appropriate value of f. For example,

$$f = \frac{1}{4}\left(\frac{V_5}{V_4} + \frac{V_4}{V_3} + \frac{V_3}{V_2} + \frac{V_2}{V_1}\right)$$

Similarly, period time T also determined by averaging over several cycles. Once the peak coil voltage, V_1 obtained from the current oscillogram and peak discharge current, I_0 of capacitor is obtained, the calibration factor can be determined and express as:

$$K = \frac{I_0}{V_1} A/\text{volts}$$

A typical short circuit signal of deuterium discharge at 10 *mbar* is given in Figure 3.6.

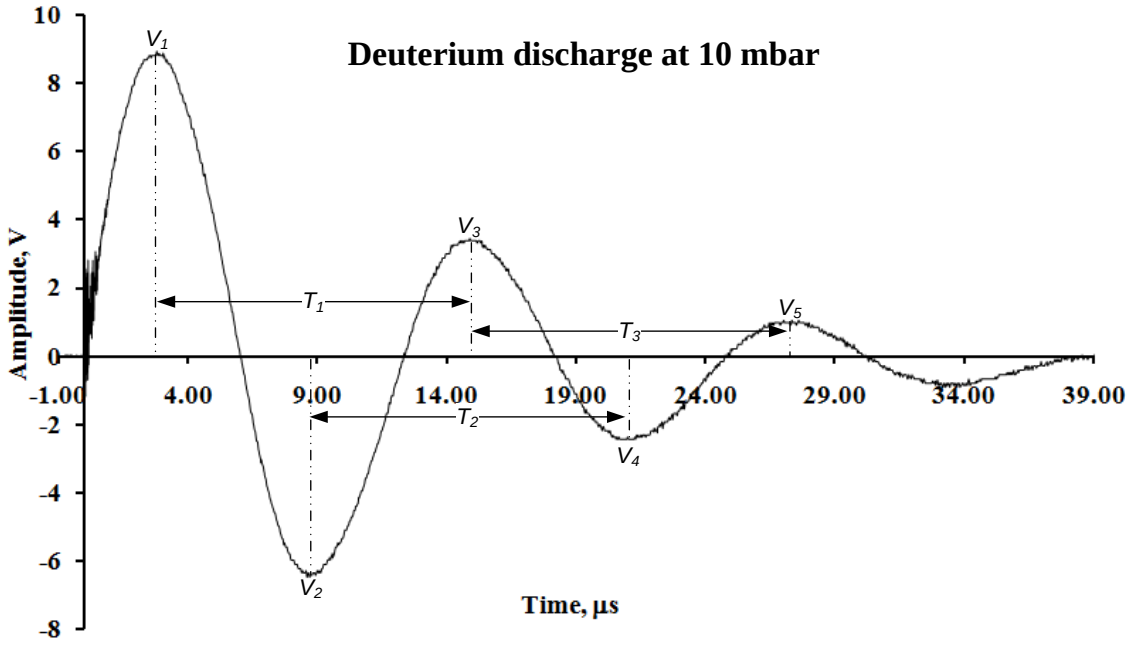

Figure 3.6: Typical short circuit signal (10 *mbar* deuterium discharge).

The calibration constant for the Rogowski coil used in current experiment has been determined to be about K = 20.7 *kA/V*. The value has been calculated by averaging over 5 shots of short circuit signals.

3.3.2 Measurement of Discharge Voltage

The transient voltage across the focus tube and plasma during the whole discharge process is measured with a high voltage probe. It is practically a resistive high voltage probe working on the principle of voltage divider. It consists of a series of ten 510 Ω*/1W* resistors shunted by a 51 Ω resistor at one end of the chain. The chain of resistors is shielded by PVC pipe and enclosed in a copper tube of 20 *mm* diameter. Upon registration of high voltage pulse across the high voltage probe, the voltage signal is measured across the 51 Ω shunting resistor with the amplitude being attenuated. The attenuation factor for the voltage signal is further increased by using a 5 times attenuator with the characteristic impedance of 50 Ω before transmit the signal from coaxial cable to the oscilloscope.

This high voltage probe was calibrated with the Tektronix High Voltage Probe, model P6015A of 1000 times attenuation and capable of registering up to 40 *kV* peak voltage of pulse signal. The use of the Tektronix high voltage probe here is for the calibration purpose. It has rise time of less than 4.67 *ns* and frequency response of 14.7 *ns*. The discharge voltage is measured directly from the Tektronix probe without connecting it to any attenuator. Both of the probes are connected beneath the backwall of the focus tube across the high voltage plate and ground plate. The output signal from the homemade high voltage probe was calibrated against the Tektronix high voltage probe and the total attenuation of the probe was determined to be 1650 times. The rise time of the homemade high voltage probe is approximately 2 *ns* and the frequency response of better than 15 *ns* has been achieved.

A design of the resistive high voltage probe and Tektronix probe is shown in Figure 3.7 below.

(a)

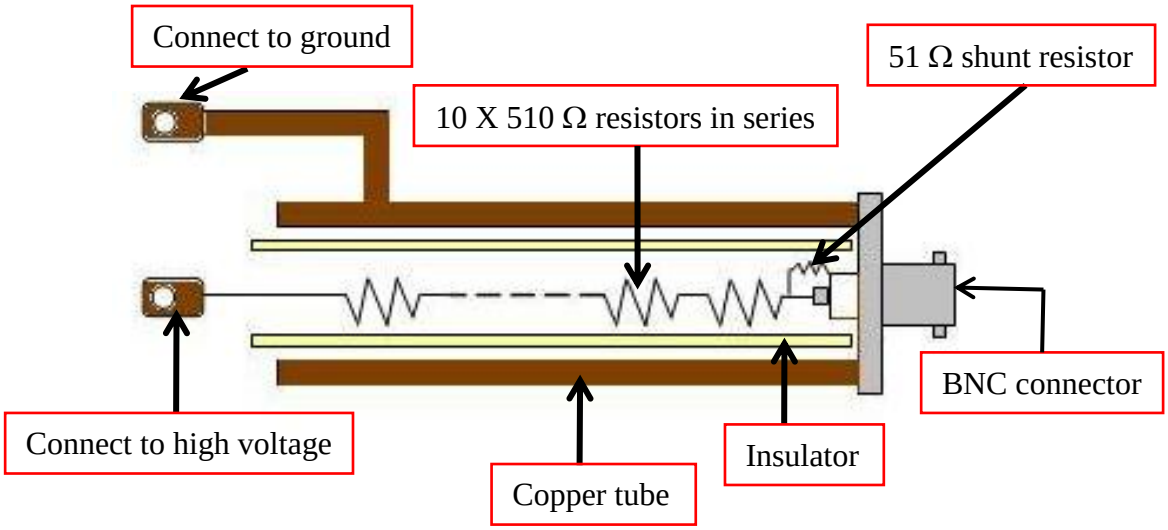

b)

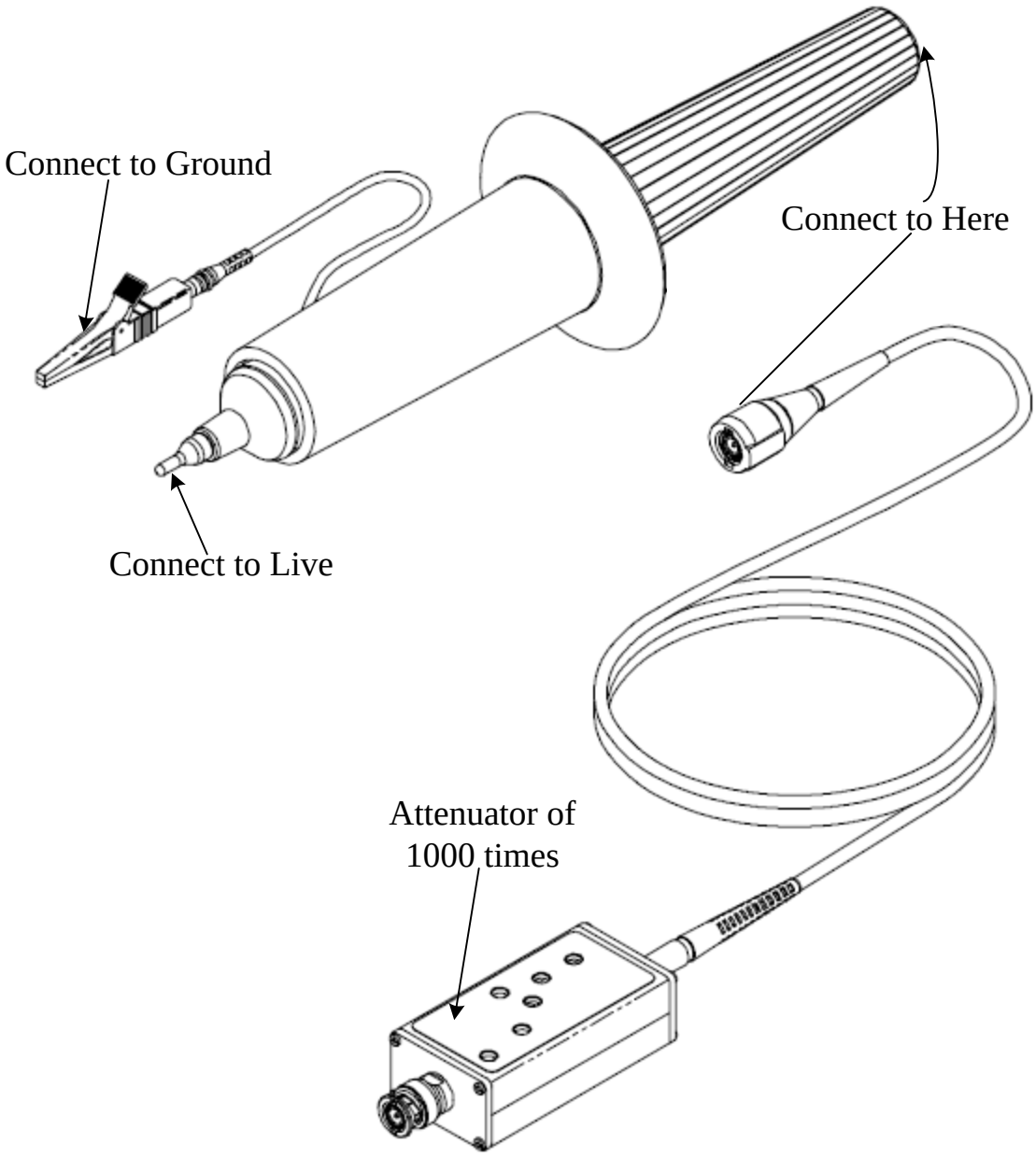

Figure 3.7: a) Schematic diagram of high voltage probe.

b) Design of Tektronix high voltage probe.

3.3.3 Ion Beam Measurement by using the Biased Ion Collector

There are several diagnostic techniques that can be used for the measurement of the characteristic of ion beam emission. In this work, biased ion collectors were used for the determination of ion beam profile. Such detector is employed for its simplicity in construction and provides sufficient time resolution for ion beam measurement.

The ion collector is essentially made from a piece of copper collector plate and negatively biased to certain potential, which is then called as biased ion collector. A photo of the biased ion collector used in the experiments is shown in Figure 3.8.

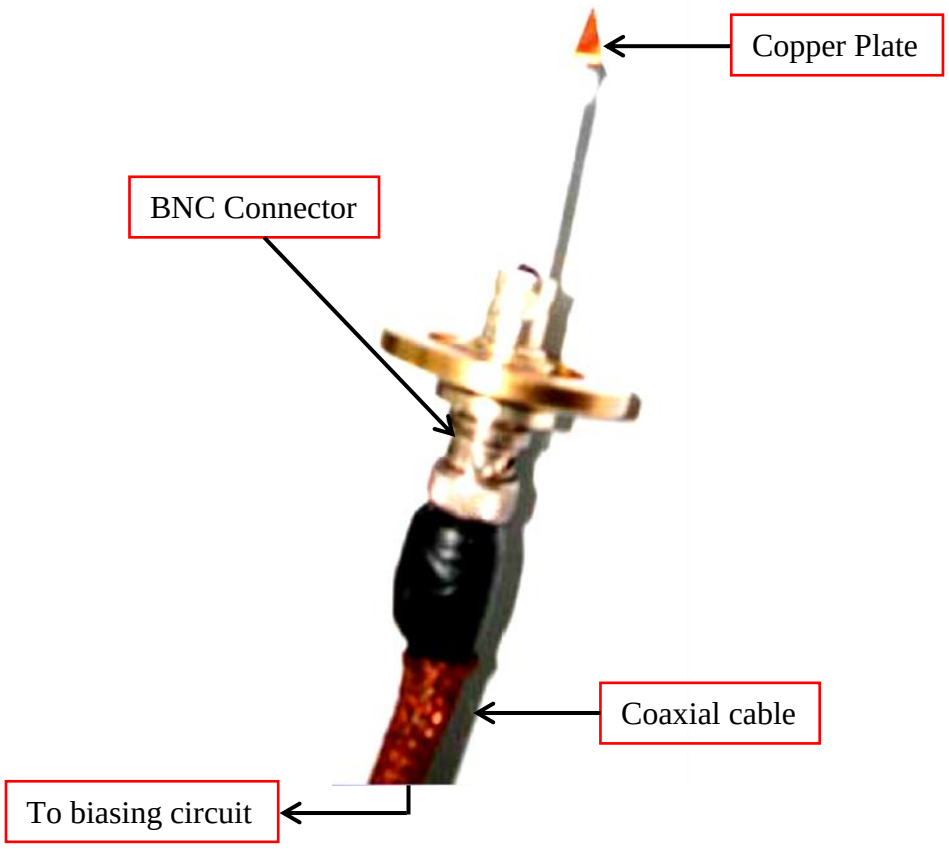

Figure 3.8: Biased ion collector.

The biased ion collector is connected to BNC connector and a biasing circuit via coaxial cable, which provides the biasing voltage to the ion collector. The negative potential applied to ion collector is to screen out the incoming electrons and secondary electron from photoelectric effects. A schematic diagram of the biased ion collector and biasing circuit is given in Figure 3.9.

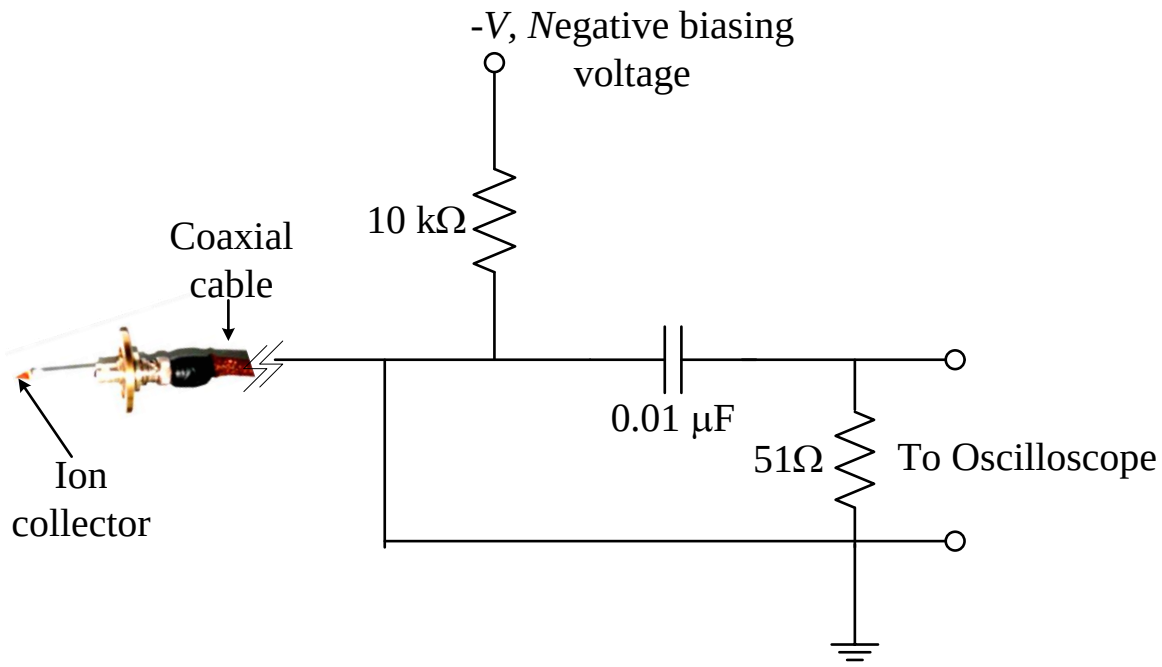

Figure 3.9: Biasing circuit.

The detector works in a simple way. Upon pickup of ion beam, the voltage signal will be registered as a spike or sequence of spikes on the oscilloscope. From the voltage signal, the number of charges being carried in the ion beam is possible to be determined upon careful analysis. An extra care must be taken when determining ion flux as some source of errors may be introduced to the ion beam signal. These are the escaping of secondary electrons due to collision of high energetic ions on surface of ion collector and back scattering of the incident particles, which leaves the detector surface and cause the ion fluxes to be less.

At least two biased ion collectors have to be used to give a time resolved signals for the estimation of the kinetic energy of ion beam. Let the two biased ion collectors arranged in parallel and separated at known distance. If time taken for the ion beam to travel from first ion collector to second collector is known, the kinetic energy of the ion beam can be determined from the information of time and distance. The characteristic of ion beam will be discussed in more detail in chapter 4.

For the time of flight measurement, three biased ion collectors have been employed for the detection of axial ion beam emitted from plasma focus discharge. Arrangement of the biased ion collectors in the differentially pumped drift tube is demonstrated in Figure 3.10.

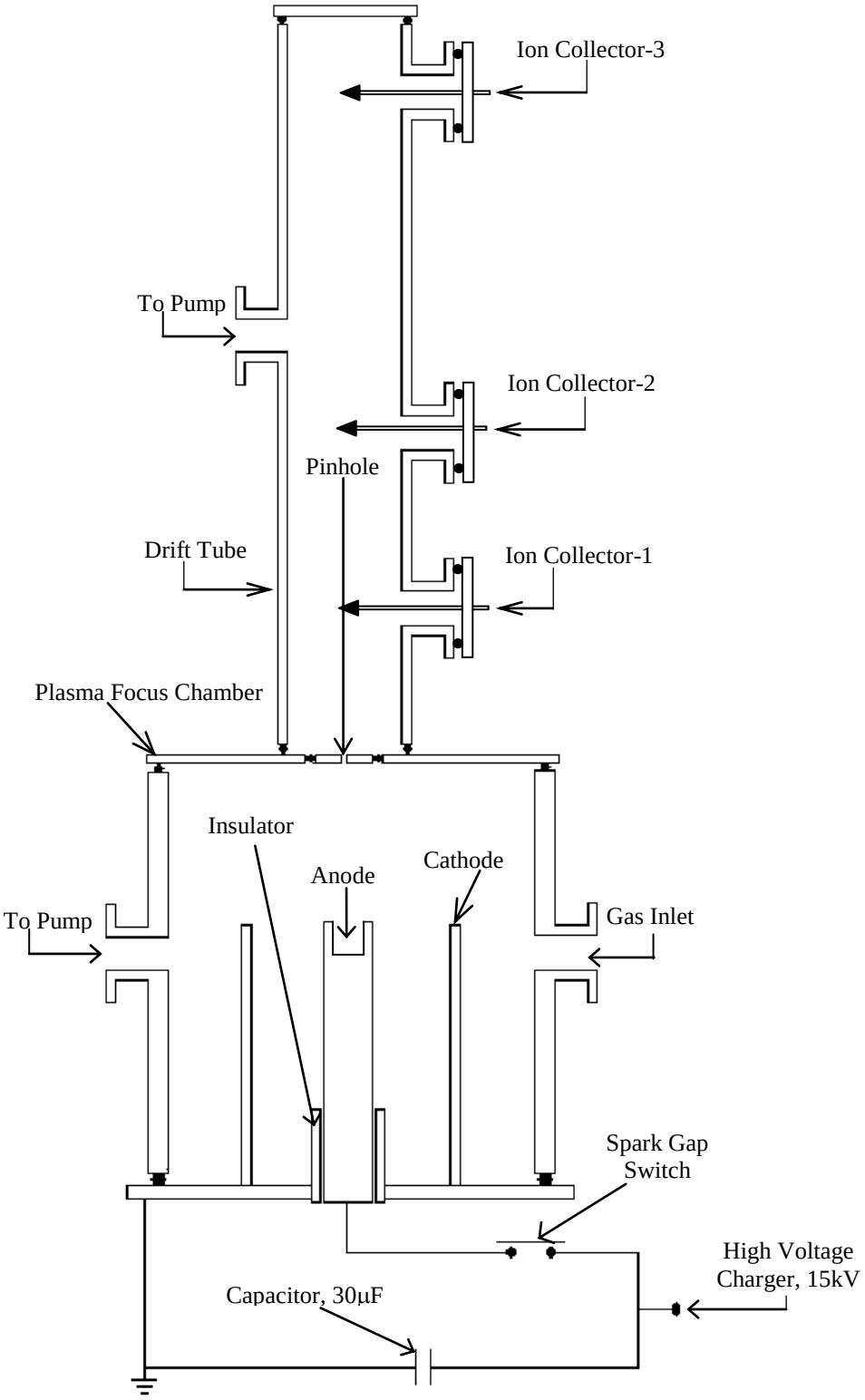

Figure 3.10: Schematic arrangement of the biased ion collectors.

All the biased ion collectors are installed inside a differentially pumped drift tube at the end on direction of the anode. The pressure inside the drift tube is kept below 10^{-4} *mbar* with the aid of turbo molecular pump. The drift tube is attached to the top plate of the plasma focus chamber with a 2 *mm* diameter pinhole.

The purpose of pinhole is to protect the biased ion collector from strong shock wave. It also reduces the equalization of pressure upon open up of high vacuum valve due to pressure difference between the discharge chamber and drift tube. The biased ion collectors are arranged in such a way that the subsequent detector does not block the previous detector.

The first, second and third ion collector is located 26 *cm*, 39.5 *cm* and 66.5 *cm* away from the open end of inner electrode. All the biased ion collectors are negatively biased to 15 *V* by DC power supply unit. The first ion collector is made from a piece of copper wire with 0.505 *mm* diameter and 2 *cm* long. The second ion collector is made of an octant of 2 *cm* diameter copper disc while third ion collector is made of quadrant of a 2 *cm* diameter copper disc. The area of ion collectors from nearest to farthest is 1.01 x 10^{-5} m^2, 3.93 x 10^{-5} m^2 and 7.85 x 10^{-5} m^2.

The reason to use third ion collector in time of flight measurement is that it provide additional confirmation for the estimation of the ion beam energy spectrum. If same group of ions are accelerated under same electric field, then the flight time of ions measured should be correlated to each other from either ion collectors.

3.3.4 X-Ray Measurement by using the Pin Diode Detector

In plasma focus discharge, it is crucial to have a special designed experimental technique and instrument for the diagnosis of the radiations emitted naturally from the plasma. The diagnostics would need to have enough resolution to follow the rapid changes of the plasma event.

Commonly, BPX 65 Silicon PIN diodes are used for the detection of X-ray, particularly in the field of plasma diagnostic. It is preferred due to its simple installation, fast response and high sensitivity for the measurement of pulsed radiation between 1 – 30 keV (Van Paassen, 1971). In this project, the X-ray emission is observed by BPX 65 PIN diodes.

The PIN diode is similar to PN junction diode with an extra light doped intrinsic silicon layer between a *p*-type and *n*-type semiconductor region, which are typically heavily doped. The *n*-type region is called as 'dead layer', which is maintained at ground potential and used as the entrance window of the diode. As a photo-detector, each diode is reversed biased where the *p*-type layer is maintained at negative potential with respect to *n*-type layer.

The typical parameters of the BPX 65 PIN used are given below:

- ✓ Effective detection area $1\ mm^2$
- ✓ Intrinsic Si wafer thickness (estimated) $\sim 10\ \mu m$
- ✓ Dead layer thickness (estimated) $\sim 0.5\ \mu m$
- ✓ Rise time (typical) $0.5\ ns$

The diode is contained inside a T0-18 casing protected by a glass window meant for visible light detection. In this work, the glass window is removed from the PIN diode for the purpose of X-ray detection. Each diode is connected to a biasing circuit and negatively biased at 45 *V* by two 22.5 *V* dry cells connected in series. A setup of the PIN diode with biasing circuit is depicted in Figure 3.11.

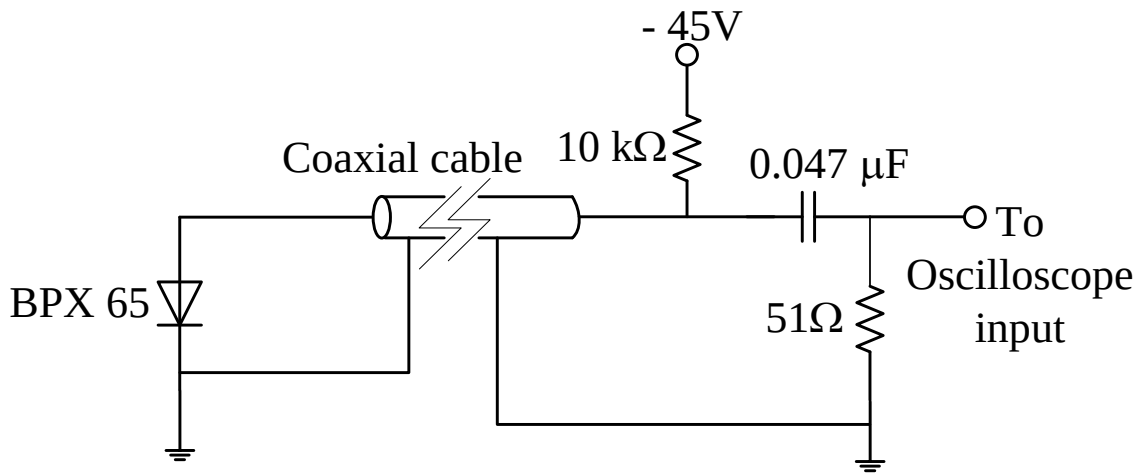

Figure 3.11: PIN diode with biasing circuit operated in time resolved mode.

The working principle of PIN diode is straightforward. Under reversed bias, the diode does not conduct. However, when the diode absorbs an X-ray photon of energy equal or more to form an electron-hole pair in the intrinsic layer, one or more electron-hole pairs will be created resulting in charge flow in the biasing circuit. For the case of silicon at room temperature, average energy needed to form an electron-hole pair is 3.55 *eV* (Siegbahn, 1965). Therefore, for every joule of X-ray energy absorbed in the intrinsic layer will results in charge flow of about 0.282 coulombs of charge.

An array of five windowless BPX 65 PIN diodes is used to monitor the X-rays temporal and spectral profile. The five diodes are glued on five good fit holes on a circular brass flange of diameter 7 *cm* and thickness 5 *mm* with one of the diodes situated at the centre of the flange. The schematic arrangement of the 5-channel PIN diode array is illustrated in Figure 3.12. Each diode is labeled as Ch. 1 through Ch.5 with Ch.1 at the middle.

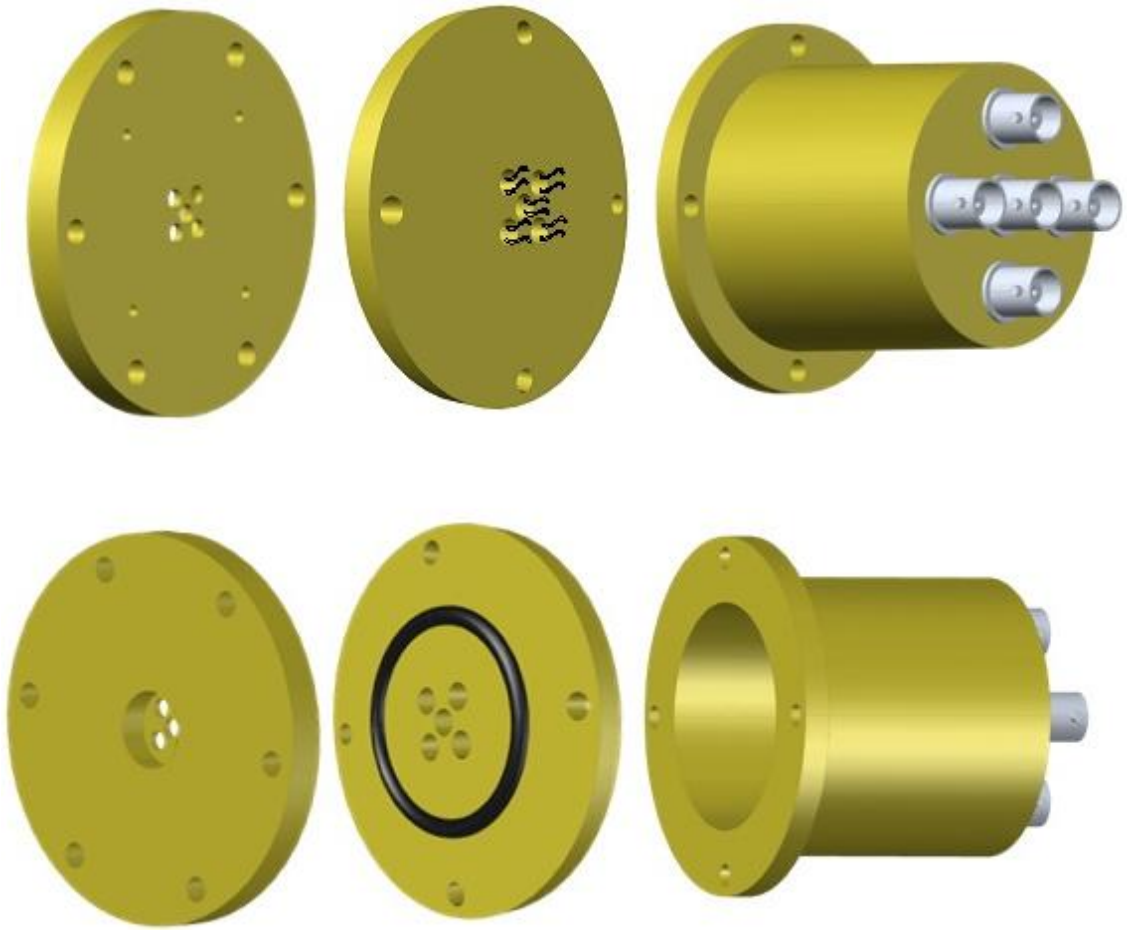

Figure 3.12: Design of five PIN diodes.

Each diode is made vacuum tight by mounting the circular brass plate onto a cylindrical brass casing with an O-ring. This is required to reduce the attenuation of X radiation through the ambient gas from reaching the diode. The casing containing five

BNC free sockets and all the diodes are connected to it via short wires. It is then adapted to the view port of the plasma chamber coupled with an O-ring.

Each of the diode is covered with aluminium filter of different thickness. Electron temperature of the plasma can be determined provided the detectors are calibrated. This is done by exposing all the PIN diodes that are covered with same foil thickness, 23 μm aluminized Mylar simultaneously to X-ray emission. The purpose is to normalize the geometrical differences of the detector due to different position and the sensitivity of each diode with respect to each other.

The diode used is suitable to detect X-ray for the wavelength in the region of 0.3 – 10 $\AA$. The sensitivity of BPX 65 diode for wavelength below 20 $\AA$ is presented in Figure 3.13.

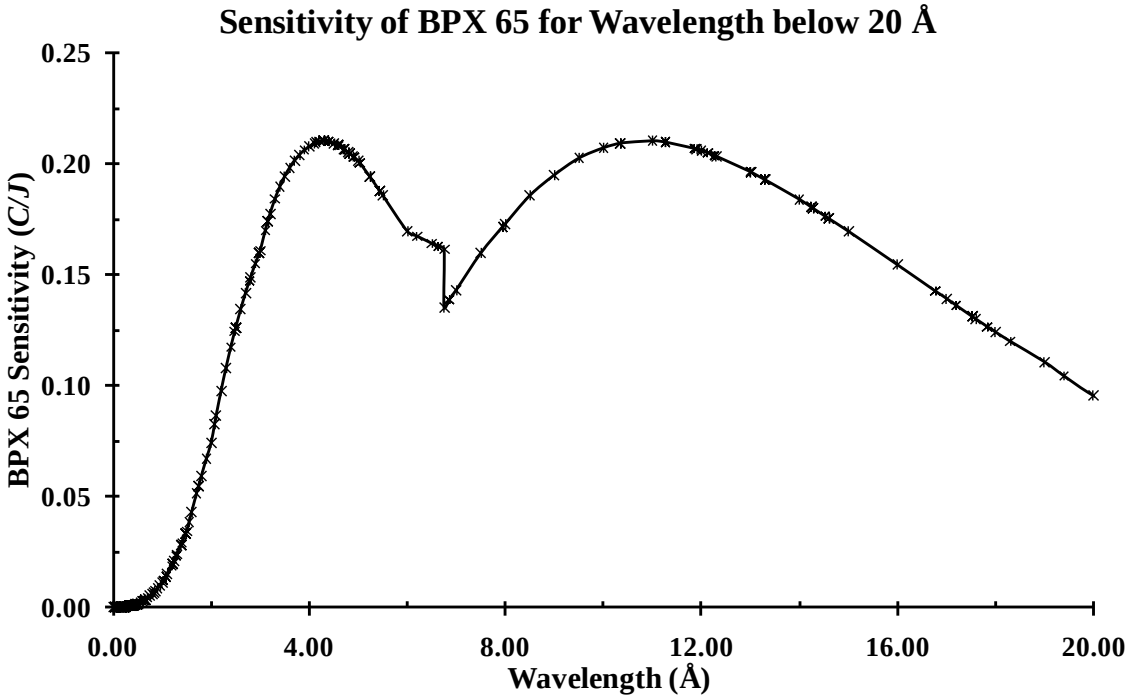

Figure 3.13: Sensitivity of BPX 65 PIN diode in X-ray region below 20 $\AA$.

The experimental arrangement of the multi channel PIN diodes is displayed in Figure 3.14 below for the detection of axial emitted X-rays inclined about 45^0 with respect to the anode axis.

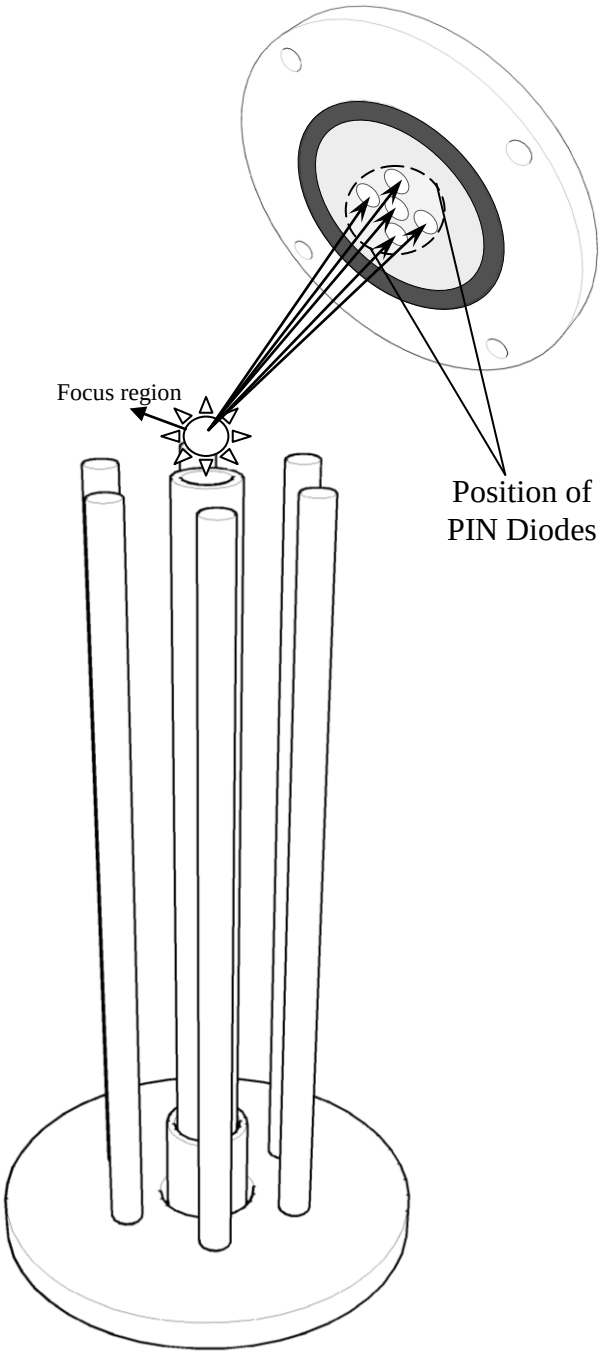

Figure 3.14: Schematic arrangement of the multi channel PIN diodes.

Below is the description for the filter thickness used for the five PIN diodes at different channel.

Channel 1 – 23 μm aluminized mylar

Channel 2 – 23 μm aluminized mylar + 30 μm aluminium foil

Channel 3 - 23 μm aluminized mylar + 60 μm aluminium foil

Channel 4 - 23 μm aluminized mylar +100 μm aluminium foil

Channel 5 - 23 μm aluminized mylar + 120 μm aluminium foil

There are some factors that can affect the detection efficiency of the PIN diode, which is predominantly dependent on the wavelength of the X-rays and thickness of the filter used. The sensitivity of the PIN diode can be expressed by a two thickness model as (Corallo, Creek, & Murray, 1980)

$$S(\lambda) = 0.282 e^{-\mu(\lambda)\cdot x_1}(1 - e^{-\mu(\lambda)\cdot x_2}) \quad A/W,$$

where, $\mu(\lambda)$ = X-ray mass-absorption coefficient of silicon in cm^2/g

x_1 = Mass thickness of the entrance windows in g/cm^2

x_2 = Effective depletion region of the intrinsic layer in g/cm^2

The first exponential term represents the transmission of X-rays through the entrance window (*n*-type layer) of PIN diode and the second term in the bracket represents the absorption coefficient of the intrinsic layer. The overall sensitivities of each PIN diodes coupled to different aluminium foil thickness are depicted in Figure 3.15.

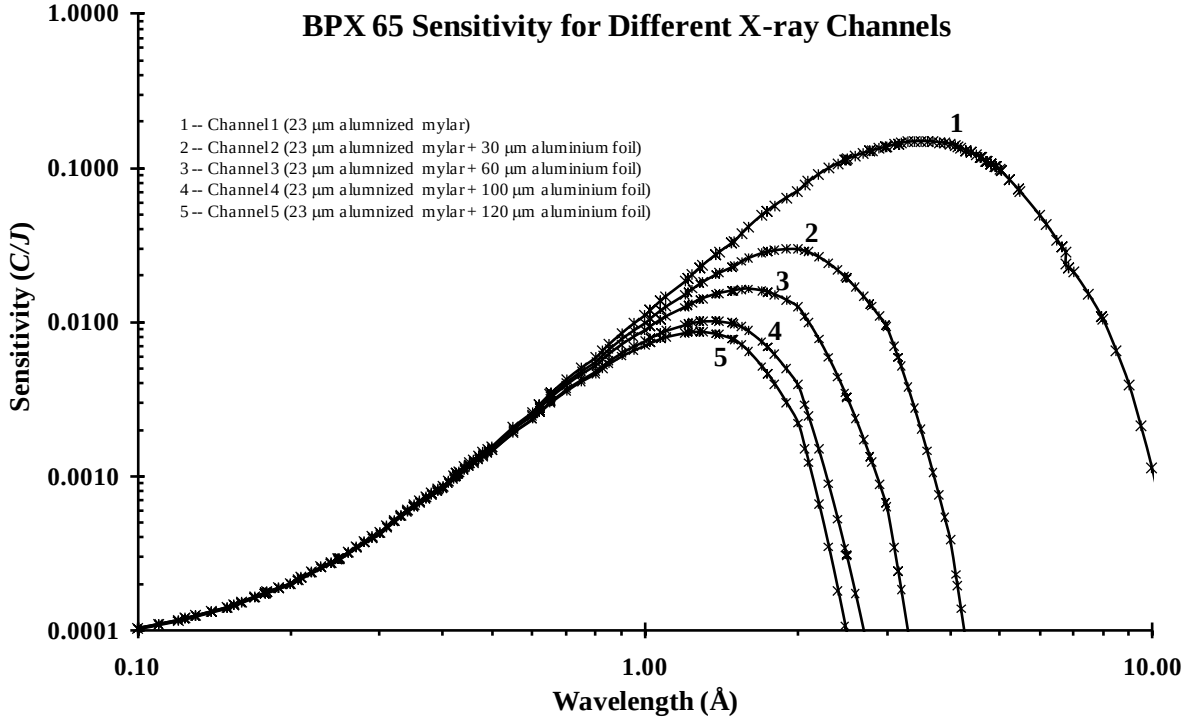

Figure 3.15: Sensitivity of BPX 65 PIN diodes with foil absorption folded in.

In each of the channel, a 23 μm thick aluminized Mylar is used in conjunction with the aluminium foil. It is actually a piece of Mylar sheet coated with aluminium. Aluminium coating is employed for the purpose of filter off the visible light and ultra-violet radiation that are emitted together with X-ray while it attenuates the X-ray as well. This in turns helps to reduce the impurity of signal recorded during the moment of focusing discharge. It is shown in the Fig 3.15, maximum sensitivity for 60 and 120 μm thick aluminium foil is suitable for the detection of X-ray with wavelength around 1.38 $\AA$ and 1.54 $\AA$. This suggests that such foil thickness can be employed for the detection of copper line radiation other than continuum radiation of X-rays photons.

Chapter 4

Experimental Results and Discussions

4.1 Introduction

In this chapter, the experimental results and data analysis on a 3 *kJ* plasma focus device are presented. In this project, deuterium was used as the working gas throughout the experiment. An attempt was carried out to find the optimum condition for ion beam production. The geometrical and electrical parameters are fixed, while the optimization of ion beam production is investigated by varying the operating pressures.

Experimental studies were performed for the operating pressure below 1 *mbar*. Diagnostics technique employed includes Rogowski coil, resistive voltage divider, biased ion collectors and filtered PIN diodes. Simultaneous measurement of these signals were carried out and some correlations have been discussed from these data in order to have a better understanding concerning the production mechanism of ion beam as well as X-rays emission.

4.2 Basic Measurement of Electrical Signals

Transient voltage across the focus tube and the discharge current is measured by resistive voltage divider and Rogowski coil, respectively. Careful analysis has been carried out to gauge from the signals, the performance of the plasma focus, the input power/energy and the average axial velocity of the current sheath. Furthermore, the current and voltage signals were used to correlate to other time resolved signals.

4.2.1 Discharge Current and Voltage Signal

Measurements of the discharge current and discharge voltage across the plasma focus tube have been carried out for all the operating pressure. The spike and dip in the voltage and current signals were used to estimate the performance of the discharge. Good performance of the plasma focus has been observed in the pressure range of 0.05 to 0.5 *mbar*. Typical discharge voltage and current signals at different operating pressure are shown in the Figure 4.1.1 to 4.1.6.

Holding of the high voltage has been observed where the breakdown occurred with a slight delay at pressure of 0.05 to 0.5 *mbar*. Multiple focusing actions have also been observed at these pressure regimes. Multiple compressions of the current sheath could be the result of a poorly formed or diffused current sheath, which is usually dependent on the operating pressure.

The plasma focus occurred at around 3.40 μs at 0.5 *mbar* and 2.37 μs at 0.1 *mbar*. The plasma focus occurred earlier with decreasing pressure. Noted that,

focusing discharge at 0.1 *mbar* occurs at time between 2.37 μs - 2.43 μs which is near or at the moment of maximum discharge current.

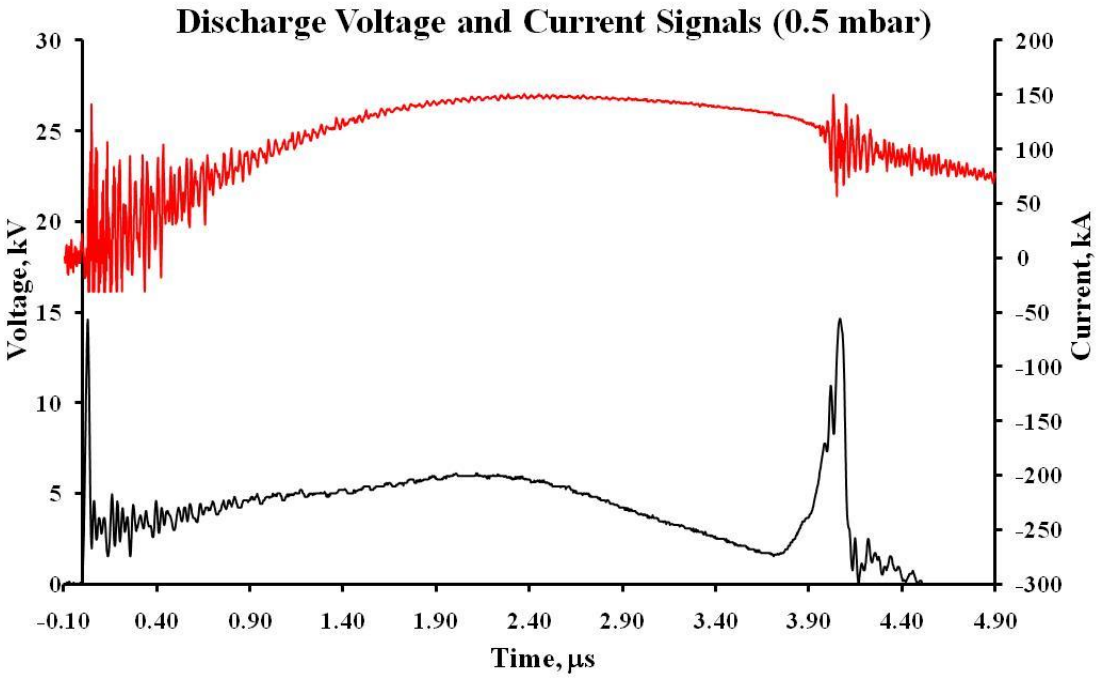

Figure 4.1.1: Typical discharge voltage and current signal at 0.5 *mbar* deuterium discharge.

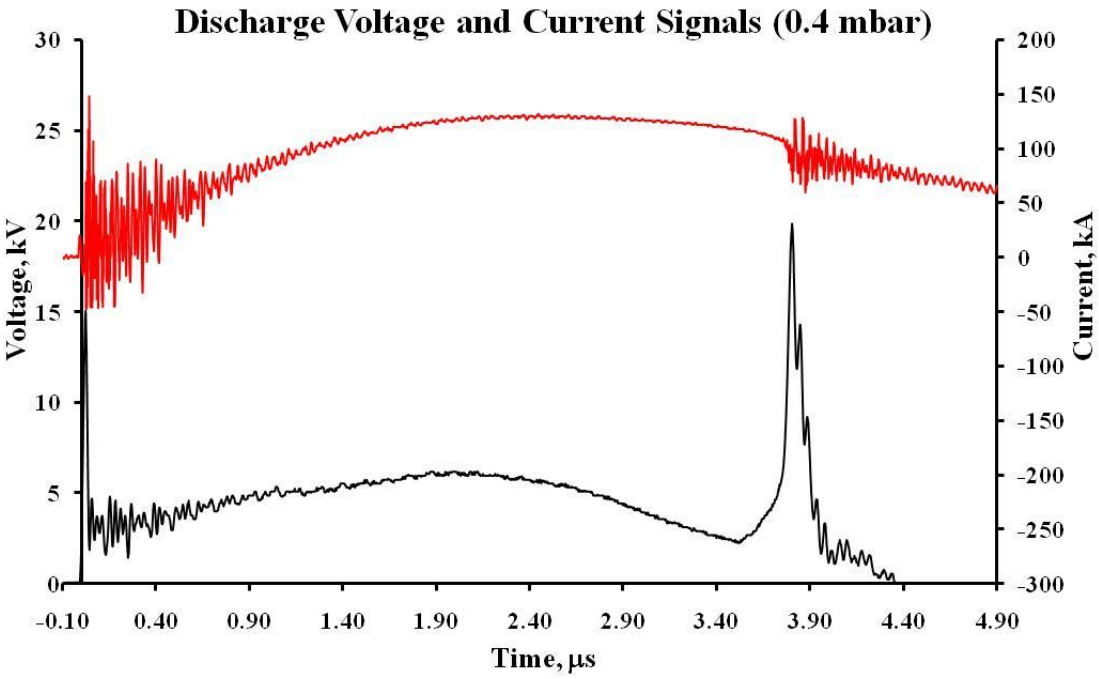

Figure 4.1.2: Typical discharge voltage and current signal at 0.4 *mbar* deuterium discharge.

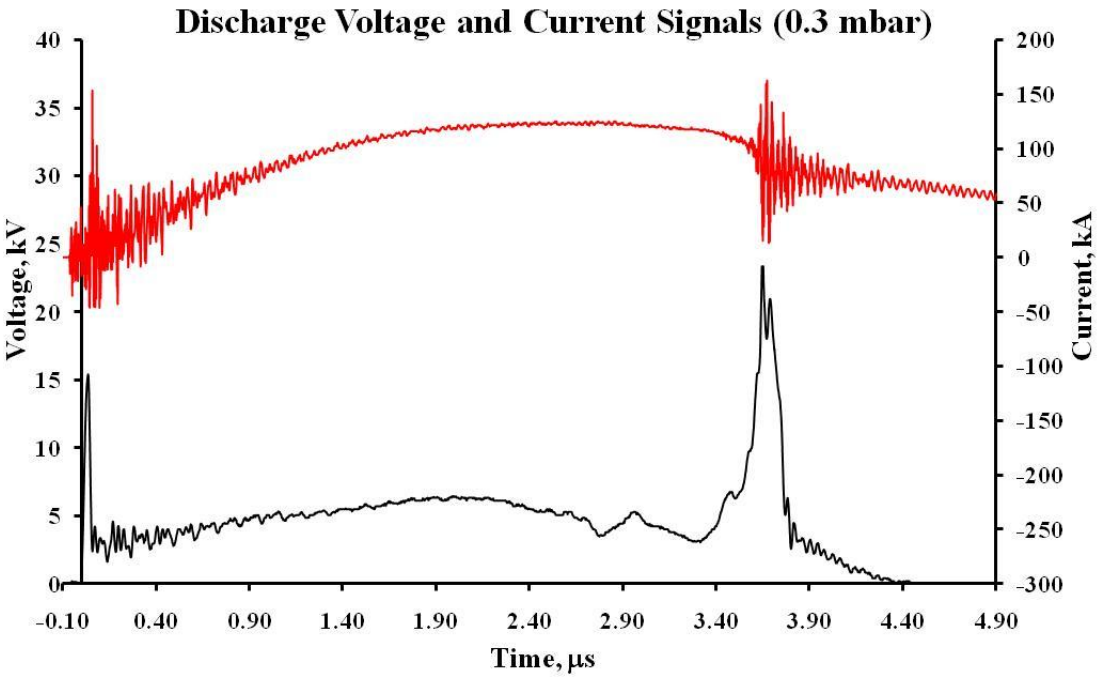

Figure 4.1.3: Typical discharge voltage and current signal at 0.3 *mbar* deuterium discharge.

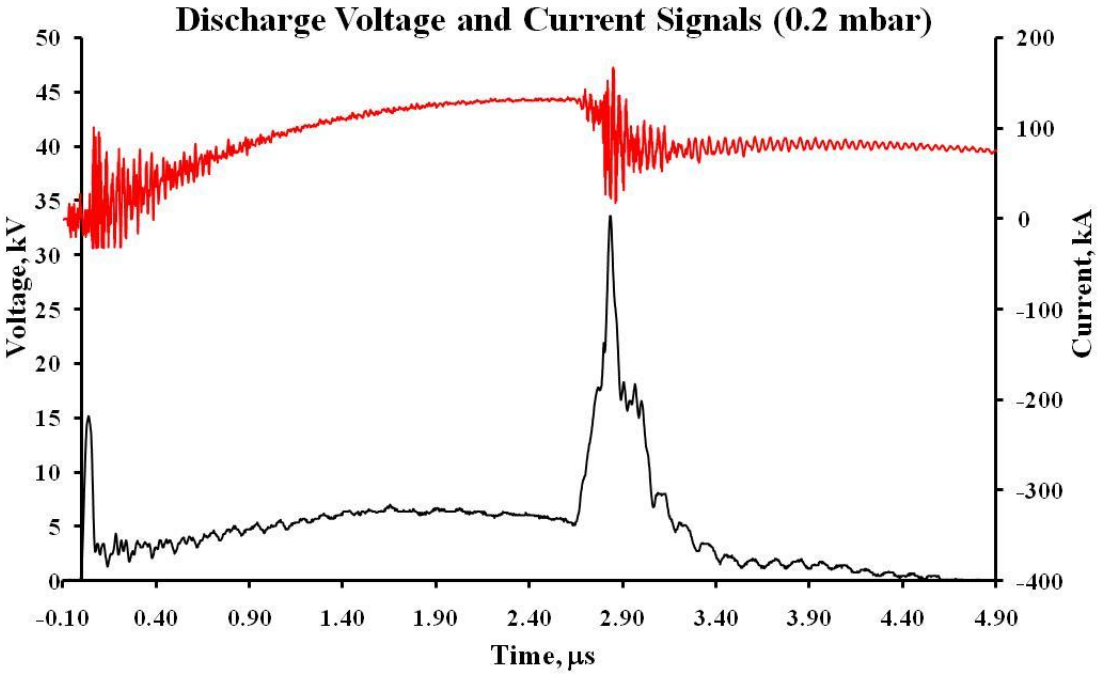

Figure 4.1.4: Typical discharge voltage and current signal at 0.2 *mbar* deuterium discharge.

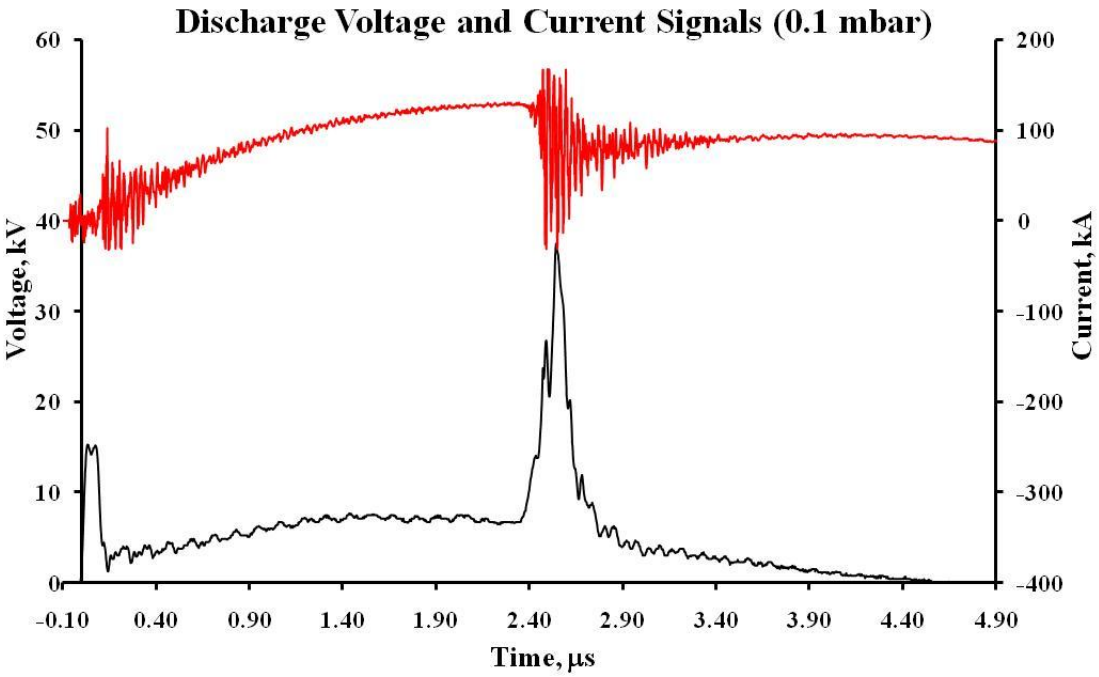

Figure 4.1.5: Typical discharge voltage and current signal at 0.1 *mbar* deuterium discharge.

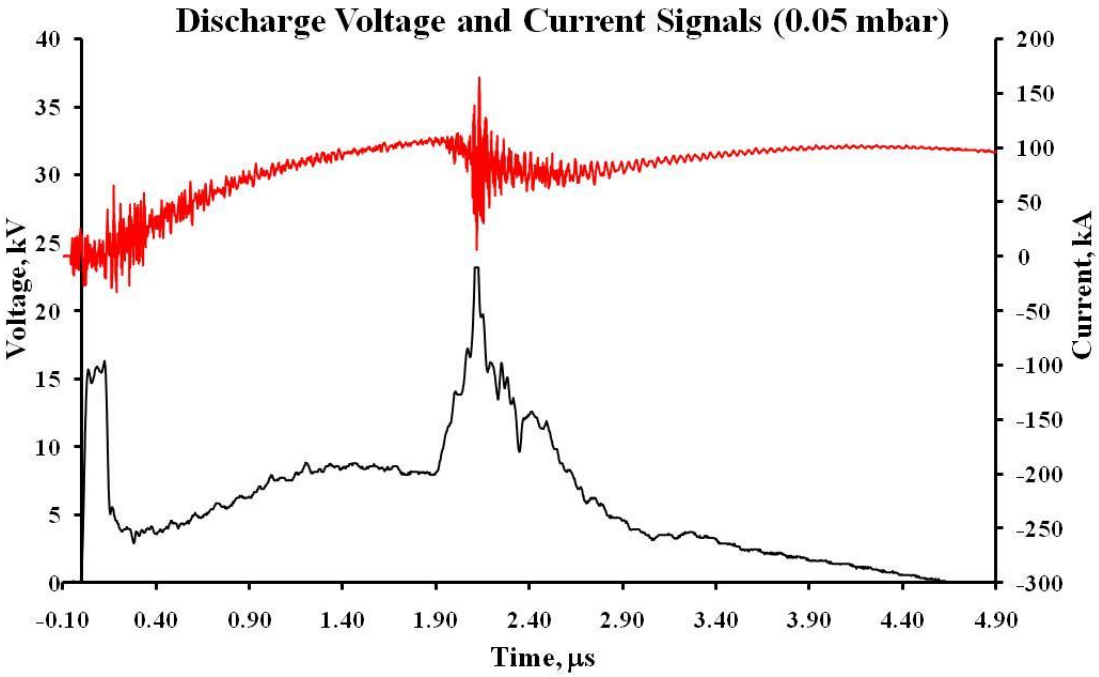

Figure 4.1.6: Typical discharge voltage and current signal at 0.05 *mbar* deuterium discharge.

The dependence of the time of focusing discharge to the operating pressure can be correlated to the run down speed of the current sheath. The average run down speed of the current sheath from breakdown to the end of the electrode can be estimated by taking the time between the breakdown (depicted as '*A'* in Figure 4.2) and the plasma compression, indicated by the voltage spike (depicted as '*B'* in Figure 4.2).

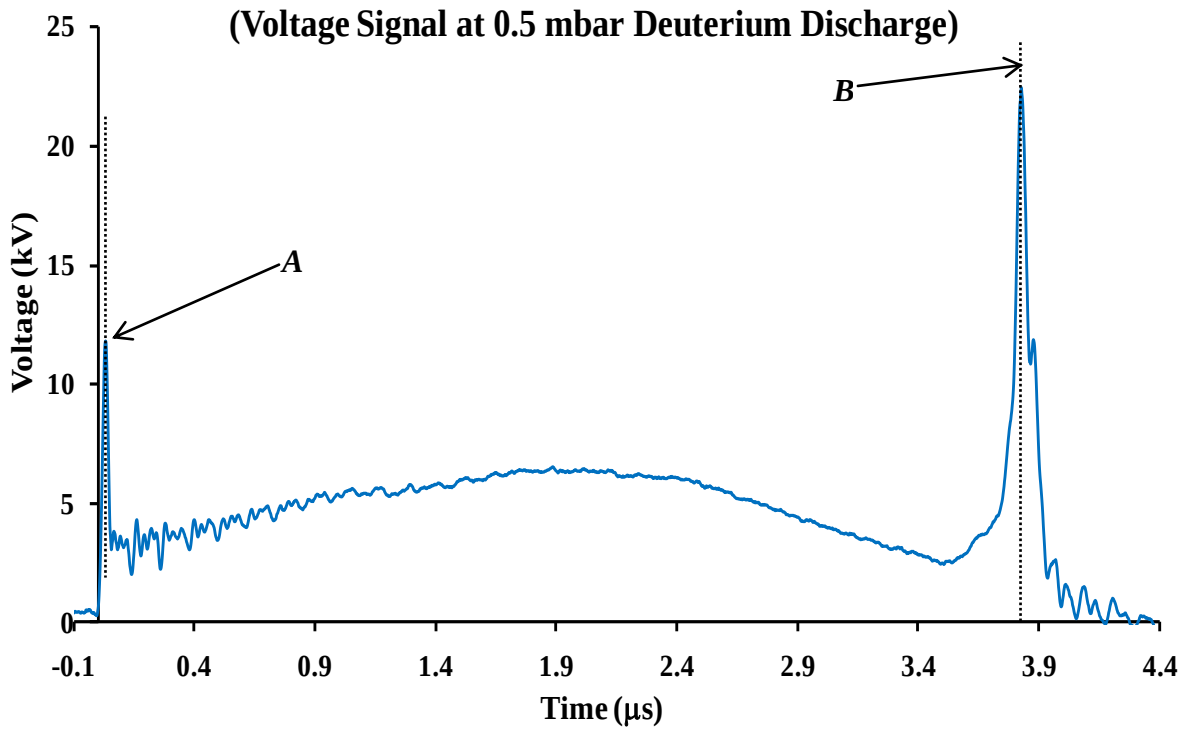

Figure 4.2: Estimation of average current sheath velocity.

A summary of the average velocity of the current sheath as a function of filling pressure is demonstrated in the Figure 4.3. It is shown that the current sheath run down at faster speed during the axial acceleration phase at lower operating pressure. This support the hypothesis of faster focus at lower pressure as observed in Figure 4.1.1 – 4.1.6. An average axial velocity of current sheath of about 11 *cm*/μs is obtained at 0.1 *mbar* where the discharge occurs near the time of maximum discharge current. At this pressure, intense focusing discharge with good reproducibility and consistent high amplitude of voltage spike is usually observed which will be discussed later.

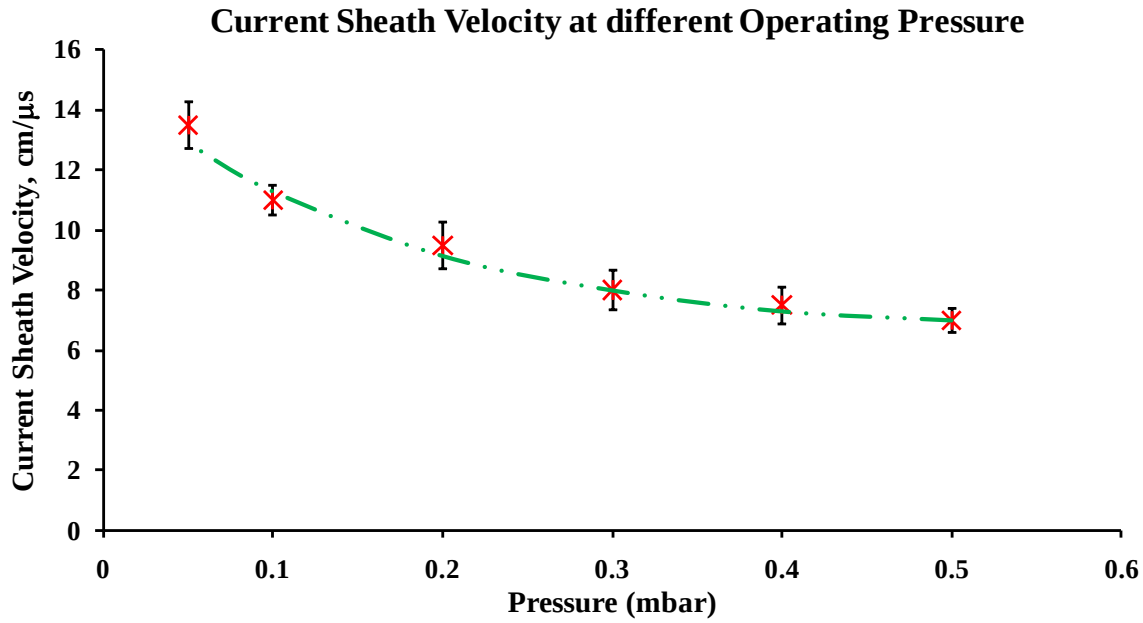

Figure 4.3: Average velocity of current sheath at deuterium discharge from 0.05 – 0.5 *mbar*.

The voltage surge and a voltage spike registered when the impedance rises during plasma focus. The amplitudes of the voltage spikes obtained at different operating pressures have been summarized in Figure 4.4. The highest voltage spike has also been obtained at 0.1 *mbar*.

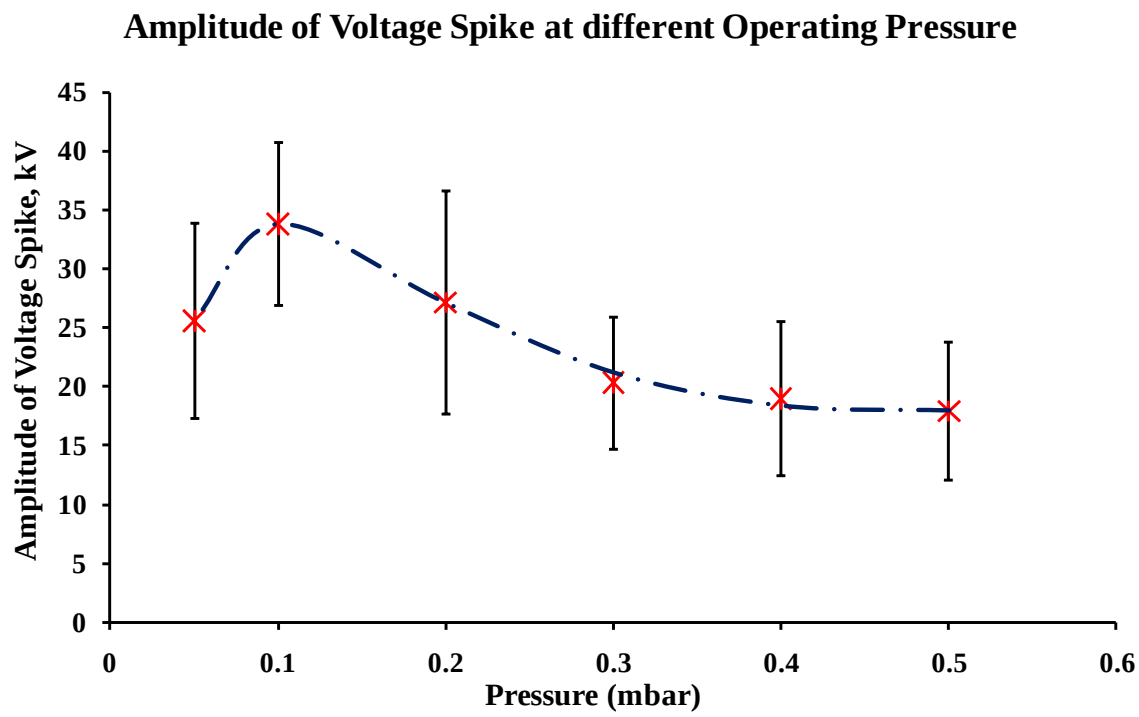

Figure 4.4: Average amplitude of voltage spike for deuterium discharge of 0.05 – 0.5 *mbar*.

The reproducibility of the focusing shots at different pressure has also been checked (Figure 4.5). Focusing has been obtained consistently for pressure 0.4 *mbar* and below. Some of the shots are registered with multiple spikes and some with single spike. Good focus shot with single spike frequently registered are obtained at 0.1 *mbar* and 0.2 *mbar*.

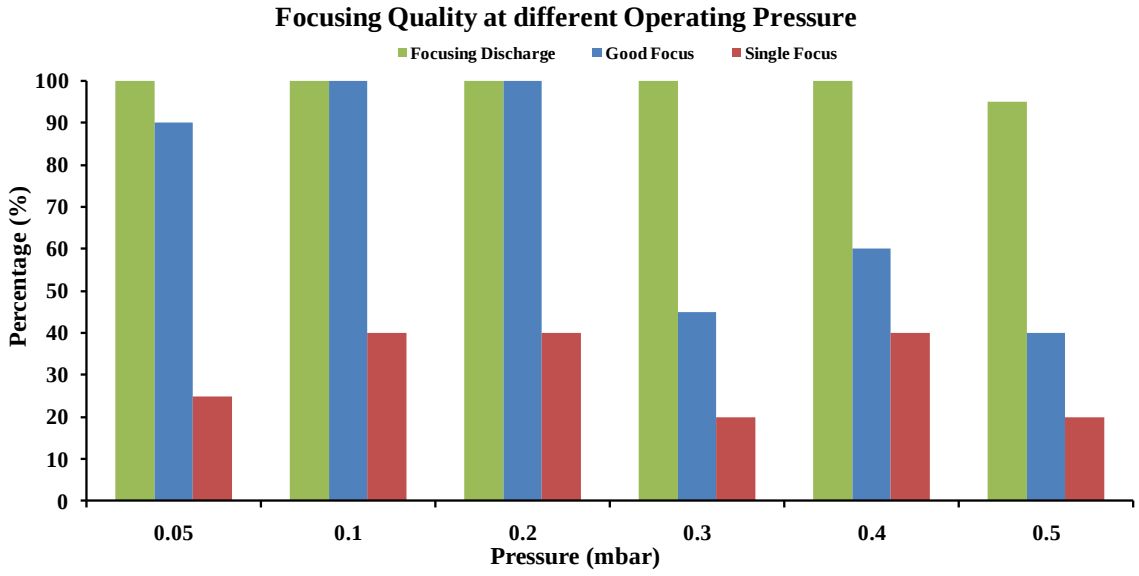

Figure 4.5: Focusing quality of deuterium discharge at respective operating pressure.

The power and energy involved during the current sheath compression onto the axis can be estimated from the changes in the discharge current and voltage measured during the compression. The power can be calculated from discharge voltage *V(t)* and current *I(t)* waveforms by taking multiplication among them. Energy output during the plasma focus can be obtained by integrating the area under the curve of calculated input power signals (Shaded area in Figure 4.6).

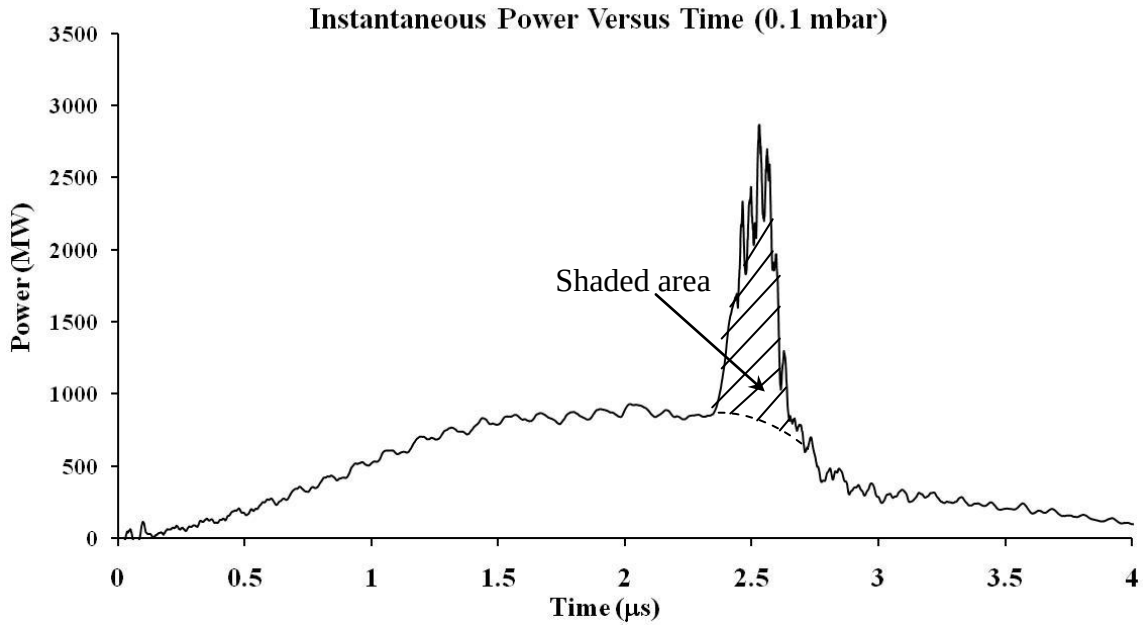

Figure 4.6: Input power *P(t)* against time at 0.1 *mbar* deuterium discharge.

The average energies converted into the compressing plasma are summarized in Figure 4.7. Within the pressure range of 0.05 *mbar* to 0.5 *mbar*, the maximum power input into the plasma column varies from 1000 Mega watts up to 4000 Mega watts for the case of 0.1 *mbar* at the instant of focusing. The average energies calculated are about 220 *J* to 360 *J* with the standard deviation varying from 20 *J* to 90 *J* for the pressure regime of 0.05 – 0.5 *mbar*. It is worth to note that the standard deviation of input energy at 0.1 *mbar* is the smallest among other operating pressure. This implies that the focusing action is almost consistent with good quality and high reproducibility

of plasma pinch. Higher input energy is found at 0.1 *mbar* compared to discharge at other operating pressure.

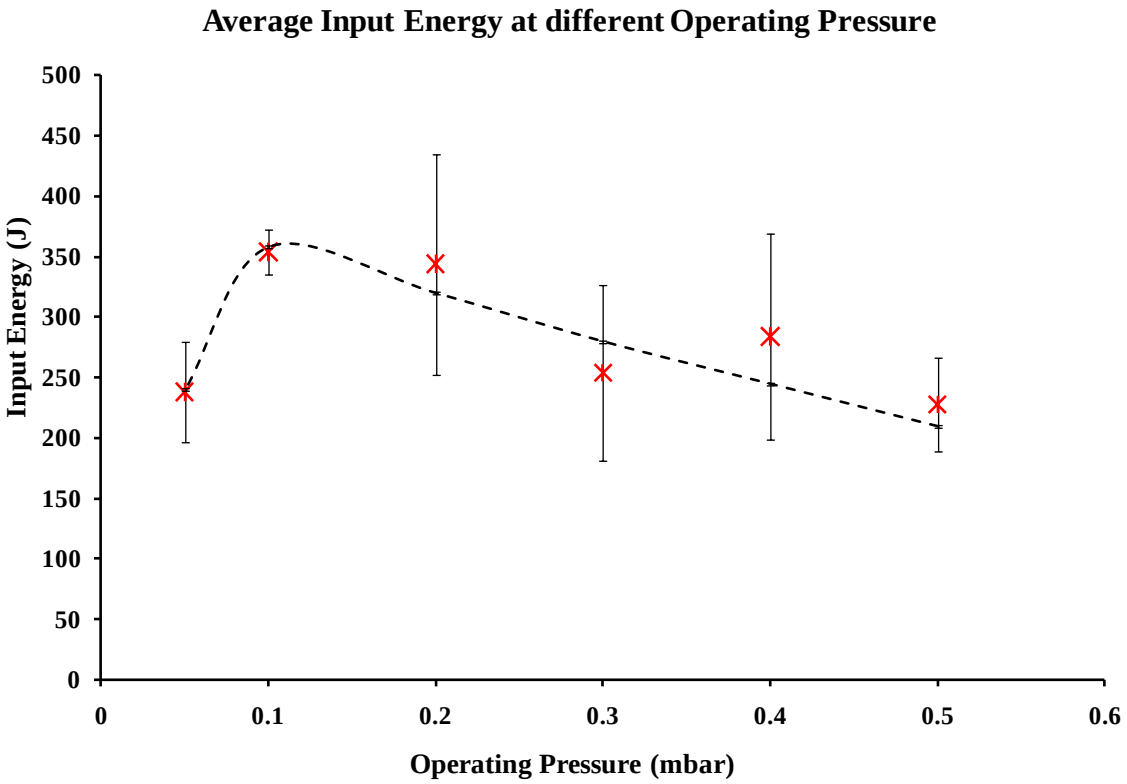

Figure 4.7: Average energy injected into plasma column calculated from the shaded area of *I(t) X V(t)* signal traces.

4.3 Ion Beam Emission of the Plasma Focus

The characteristic of the plasma focus device operated as an efficient source of ion beam when deuterium is used as the filling gas has been investigated. Efforts made to enhance the ion beam emission of the plasma focus device employed here include the extension of the electrode length and the pre-ionization making use of the set of plasma gun. The ion beam emission could also owe to the development of the instability in the pinched plasma. Time of flight technique is employed to investigate the ion beam emission and to determine the energy of the ion beam.

4.3.1 Correlation of Ion Beam Emission with Operating Pressure

Six operating pressures in the range from 0.05 – 0.5 *mbar* are employed. For the operating pressure more than 0.5 *mbar*, the reproducibility of the focusing action are found significantly less and the ion beam signal is insignificant. Ion beam signals obtained at various pressures are summarized in Figure 4.8.

The ion beam signals shown are registered by the biased ion collector-2. The amplitudes of ion beam signals are seen to increase gradually from pressure at 0.5 *mbar* to 0.1 *mbar*. The duration or FWHM of the ion beam signals is also found to be longer at lower operating pressure.

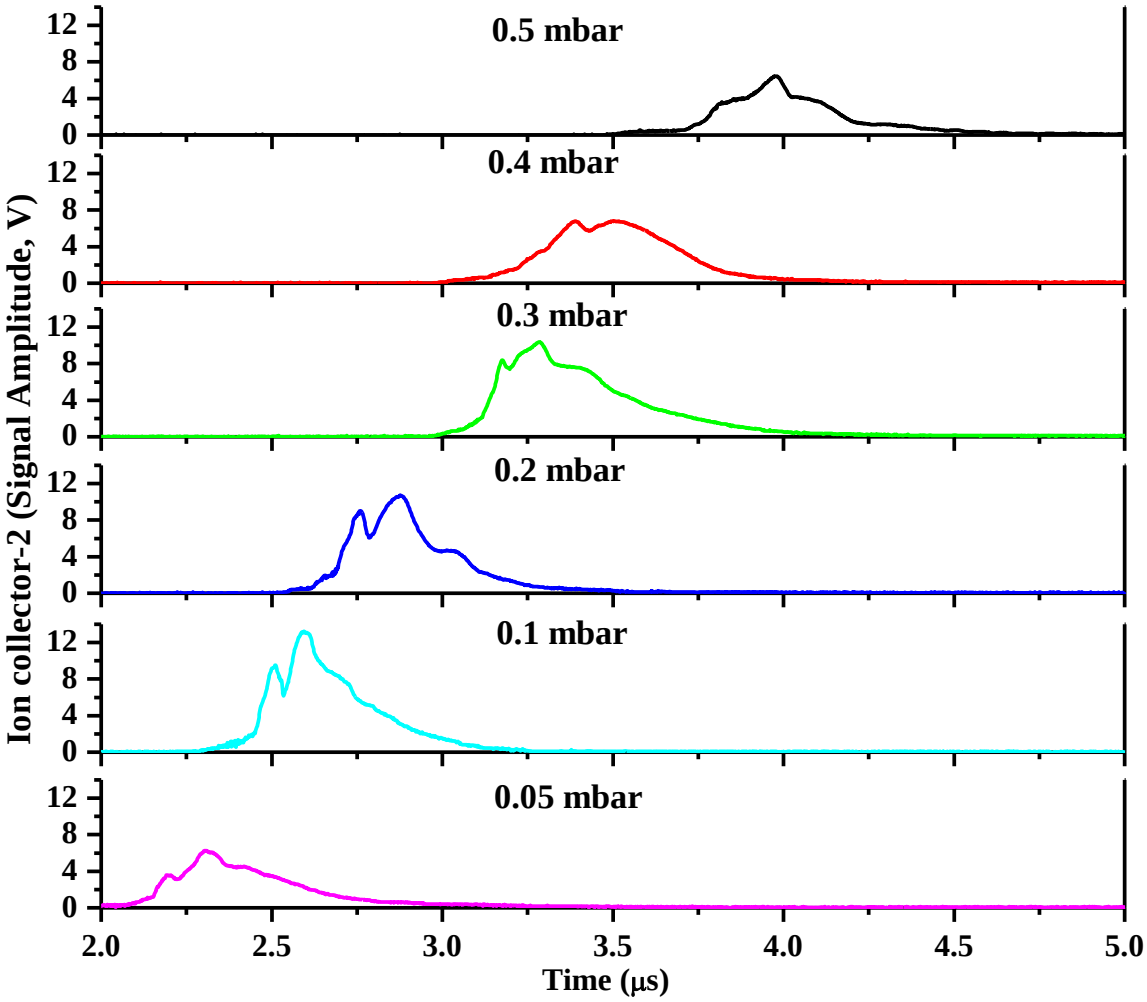

Figure 4.8: Ion beam signals at six different operating pressures from 0.05 - 0.5 *mbar* deuterium discharge.

On the other hand, the flux of the ion beam is found dependant on the filling pressure (Figure 4.9). The curve represent the results of 120 shots being fired for deuterium discharge in the pressure range of 0.05 – 0.5 *mbar*. Generally, a trend can be observed where the ion beams flux is peaked at 0.1 *mbar* and become lower at higher or lower pressures.

Assuming the ion beam is deuteron beam, the number of deuterons registered by the biased ion collector can be calculated, and shown in Figure 4.10. The average total

deuteron flux per shot is estimated to be around 2.1 x 10^{18} cm^{-2} at 0.1 *mbar*, which is the highest, compared to other pressure.

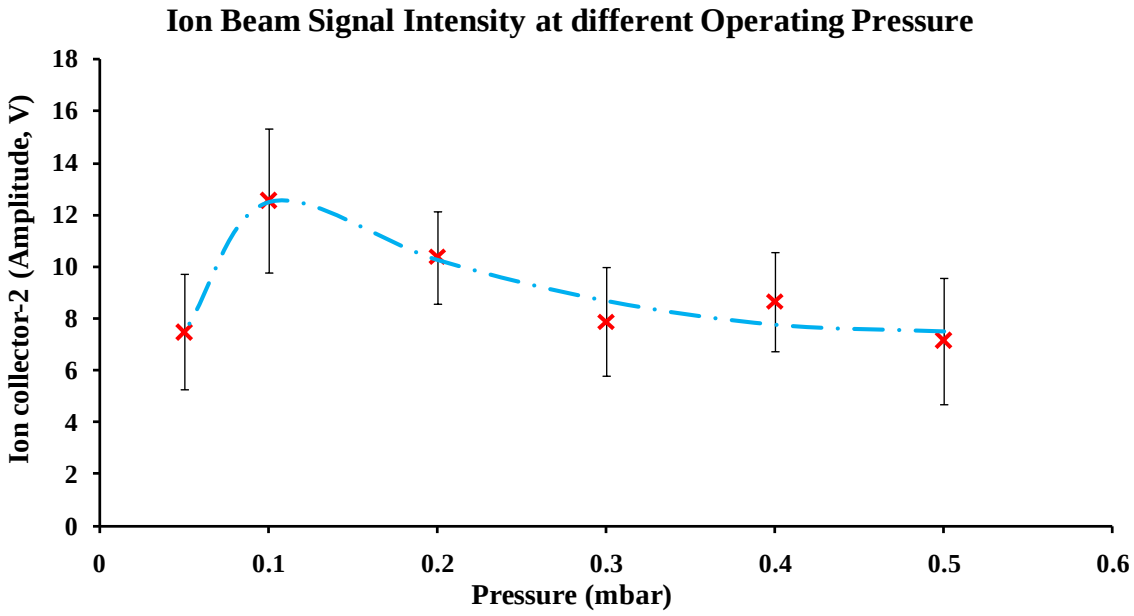

Figure 4.9: Average maximum ion beam signal intensity as a function of filling pressure.

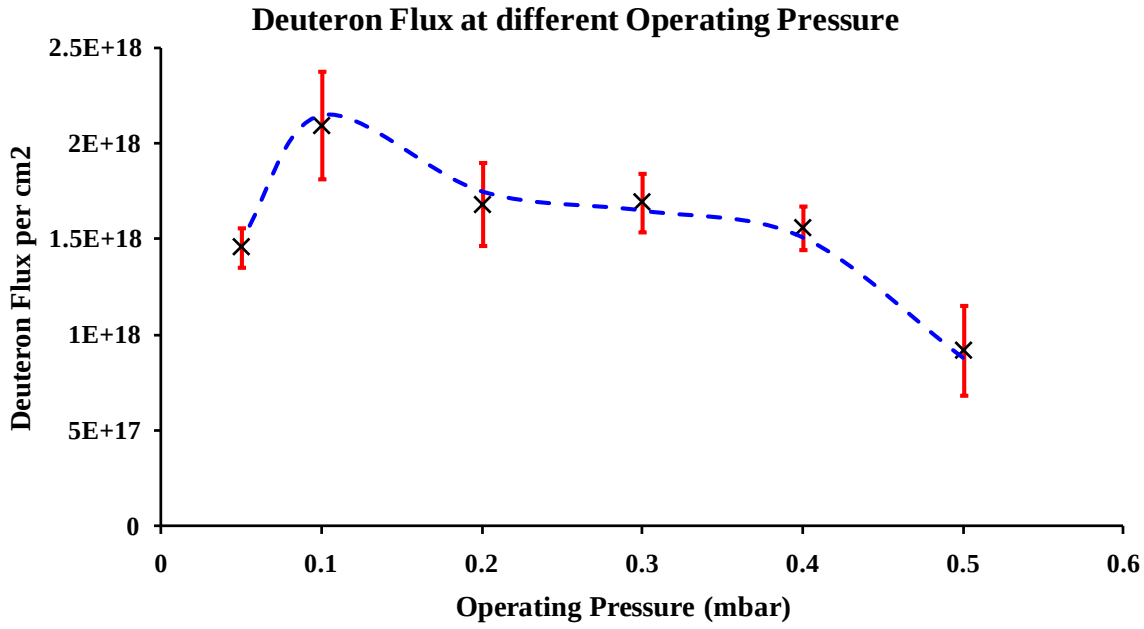

Figure 4.10: Average deuteron flux per cm^2 at different filling pressure.

4.3.2 Time of Flight (TOF) Measurement of Ion Beam Emission

For time of flight analysis, the ion beam emission from a plasma focus discharge in the axial direction of the focus tube is investigated with three biased ion collectors. The ion beams emitted will first be picked up by the first ion collector and reach the further ion collectors at a later time. Hence, ion beam energy is then to be determined from the peak-to-peak time difference of the corresponding time resolved ion beam signals. Signals registered by the third ion collector can be used to confirm our time of flight calculation, while the voltage spike is used to mark the emission time of the ion beam.

Typical voltage and biased ion collectors signals at 0.1 *mbar* deuterium discharge are shown in the Figure 4.11. A sharp rise of voltage spike can be observed in the voltage signal, which indicates a strong compression of the pinch plasma has been obtained. The ion beam signals registered by the three biased ion collector are clearly shown.

Although there are usually some plasma jet measured after the ion beam produced by the plasma focus (Lim, et al., 2009), plasma jet is not presence in our discharged and not observed in all the pressures from 0.05 *mbar* to 0.5 *mbar*.

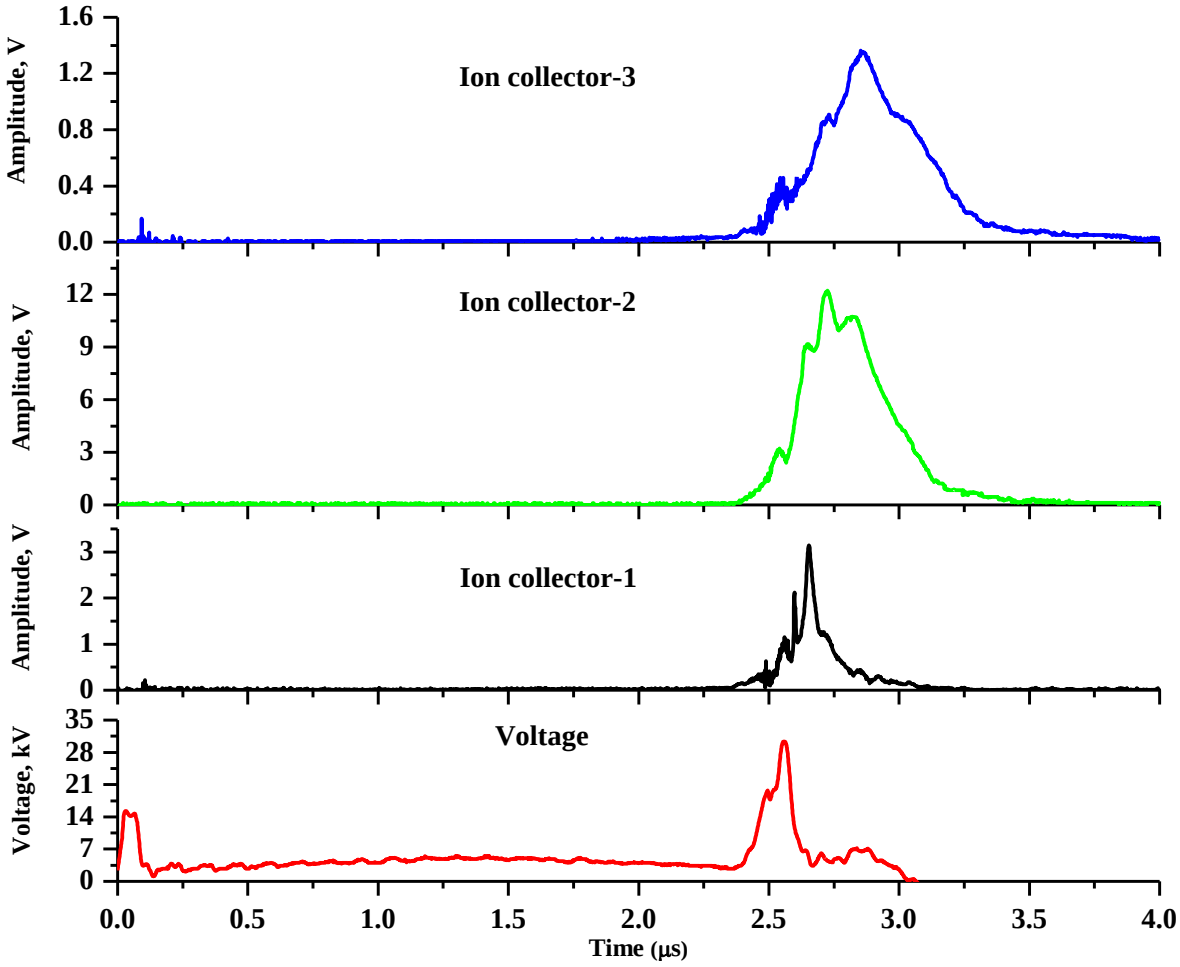

Figure 4.11: Typical discharge voltage and biased ion collectors signals at 0.1 *mbar* deuterium discharge.

The time scale of the graph in Figure 4.11 is enlarged to show the detail of the ion beam signal (Figure 4.12). Here, it is noticed that the ion beam signals have multiple peaks where at least three distinctive ion peaks (marked as 1, 2, 3) can be identified. With careful examination, the first peak (Peak 1, 1', 1") measured from all the ion collectors occurs simultaneously at the same time and explicitly corresponds to the voltage spike. Thus, this is the signal of the photoemission due to the radiation produced during the radial compression phase.

Careful analysis must be taken when recognizing the peak-to-peak time difference of the corresponding ion beam signals. In current setup, the distance between ion collector-2 to ion collector-3 is set at two times the distance of ion collector-1 to ion collector-2, hence the ion beam should take double time to travel from the location of the collector-2 and reaching collector-3.

Noticed that in Figure 4.12, ion beam signal is registered by ion collector-1 (marked as 2) ion collector-2 (marked as 2') and ion collector-3 (marked as 2'') at different time. Broadening of the ion beam signal is also observed. Ion beam signal registered at second ion collector exhibit pulse shape of broader width compared to first ion collector. This is because the ion beam has certain energy spread.

We can quickly determine the identification of the corresponding peaks by estimating the time difference between peaks. In the example shown in Figure 4.12, the peak-to-peak time difference between ion collector-1 (Peak 2) and ion collector-2 (Peak 2') is 42 *ns* while the corresponding time difference registered between ion collector-2 and ion collector-3 (Peak 2") is 84 *ns*. The trajectory time of the ion beam from ion collector-2 to ion collector-3 is seen to be twice from ion collector-1 to ion collector-2. By checking the time difference between other peaks, we can confidently label the peaks that are due to the same group of ion beam.

To calculate the ion beam energy, the mass, m is taken as the mass of deuteron, and v as the velocity of the ion beam, that the kinetic energy of a deuteron ion is obtained:

Kinetic energy, $E = \frac{1}{2} mv^2$.

Figure 4.12 also shows presence of two groups of ion beam, which the deuteron beams energy have been determined to be ~ 108 *keV* and ~ 39 *keV*. Since there is only single voltage spike observed which indicates the plasma compression, the ion beams produced could be due to the induced electric field during the moment of maximum compression and the m = 0 instability.

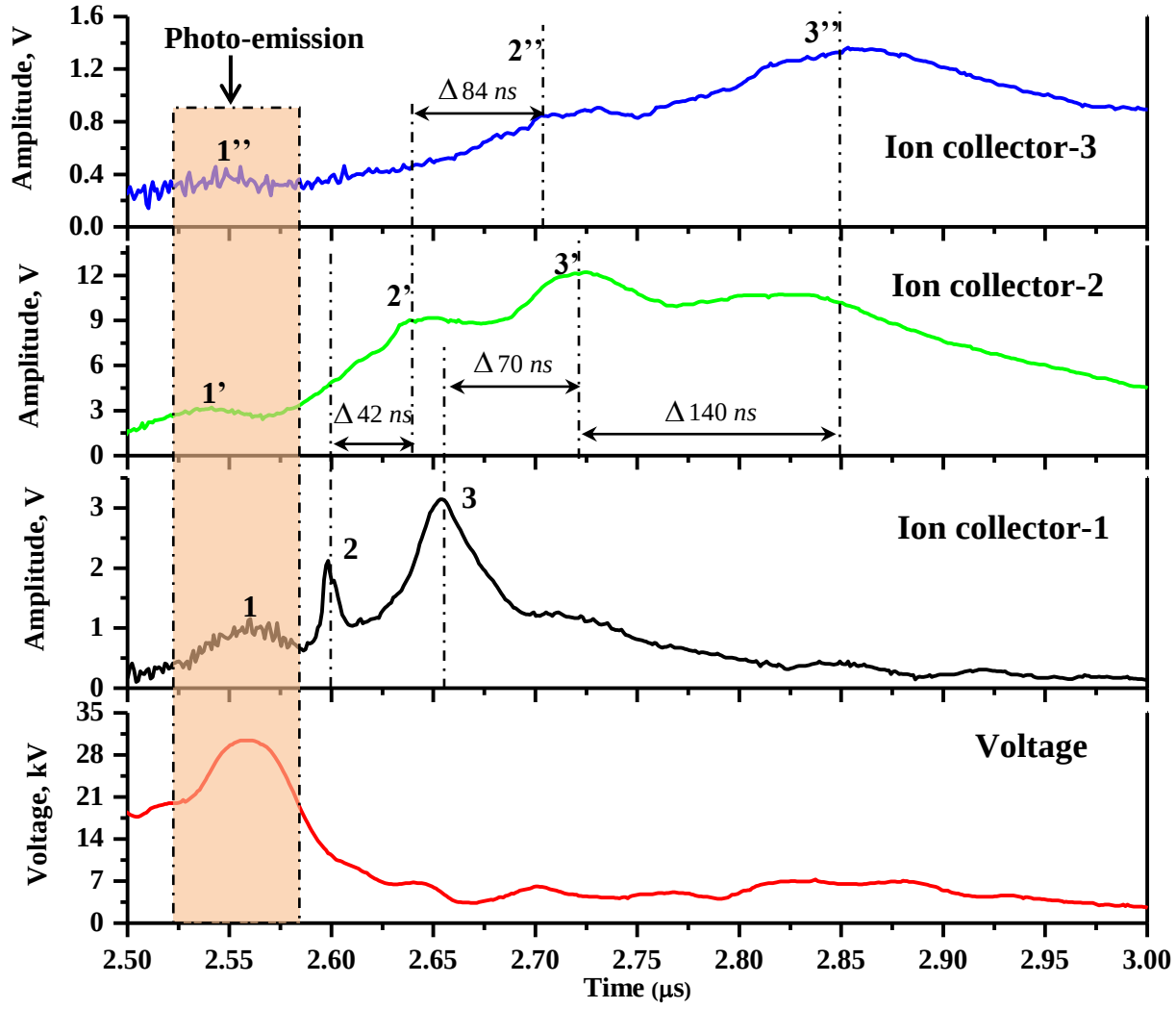

Figure 4.12: Typical biased ion collectors signal at 0.1 *mbar* deuterium discharge.

In Figure 4.13, there are multiple voltage peaks, correspond to the peaks registered by the ion collectors. In this case, the deuteron beam energy can be determined by identifying the corresponding voltage and ion peaks. The deuteron beam

energy of a particular shot was determined by taking the highest peak in the voltage and ion beam signal.

The deuteron beam energy determined is 30 *keV*, while the voltage spike measured is about 30 kV. It showed that the electric field induced at the moment of plasma pinching could be responsible for accelerating the deuteron beam.

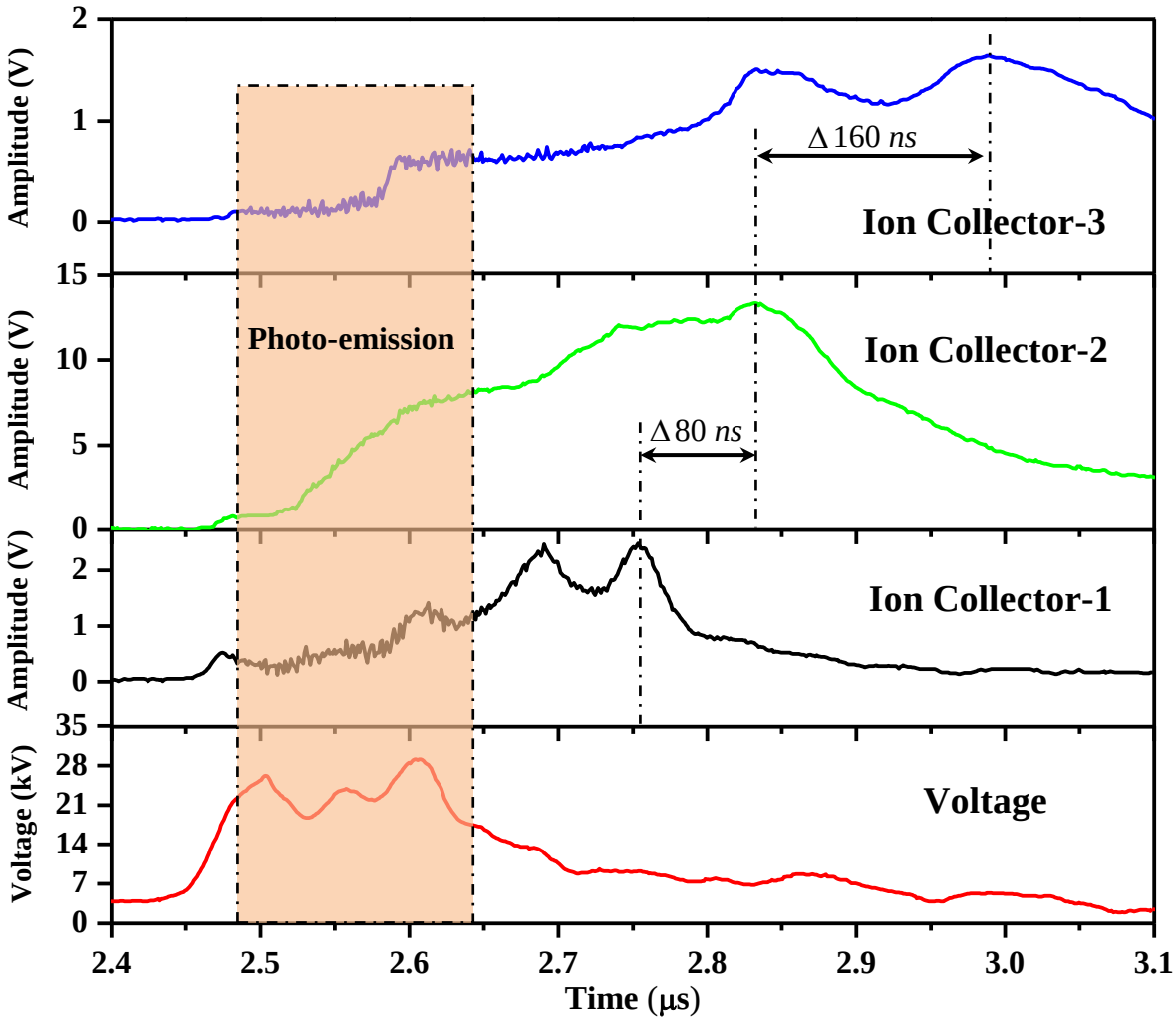

Figure 4.13: Time of flight ion beam signals with the corresponding voltage signal at 0.1 *mbar*.

Deuteron beam energy obtained at six different operating pressures ranged from few *keV* to 170 *keV*. It was found that the ion beam energy is larger at lower operating pressure, typically at filling pressure of 0.1 and 0.2 *mbar*. The average energy of

deuteron beam as a function of filling pressure is shown in Figure 4.14. The results show that the ion beam energy increases almost linearly with the decrease of operating pressure and reaches a maximum at 0.1 *mbar* and subsequently decreases at lower pressure. The deuteron beam with average energy in the range of 25 – 80 *keV* has been obtained.

By comparing Fig 4.14 and 4.4, we see that the ion beam energy is correlated with the amplitude of the voltage spike. The highest ion beam energy and strongest compression of the plasma column are obtained at operating pressure of 0.1 *mbar*.

A very high amplitude voltage spike corresponds to severe focusing action which is due to the large surge of plasma column impedance during the plasma pinch. It is this change of the impedance or inductance resulting the induced electric field that could accelerate the ion beam to very high energy in the downstream direction. High voltage spike indicate high induced electric field. The highest amplitude of voltage spike at 0.1 *mbar* deuterium discharge is also shown in Figure 4.4.

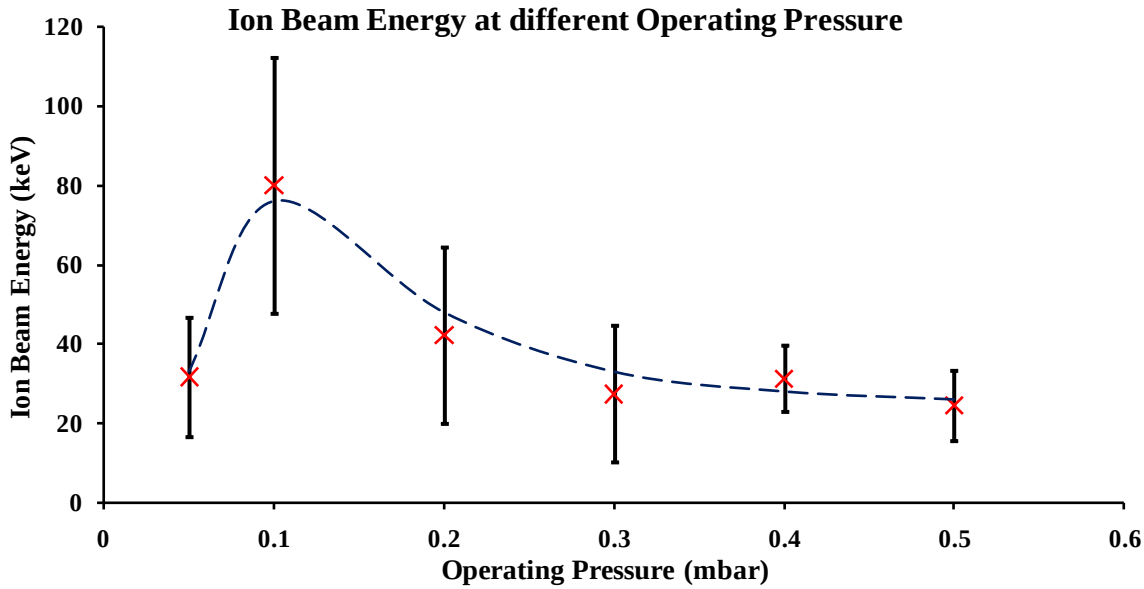

Figure 4.14: Average ion beam energy of deuterium discharge at different operating pressures.

Figure 4.15 presents the ion beam energy and the amplitude of voltage spike at six different operating pressures. At each working pressure, the ion beam energy determined is measured simultaneously with the voltage signal. Voltage signal is obtained by the Tektronix high voltage probe and the amplitude of the voltage spike is taken by considering the highest peak of voltage spike in the voltage signal.

Results showed that the stronger voltage spike is measured at lower operating pressure. The ion beam energy increases with the amplitude of voltage spike. This is reasonable as the high amplitude voltage spike represent the strong induced electric field, which can accelerate the ion beams.

The focusing discharge at 0.05 mbar occurs before the first quarter cycle of the discharge at only about 70 – 80 % of the maximum discharge current. The amplitude of the voltage spike measured is lower compared to the highest value measured at 0.1 mbar. The ion beam energy determined is only about 30 keV.

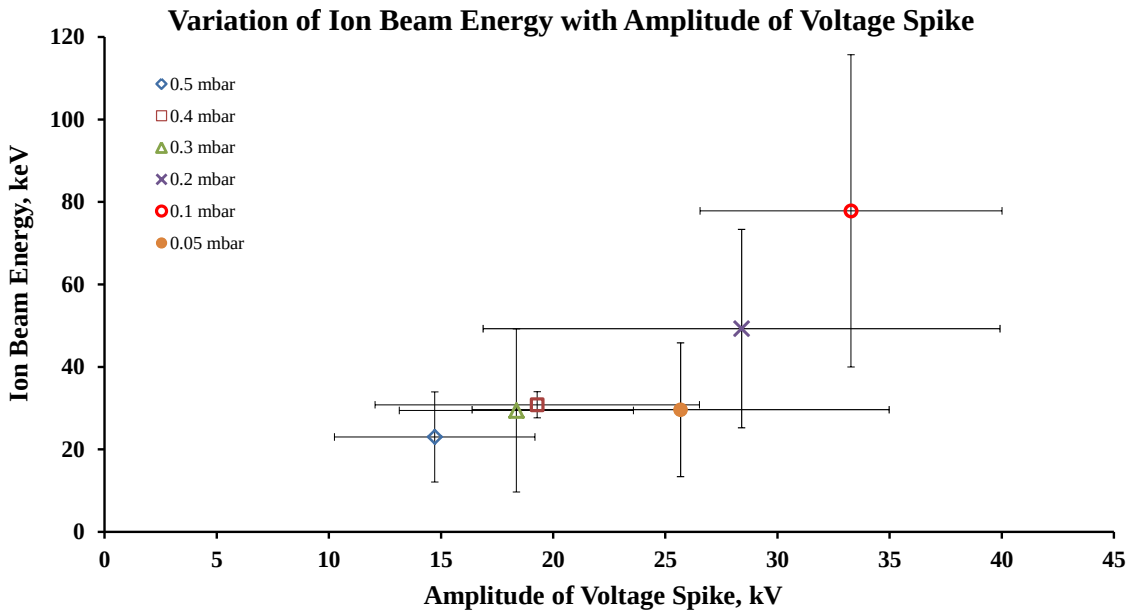

Figure 4.15: Variation of average ion beam energy with average amplitude of voltage spike at deuterium discharge for pressure ranged from 0.05 – 0.5 *mbar*.

If the signal intensity of the ion beams obtained at different operating pressures are analyzed (Figure 4.16), it shows that the intensity of ion beam is also dependent on the pressures, and thus correlated with the amplitude of the voltage spikes. Again, results obtained for 0.05 *mbar* does not follow the trend. Amplitude of the voltage spike at 0.05 *mbar* did not reach higher value than that of 0.1 *mbar*, but measured to be much smaller. The flux of the ion beam is also lower.

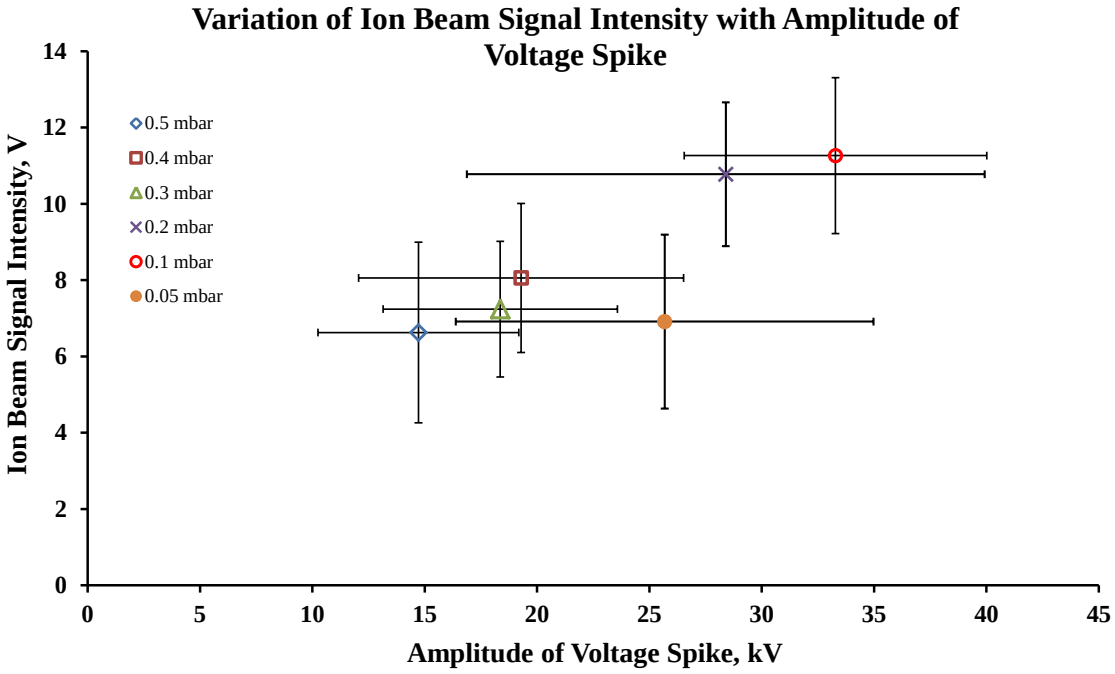

Figure 4.16: Variation of maximum amplitude of ion beam with amplitude of voltage spike at deuterium discharge from 0.05 - 0.5 *mbar*.

Correlation of the ion beam energy with the energy consumed during the plasma focus is shown in Figure 4.17. It is obvious that when more energy is consumed in the plasma focus, the discharge produces more energetic ion beam. The focused plasma of higher temperature would have ions of higher energy. Furthermore, together with the emission of ion beams due to the instabilities, energetic electron beams are also emitted.

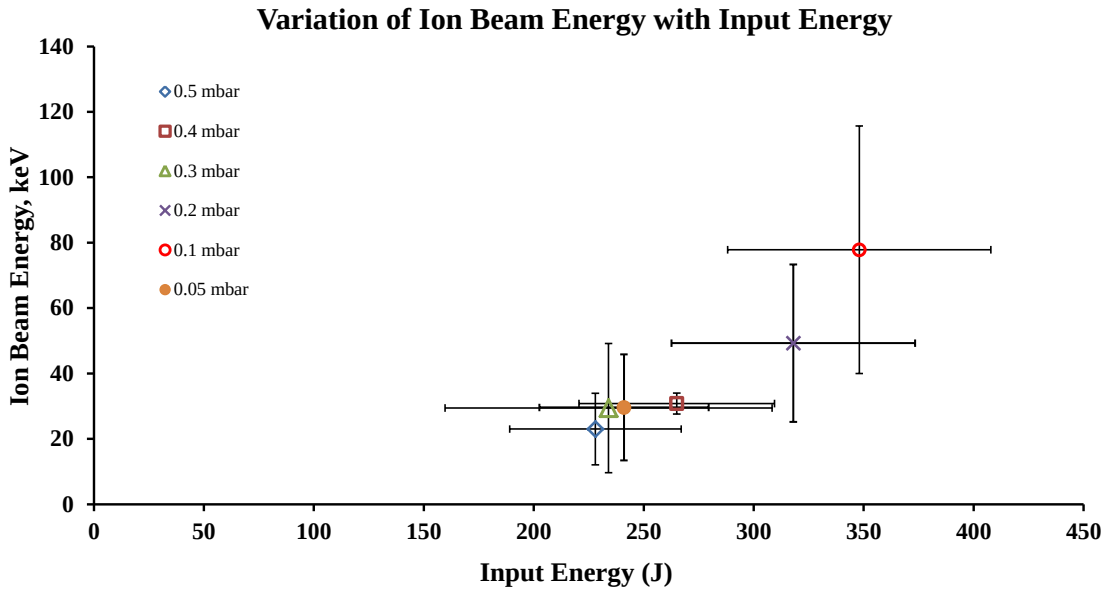

Figure 4.17: Ion beam energy as a function of energy pumped into the focus tube during the focusing discharge.

4.3.3 Summary of the Results

Experimentally, consistent and reproducible plasma focus discharge can be achieved at pressure of about 0.05 to 0.3 *mbar*. Nevertheless, the study includes a broader range of 0.05 *mbar* to 0.5 *mbar*. It was found that lowering the pressures improve the output of ion beam in terms of both the energy and intensity, with the lower pressure limit at 0.1 *mbar*. Table 4.1 summarized all the results of the study of the ion beam production against the operating pressure.

Table 4.1: Comparison of ion beam properties at 0.05 - 0.5 *mbar* deuterium discharge.

Operating Pressure (*mbar*)	Reproducibility of good Ion Beam Signals	Average Ion Beam Energy (*keV*)
0.5	~50%	~ 25
0.4	~70%	~30
0.3	~80%	~30
0.2	~80%	~50
0.1	~100%	~80
0.05	~90%	~30

The reproducibility of good ion beam production or good focusing discharge is the highest at the operating pressure of 0.1 to 0.2 *mbar*. Thus, application-making use of ion beam, like study of beam target reaction or treatment of sample with ion beam can be tested under these favorable conditions for the plasma focus ion beam production.

4.4 X-Ray Emission of the Plasma Focus

X-ray produced at each shot is recorded simultaneously with the discharge voltage, discharge current and ion beam signal. The diagnostic used to measure the soft X-ray emission from deuterium plasma is monitored by a 5-channel windowless BPX-65 PIN diodes covered with aluminized filter of different thickness. The combination of the filters used allows us to determine the plasma temperature if the emission is dominated by the Bremsstrahlung. All the channels of the PIN diode detectors have to be cross-calibrated.

Significant soft X-ray emissions are observed for all the discharge for the pressure range from 0.05 *mbar* to 0.5 *mbar*. Often, X-ray signal observed with a sharp spike followed by single or multiple broader peaks (Figure 4.18). The first spike usually exhibits a very sharp rise time, same time as the voltage spike. This is the signal of the maximum compression of the plasma column, thus can be taken as the zero time (t = 0) reference for the ion beam measurement.

A typical X-rays signal is shown in Figure 4.18 together with the discharge voltage and ion beam signal. The X-rays emission last for about 400 *ns*, where the second peak could be ascribe to the decay phase of the plasma column. The third peak (marked as '*X*') which is registered at about 400 *ns* after the maximum compression is speculated to be associated with the vaporized copper from the anode, which arrive later than the ion beams.

At least 3 ion peaks (Peak-1, 2, 3) in the ion beam signal can be identified here. First peak of the ion beam signal is too near to the voltage spike and X-ray spike that could be dominated by photo-emission. The time of flight of the ion beam can be checked after calculating the ion beam energy from the two ion collectors. The ion beam energy at this shot is determined to be 60 keV. At this energy, the time of the ion beam emitted from the plasma column is found to coincide with the time of the first peak in the voltage and X-ray signal (marked as 'A').

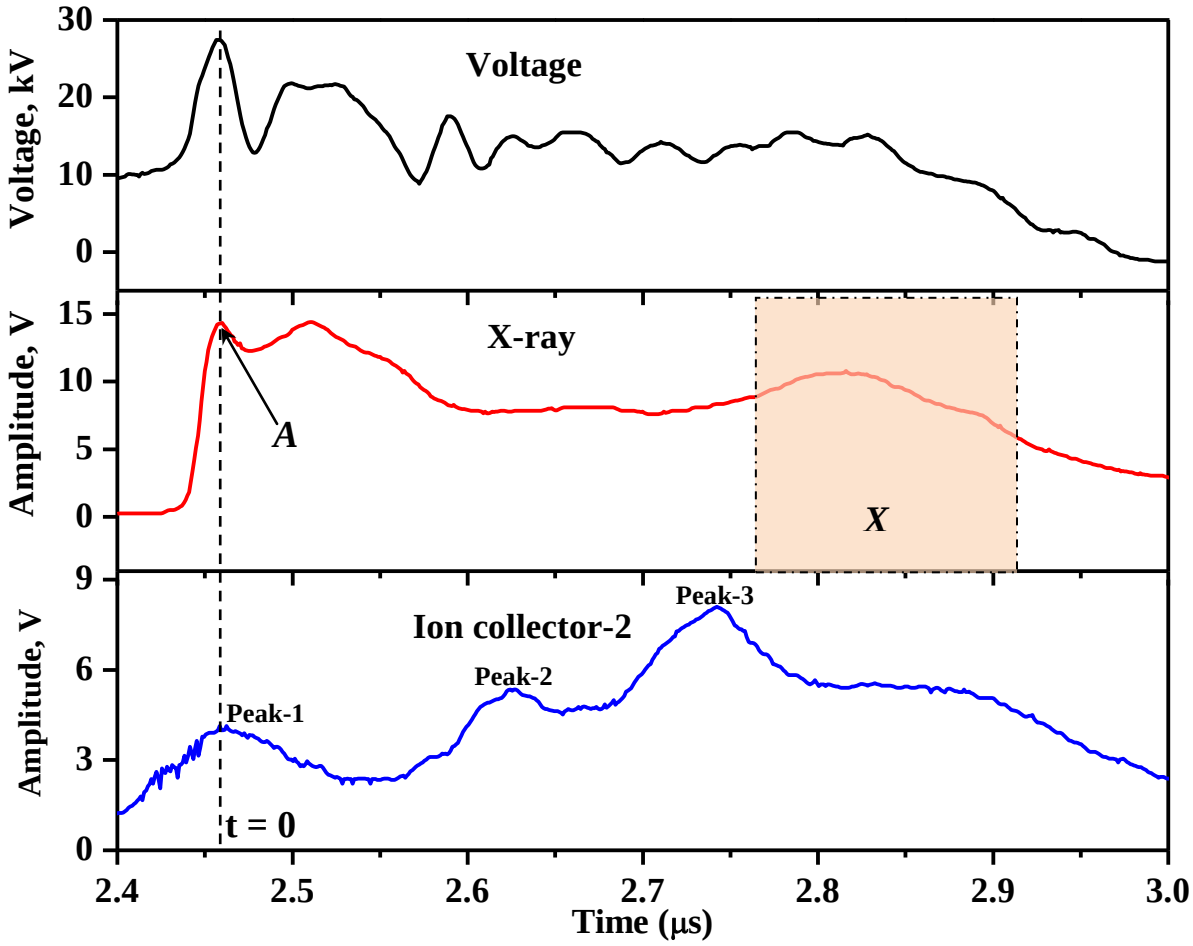

Figure 4.18: Simultaneously measured voltage signal, X-rays signal and ion beam signal at 0.1 *mbar* deuterium discharge.

Soft X-rays production is seen to be pressure dependent, as shown in Figure 4.19. The trend is similar to the ion beam emissions obtained. It was found that the soft X-rays production is maximum at deuterium discharge of 0.1 *mbar* where the highest

ion beam signal intensity also obtained at the same operating pressure. Similar trends exhibited by the ion beam and X-rays emission at operating pressure in the range of 0.05 – 0.5 mbar suggesting that the X-rays emission are produced by the activity of the corresponding electron beams.

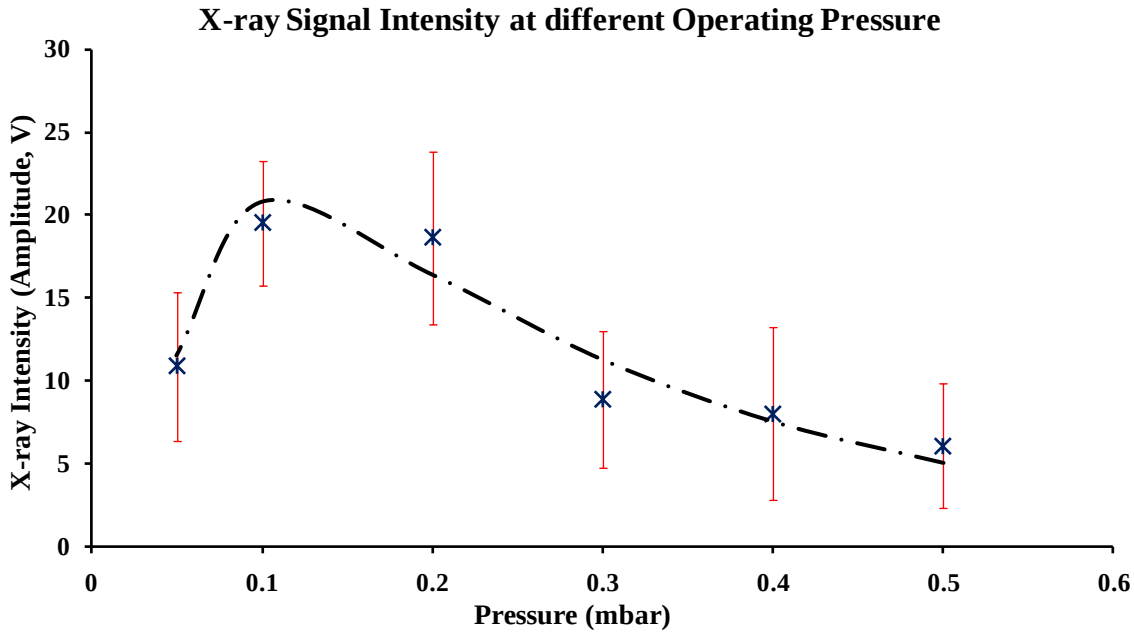

Figure 4.19: Average maximum X-ray signal intensity at deuterium pressure ranging from 0.05 *mbar* to 0.5 *mbar*.

Chapter 5

Conclusion and Suggestions for Further Studies

5.1 Conclusion

In the present study, the ion beam and X-ray emissions produced by a 3 *kJ* plasma focus device operated in deuterium gas have been investigated and reported. The discharges are carried out at pressure of 0.5 – 0.05 *mbar*, aims to enhance the plasma focus and allow acceleration of the current sheath to higher speed. However, formation of plasma focus observed is followed by severe disruption due to instabilities. These instabilities have been observed in the early study of plasma focus (Mather & Bottoms, 1968) and was known to disrupt the plasma. However, we believe that the instability also enhanced emissions of ion beams and X-rays. Energy of ion beam produced by the plasma focus is dependent on the instability that accelerated the ions to high energy (Imshennik, et al., 1973), (Haines, 1983), (Zambreanu & Doloc, 1992). Characteristic of the ion beam and Xradiation produced were studied by time resolved techniques. Energy of ion beam was determined with time of flight technique, while the X-rays were measured simultaneously by using an array of filtered PIN diodes. Ion beam and X-rays emissions were found correlated to the discharge current and voltage.

The production of ion beam from the plasma focus discharge was pressure dependent. Correlation of the ion beam flux and energy with the pressures are obtained. Ion beam is observed to be emitted at or after the maximum compression of the plasma column. In each of the discharge, at least two ion peaks can be identified where the first

peak may be due to photo-emission during the plasma pinching and the second peak is corresponds to the ion beam emission. In some of the shots, ion beam signal with more than two ion peaks can be observed. The ion peaks measured is either emitted from multi compressions of the plasma column or due to different pinch stages.

Generally, good focusing discharge was obtained in the pressure range from 0.05 – 0.5 *mbar*. Consistent good focus was observed particularly between 0.05 *mbar* to 0.2 *mbar*, with the reproducibility of 90 % to 100 %. Discharge with severe plasma focus indicated by the single voltage spike was obtained predominately at 0.1 and 0.2 *mbar*.

The energy transferred to the plasma upon focusing is calculated by considering the work done due to the electromagnetic compression of the current sheath by referring to the change in the measured time varying voltage and current. An average energy of 220 *J* to 360 *J* was estimated for discharges in the pressure range of 0.05 – 0.5 *mbar*, being highest at 0.1 *mbar*, which is 360 *J*. The voltage spike measured during plasma focus surged to 15 - 35 *kV*, which is within the limit of the high voltage probe of 40 *kV*. However, the instantaneous voltage rise could exceed the respond bandwidth of the probe, thus the value could be underestimated.

The average deuteron beam energy obtained was in the range of 25 – 80 *keV*. The X-ray measured follows a similar trend with ion beam when plotted against the pressures. As the ion beams increased, X-rays emission increased, thus suggesting those are produced by the corresponding electron beams.

The highest ion beam energy has been consistently measured at pressure 0.1 – 0.2 *mbar*. The highest ion beam energy of 80 *keV* obtained was at 0.1 *mbar*, with the relatively highest voltage spike. This implies that very high electric field strength has been induced at the moment of plasma pinching and thus accelerates the ion beam to very high energy. Thus, it can be concluded that 0.1 *mbar* is the optimum pressure for the ion beam production. On top of that, maximum deuteron flux isobtained at 0.1 *mbar* and the average total deuteron flux per shot is estimated to be around 2.1 x 10^{18} cm^{-2}.

On the other hand, significant amount of Xradiation has been obtained within the same pressure range as ion beam and is also found to be dependent on filling pressure. The maximum X-ray yield is also observed at 0.1 *mbar* deuterium discharge. In each focusing discharge, multi burst of X-rays pulses is observed in the X-rays signal. The origin of these X-rays pulses may come from the pinch column itself as well as interaction of electron beam with anode vapor.

The first X-rays spike is registered at the same time with the voltage spike, where the biased ion collectors also register a bump at the same time. Thus, the first ion peak in the ion beam signal is attributed to the photo-emission of the plasma during maximum compression. The optimum pressure for ion beam and X-rays generation is around 0.1 *mbar*. The consistent production of ion beam with average flux of 2.1 x 10^{18} cm^{-2} and average energy of 80 *keV* make the plasma focus a possible pulsed ion beam source for various applications.

5.2 Suggestions for Further Studies

In recent years, Plasma focus device has been considered as an alternative neutron source. Production of neutron yield from the plasma focus when deuterium gas is used can be enhanced via the beam target fusion reaction. Intense axial ion beam emission from the plasma focus can be utilized for this purpose.

There are few aspects that have to be considered to develop the plasma focus device for applications in beam target fusion. The reproducibility and efficiency of the plasma focus device to produce an intense ion beam and its energy spectrum has to be understood.

Works to enhance the ion beam emission have suggested the use of a longer electrode of length 27 cm (Yap, 2006). In this current project, optimum pressure with deuterium filling has been investigated, while for the operation with deuterium-tritium can be investigated in future.

The current sheath velocity at different operating pressures in this project is estimated by computing the time interval between the initial discharge to the time of focus. Measurements and computation of the current sheath profile during the axial acceleration and before the pinching effect can be investigated in more detail using magnetic probes. By obtaining the current sheath profile at various stages of the current sheath development, a better understanding of the dynamics of the plasma focus can be obtained.

To improve the current understanding of the ion beam production mechanism, the ion beam, X-rays and electron beam should be investigated simultaneously in correlation to the discharge voltage and current signals. Imaging of the plasma focus to indentify the zone where the ion beams are emitted can also give meaningful results.

Thomson parabola spectrometer can be used to measure the energy spectrum of the ion beams. This method has the advantage of resolving ion beam energy up to the range of MeV with suitably selected electric and magnetic field. Furthermore, accelerated ions with various charge states, ion mass number, atomic mass and ion beam energy can also be distinguished.

The purity of the ion beam emitted is also a concern for its application as an ion beam source. During focusing, impurities may be introduced due to irradiation of the electron beam on the electrode. Thus, studies on the effect of different electrode material especially those with the characteristic of high resistant to ablation can be carried out.

The miniaturization of the plasma focus device to a portable one is of importance for radiography application. The advancement in pulsed power technology to engineer a fast high current source is one of the important factors in the development of the pulsed sources in smaller dimension but with higher yield.